ISOLATION OF ACE2 INHIBITORS FROM RICE BRAN OIL BY-PRODUCT

Mr. Muhammad Waqar Nasir

จุฬาลงกรณ์มหาวิทยาลัย
CHULALONGKORN UNIVERSITY

A Thesis Submitted in Partial Fulfillment of the Requirements

for the Degree of Master of Science in Chemistry

Department of Chemistry

FACULTY OF SCIENCE

Chulalongkorn University

Academic Year 2022

Copyright of Chulalongkorn University

การแยกสารยับยั้ง ACE2 จากผลิตภัณฑ์พลอยได้ของน้ำมันรำข้าว

นายมูฮัมหมัด วากา นาเซอร์

Thesis Title	ISOLATION OF ACE2 INHIBITORS FROM RICE BRAN OIL BY-PRODUCT
By	Mr. Muhammad Waqar Nasir
Field of Study	Chemistry
Thesis Advisor	Associate Professor SURACHAI PORNPAKAKUL, Ph.D.

Accepted by the FACULTY OF SCIENCE, Chulalongkorn University in Partial Fulfillment of the Requirement for the Master of Science

--- Dean of the FACULTY OF SCIENCE
(Professor POLKIT SANGVANICH, Ph.D.)

THESIS COMMITTEE

--- Chairman
(Professor PREECHA PHUWAPRAISIRISAN, Ph.D.)

--- Thesis Advisor
(Associate Professor SURACHAI PORNPAKAKUL, Ph.D.)

--- Examiner
(Associate Professor SOMSAK PIANWANIT, Ph.D.)

--- External Examiner
(Assistant Professor Jirapast Sichaem)

มูฮัมหมัด วากา นาเซอร์ : การแยกสารยับยั้ง ACE2 จากผลิตภัณฑ์พลอยได้ของน้ำมันรำ
ข้าว. (ISOLATION OF ACE2 INHIBITORS FROM RICE BRAN OIL BY-PRODUCT)
อ.ที่ปรึกษาหลัก : รศ. ดร.สุรชัย พรภคกุล

การศึกษานี้มีวัตถุประสงค์เพื่อแยกแกมมาออริซานอลจากน้ำมันกรด (ผลพลอยได้จาก
การสกัดน้ำมันรำข้าว) และเพื่อประเมินฤทธิ์ยับยั้งเอนไซม์แองจิโอเทนซิน-คอนเวอร์ติง (เอซีอี
2) การแยกส่วนสกัดน้ำมันกรดด้วยเทคนิคโครมาโทกราฟีได้ 3 ส่วนสกัดแกมมาออริซานอลซึ่ง
ประกอบด้วย cycloartenyl ferulate, campesteryl ferulate, sitosteryl
ferulate, stigmasteryl ferulate และ cyclobranyl ferulate แกมมาออริซานอลที่มี
cycloartenyl ferulate และ campesteryl ferulate เป็นองค์ประกอบหลักแสดงฤทธิ์ยับยั้ง
เอนไซม์เอซีอี 2 ได้ดีที่สุดโดยมีค่าการยับยั้งที่ร้อยละ 50 (IC_{50}) เท่ากับ 10.57 ไมโครกรัมต่อ
มิลลิลิตร นอกจากนี้การศึกษาอันตรกิริยาของแกมมาออริซานอลทั้ง 19 โครงสร้างในการยับยั้ง
การทำงานของเอนไซม์เอซีอี 2 ด้วยวิธีการจำลองการจับเชิงโมเลกุล (Molecular docking) จาก
การศึกษาทาง ADME และการทำนายความพิษของ cycloartenyl ferulate และ campesteryl
ferulate โดยโปรแกรมคอมพิวเตอร์พบว่ามีศักยภาพที่จะพัฒนาเป็นตัวยับยั้งใหม่สำหรับยับยั้ง
เอนไซม์เอซีอี 2 ผลการศึกษานี้แสดงให้เห็นว่าแกมมาออริซานอลที่แยกได้จากน้ำมันกรดมี
ศักยภาพที่จะใช้เป็นตัวยับยั้งเอนไซม์เอซีอี 2 อย่างมีนัยสำคัญ ซึ่งสามารถนำไปใช้เป็นต้นแบบใน
การพัฒนาวิธีการรักษาแบบใหม่ที่มุ่งเป้าในการรักษาโรค COVID-19.

จุฬาลงกรณ์มหาวิทยาลัย
CHULALONGKORN UNIVERSITY

สาขาวิชา   เคมี   ลายมือชื่อนิสิต ....
ปีการศึกษา   2565   ลายมือชื่อ อ.ที่ปรึกษาหลัก ....

6470183823 : MAJOR CHEMISTRY

KEYWORD: Rice bran oil, Crude oil acid fraction, Gamma oryzanol, ACE2, Molecular docking

Muhammad Waqar Nasir : ISOLATION OF ACE2 INHIBITORS FROM RICE BRAN OIL BY-PRODUCT. Advisor: Assoc. Prof. SURACHAI PORNPAKAKUL, Ph.D.

This study aimed to isolate **γ**-oryzanol from the crude oil acid fraction (a by-product of rice bran oil refinery) and to evaluate their Angiotensin-Converting Enzyme 2 (ACE2) inhibitory activity. Chromatographic fractionation of the crude oil acid fraction gave 3 isolated fractions of **γ**-oryzanol containing cycloartenyl ferulate, campesteryl ferulate, sitosteryl ferulate, stigmasteryl ferulate, and cyclobranyl ferulate. The **γ**-oryzanol containing cycloartenyl ferulate and campesteryl ferulate as major component showed good ACE2 inhibitory activity with the IC_{50} value 10.57 **μ**g/mL. Furthermore, the 19 structures of **γ**-oryzanol were also studied for its interaction against ACE2 through molecular docking. Based on the *in-silico* study, ADME investigation, and toxicity prediction of cycloartenyl ferulate and campesteryl ferulate were potential to be developed as novel inhibitors for ACE2. This result demonstrated that the isolated **γ**-oryzanol from the crude oil acid fraction had the potential to be ACE2 inhibitor and its significant ACE2 inhibitory activity could serve as leads for the development of novel therapeutics targeting COVID-19.

Field of Study: Chemistry   Student's Signature ....

Academic Year: 2022   Advisor's Signature ....

ACKNOWLEDGEMENTS

TABLE OF CONTENTS

LIST OF TABLES

LIST OF FIGURES

จุฬาลงกรณ์มหาวิทยาลัย
CHULALONGKORN UNIVERSITY

LIST OF ABBREVATIONS

δ	Chemical shift (NMR)
δ_C	Chemical shift of carbon (NMR)
δ_H	Chemical shift of proton (NMR)
μL	Microliter
μM	Micromolar
μg	Microgram
°C	Degree Celsius
^{1}H NMR	Proton nuclear magnetic resonance spectroscopy
^{13}C NMR	Carbon-13 nuclear magnetic resonance spectroscopy
2D NMR	Two-dimensional nuclear magnetic resonance spectroscopy
α	Alpha
ACE2	Angiotensin-converting enzyme 2
CRBO	Crude rice bran oil
CC	Column chromatography
CDCl$_3$	Deuterated chloroform
d	Doublet (NMR)
dd	Doublet of doublet (NMR)
ddd	Doublet of doublet of doublet (NMR)
DMSO	Dimethyl sulfoxide
dq	Doublet of quartet (NMR)
dt	Doublet of triplet (NMR)
EtOAc	Ethyl acetate

γ	Gamma
HMBC	Heteronuclear multiple-bond correlation spectroscopy
HPLC	High performance liquid chromatography
HSQC	Heteronuclear single quantum correlation spectroscopy
IC_{50}	Half maximal inhibitory concentration
J	Coupling constant
L	Liter
m	Multiplet (NMR)
M	Molar
MeOH	Methanol
mg	Milligram
MHz	Megahertz
mM	Millimolar
mmol	Millimoles
ppm	Parts per million
q	Quartet (NMR)
qd	Quartet of doublet (NMR)
RBO	Rice bran oil
RBAF	Rice bran acid fraction
s	Singlet (NMR)
t	Triplet (NMR)
td	Triplet of doublet (NMR)
TLC	Thin layer chromatography

ml   Microliter

Kg   Kilogram

CHAPTER I INTRODUCTION

Chemical molecules generated by plants, animals, or microorganisms are known as natural products. Cosmetics, drugs, dyes, nutritional supplements, and foodstuffs made from natural sources that are minimally processed or do not include artificial chemicals are example of natural goods in commercial usage. Natural products are organic molecules obtained and isolated from natural sources and created by the metabolic pathways or primary or secondary metabolism in organic chemistry. Within the discipline of medicinal chemistry, the term is usually narrowed to secondary metabolites, which are tiny molecules (mol wt. <2000 amu) that are not required for the organism's existence [1].

Organic substances important for growth, development, reproduction, and survival, including as nucleic acids, amino acids, proteins, carbohydrates, and different energy components involved in all living organisms' fundamental metabolic pathways, are known as primary metabolites. Secondary metabolites, unlike primary metabolites, are found exclusively in certain organisms and are expressions of species identity. Organic substances that are not required for metabolism are known as secondary metabolites. Secondary metabolites rather play a role in circumstantial adjustment or as a feasible defensive technique for the organism's self-protection [2]. Ecological pressures such as food and space contests, as well as predator and surface fouling, have resulted in the creation of secondary metabolites with a variety of biological functions. Several

secondary metabolites are poisonous to predators, stimulating allure to the identical or the different species, or colorant to entice or to threaten distinct species. Most natural compounds, by definition, have pharmacological or biological activity that can aid the treatment of disorders [3].

Rice (Oryza sativa L.) is the world's second biggest cereal grain, behind wheat. According to the United States Department of Agriculture, the world rice production in 2016/2017 was roughly 741.3 million metric tons. The majority of rice produced is grown in Asian countries. Thailand produces 30 million metric tons of paddy or 19.8 million tons of milled rice, which is split between local and export use. Because Thai people love white rice, the rice grain is milled or polished to eliminate the bran and germ. [4].

Rice bran is a byproduct of the rice milling process that accounts for 8-11% of the total weight of raw rice. Rice bran is a desirable byproduct of the rice processing industry because it contains oil, protein, dietary fiber, and important compounds such as vitamins, phytosterols, and γ-Oryzanol. One option to utilize rice bran is to extract oil for human use. Solvent extraction is a method for extracting rice bran oil. After extraction, the solvent is removed to yield crude rice bran oil, which is then refined. [5].

γ-Oryzanol is a combination of ferulic acid esters of triterpene alcohols (phytosterols) such as cycloartenyl ferulate, 24-methylenecycloartanyl ferulate, and campesteryl ferulate [6]. γ-Oryzanol is an antioxidant that has been linked to reduced plasma

cholesterol, lower serum cholesterol, and decreased platelet aggregation. However, it has been demonstrated that greater amounts of γ-Oryzanol of 200-2,000 mg offer the necessary health advantages. Several studies over the last few decades have demonstrated the favorable physiological and biological benefits of γ-Oryzanol consumption [7]. Due to the presence of the phenol moiety in its composition, the majority of biological research concerns the antioxidant activity of this γ-oryzanol. In this respect, γ-Oryzanol has been thoroughly explored for its antioxidant due to the presence of the ferulic/caffeic acid component, which allows electron donation and kills the activity of free radicals [8].

Although many researches on phytochemicals, pharmacological tests and isolation work on rice bran oil have been published, there were only few reports from the crude rice bran acid fraction. Therefore, this thesis focused on seeking ACE2 Inhibitor candidates from crude rice bran acid fraction. According to the main objective of this research, the bioactive compound from crude rice bran oil were isolated by column chromatography techniques and screened for the active compound for ACE2 SARS-CoV-2.

CHAPTER II LITERATURE REVIEW

2.1 Rice and Rice Grain Structure

Rice farming dates back over 7,000 years. Rice is farmed on enormous amounts of land all over the world and is a primary dietary staple for more than half of the world's population. Rice was the fourth largest cultivated crop produced globally in 2016-2017, with an annual global production of around 740 million metric tons of paddy. The Asian continent accounts for nearly 90% of rice production and is also the largest consumer [9]. Figure 1 depicts the mature rice grain structure. The rice grain's main components are the hull, pericarp, seed coat, nucellus, aleurone layer, endosperm, and embryo. Rice is made up of 20% husk, 1-2% rice germ, 8-9% rice bran, and 70% rice starchy endosperm. Rice caryopsis is composed of pericarp (1-2%), aleurone (4%), seed coat and nucellus (4%), embryo (2%), and endosperm (89%) [10].

2.2 Chemical Characteristics

As demonstrated in Table 1, good eating quality is associated with high stickiness, sweet flavor, gloss of cooked rice, and palatability. A tasting panel evaluates the eating quality of a particular lot of rice objectively. Taste panel scores are then used to calibrate "taste analyzers" that produce taste scores based on physicochemical parameters. White rice's flavor is mostly determined by protein, amylose, and moisture. Brown rice flavor ratings, on the other hand, are determined by protein, amylose, moisture, and

fatty acid content. The majority of fatty acids are found in the bran layer, which is removed during the milling process. Six sensory tests comprise a palpability evaluation criterion used to further evaluate table rice. Appearance, Aroma, Taste, Stickiness, Hardness, and Overall Evaluation are among them.
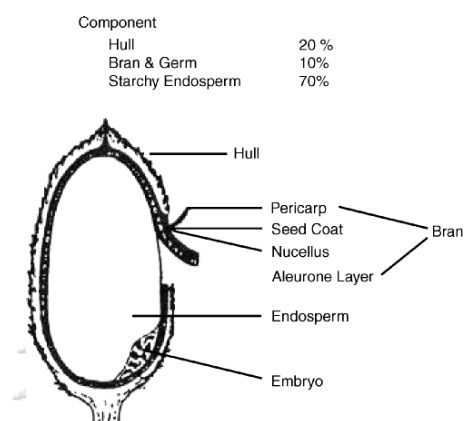
Figure 1 Structure of the mature rice grain **[10]**

Table 1 Range of Chemical and Physical Characteristics of Long, Medium and Short Gran Rice Types [11]

Characteristics	Long Grain	Medium Grain	Short Grain
Amylose (%)	23-26	15-20	18-20
Alkali spreading value	3-5	6-7	6-7
Gelatinization temperature (°C)	71-74	65-68	65-67
Gelatinization class	Intermediate	Low	Low
Water uptake (ml/100g)	121-136	300-340	310-360
Protein (%)	6-7.5	6-7	6-6.5
Parboiling stability, solid loss (%)	18-21	31-36	30-33

2.3 Rice Bran

Rice bran is an important byproduct of the rice processing industry. Rice bran (8-9 wt.% of the rice paddy) and rice germ (1-2%) are often removed during the milling process to get white rice, and the discarded by-products are commonly referred to as rice bran. Rice output now stands at 740 million tons. Rice milling removes rice hulls (164 million tons) and rice bran (59.2 million tons) throughout the rice producing process. As a result, the total amount of white rice produced is 411 million tons [12]. Rice bran is high in fiber, natural oil, and minerals such as vitamin E and γ-Oryzanol [13]. Rice bran is made up of fractions from the pericarp, aleurone, sub-aleurone layers, seed coat, nucellus, germ, or embryo, and a little amount of endosperm [14]. The physical and chemical properties of bran are affected by rice variety, grain treatment before to milling, milling type, degree of milling, and the fractionation method used before milling [15]. Rice bran is high in vitamin E, thiamin, niacin, aluminum, calcium, chlorine, iron, magnesium, manganese, phosphorus, potassium, silicon, sodium, and zinc [16]. Rice bran's relevance as a processed product is mostly due to its lipid content. Rice bran oil is gaining popularity due to its numerous health benefits [17].

2.4 Rice Bran Oil (RBO)

The oil produced from the hard outer brown coat of rice following chaff (rice husk) is known as RBO. Solvent extraction and hydraulic pressing or expeller pressing are the

two most prevalent processes for extracting oils from basic materials. Table 2 shows

the composition of crude rice bran oil (CRBO), whereas Table 3 specifies significant rice

bran oil features. Rice bran oil contains unsaturated fatty acids oleic acid (38.4%),

linoleic acid (34.4%), and linolenic acid (2.2%), as well as palmitic (21.5%) and stearic

acid (2.9%) [18]. 90% of the total fatty acids in rice bran oil are made up of three

primary fatty acids: palmitic, oleic, and linoleic. Rice bran is high in linoleic acid, which

is vital for human health [19].

Table 2 Composition of Crude Rice Bran Oil

Composition of CRBO	
Saponifiable Lipid	96%
Triacylglycerol	81-84%
Diacylglycerol	2-3%
Monoacylglycerol	1-2%
Free fatty acid	2-6%
Wax	3-4%
Glycolipids	0.8%
Phospholipids	1-2%
Unsaponifiable	4%

Table 3 Fatty acid composition for rice bran oil (% of total lipid)

Fatty acid	Rice Bran (%)
Palmitic acid (C 16:0)	21.5
Stearic acid (C 18:0)	2.9
Oleic acid (C 18:1)	38.4
Linoleic acid (C 18:2)	34.4
Linoleic acid (C 18:3)	2.2

2.5 Extraction of Rice Bran Oil

Rice bran oil is distinct among edible oils in that it has a high concentration of economically and nutritionally essential phytochemicals such as oryzanol, lecithin, tocopherols, and tocotrienols [20]. The extraction process begins with the processing of raw materials. Prior to extraction, rice bran is screened and then heated by steam at temperatures more than 100 °C to inhibit lipase hydrolysis. RBO is extracted from bran using a solvent (hexane) and a pressing method (screw press or hydraulic press). Rice bran oil must be refined once it has been extracted. This is due to the existence of extremely high levels of by-products such as gums, waxes, and free fatty acids in crude RBO. Crude RBO ranges in color from dark greenish brown to pale yellow, depending on the quality of the bran, extraction process, and bran composition.

2.6 Refining

There are two ways for refining rice bran oil: chemical and physical refining. The chemical refining process often includes processes such as degumming, neutralization, bleaching, and deodorization, whereas the physical refining process includes procedures identical to the chemical refining process except for the removal of free fatty acid. In chemical refining, free fatty acid is removed using alkali treatment (neutralization), but in physical refining, it is removed via steam distillation, similar to deodorization [21].

2.6.1 Chemical Refining

Degumming: This procedure is intended to remove phospholipids (gums) in crude oil, including hydratable and nonhydratable gums. Hydratable gums can be removed from oil by adding water or acid. This is known as water degumming or acid Degumming.

Deacidification or Neutralization: In this method, sodium hydroxide is used to remove free fatty acids and other impurities such as phosphatides, proteinaceous, and mucilaginous compounds. A slight excess of sodium hydroxide was combined with the heated oil at a temperature of 60-80 ℃ and the aqueous phase was allowed to settle. Soapstock is the aqueous phase that is separated from the neutral oil by washing with hot water, followed by settling or centrifugation. Despite the fact that the primary goal of the deacidification stage is to remove free fatty acid, the procedure also reduces phospholipid and coloring matter concentration [22].

Winterization or Dewaxing: This procedure is intended to remove waxes with high melting points from rice bran oil. Winterization is a procedure that uses temperature to manage crystallization and removes the wax from the oil by filtration to minimize clouding of the liquid fraction under colder temperature settings. The oil is heated to roughly 90 °C in a typical technique to eliminate any remaining nuclei. The oil is then cooled while stirring to roughly 20 °C and allowed to develop for at least 4 hours. Filtration in plate and frame filters to separates wax.

Bleaching: Bleaching of rice bran oil is more challenging than other vegetable oils because of the high chlorophyll and red pigment content, as well as the oxidized products of tocopherols and metallic salts of fatty acids. Bleaching rice bran oil is often done after the deacidification stage, utilizing adsorbents known as bleaching earths (Fuller's earth, acid activated monmorillonite clays, or activated carbon) to absorb coloring components. Gums, soaps, and certain oxidation products are adsorbed with the pigments during bleaching [23].

Deodorization: This step's goal is to eliminate volatile chemicals, primarily aldehydes and ketones. These chemicals have low detection thresholds by taste or smell. Deodorization is mainly a steam distillation process that takes place at temperatures ranging from 200 to 220 °C and pressures ranging from 6 to 10 mmHg. Unfortunately, this process also removed some of the natural oils' protectants, such as tocopherols and sterols. As a result, the addition of citric acid is frequently applied to chelate

residues of pro-oxidant metals, so lowering their activity that imparts to the oils, even at lower tocopherol level, thereby boosting oil stability [24].

2.6.2 Physical Refining
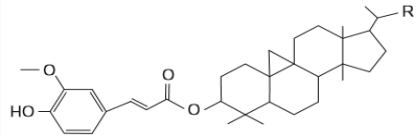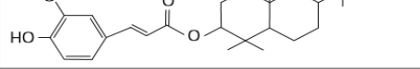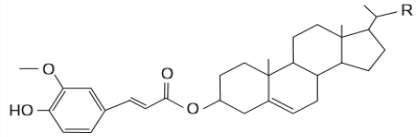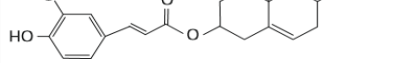
Except for the elimination of free fatty acids, the physical refining process is similar to that of chemical refining. Free fatty acid is removed by alkali treatment in chemical refining, while it is removed by steam distillation in physical refining, which is analogous to deodorization. The elimination of low volatility fatty acids (depending on length) in physical refining necessitates greater temperatures than those necessary for deodorization alone. A maximum temperature of 240-250 °C is enough to decrease free fatty acid concentration to 0.05-0.1 percent. Phosphatides must be eliminated to a level below 5 ppm (FAO) as tiny levels of phosphatides and iron are the most likely cause of heat darkening during distillation [25]. This level is easily attained during the deacidification process in chemical refining. However, in physical refining, a particular degumming procedure is required to obtain the above-mentioned phosphorus level. Prebleaching is required in addition to degumming to remove colored bodies and virtually all trace metals. When processing high free fatty acid products such as rice bran oil, the economics of deacidification by physical refining vs chemical refining often favor physical refining [26]. Furthermore, as compared to chemical refining, refined rice bran oil derived by physical refining can maintain the majority of the important component γ-oryzanol. [27].

2.7 γ-Oryzanol

γ-Oryzanol is a naturally occurring component in rice bran oil which consists of a mixture of ferulic acid esters of sterols and triterpene alcohols.

2.7.1 Structures of γ-Oryzanol

γ-Oryzanol was first recovered from rice bran oil by [28]. It was assumed to be a single compound at the time. Subsequent research reveals that γ-Oryzanol is not a single chemical, but rather a group of ferulic acid esters known as γ-Oryzanol. γ-Oryzanol has been the most thoroughly studied. γ-Oryzanol is a compound composed of two molecules [29]. The largest part is triterpene alcohols or plant sterols, and the other part is ferulic acid [30]. Among them, cycloartenol, ß-sitosterol, 24-methylenecycloartenol, and campesterol are the most abundant. Figure 2 depicts the *trans*-ferulate molecular structures of these four phytosterols.

Figure 2 Chemical structure of the four main components of gamma-oryzanol [31]

2.7.2 Phytochemical Constituent of **γ**-Oryzanol
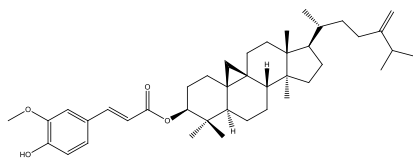
24-Methylenecycloartanyl ferulate (**1**)
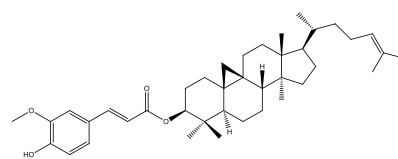
Cycloartenyl ferulate (**2**)
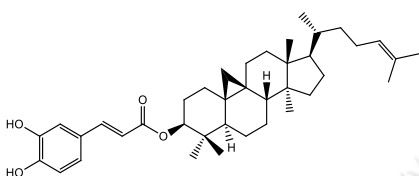
Cycloartenyl caffeate (**3**)
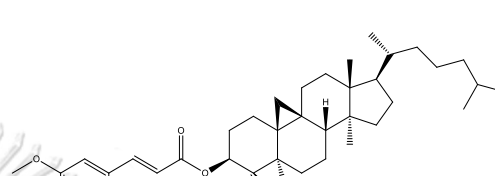
Cycloartanyl ferulate (**4**)
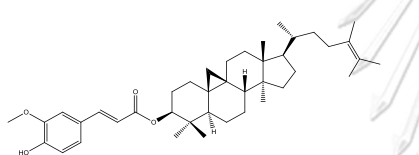
Cyclobranyl ferulate (**5**)
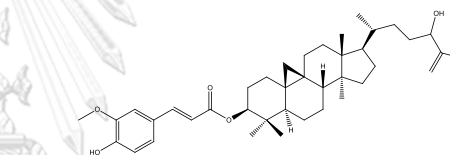
(24)-cycloart-25-ene-3*β*-24-diol-3*β*-*trans* ferulate (**6**)
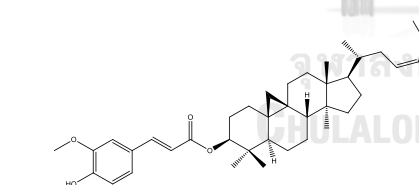
Cycloart-23-*Z*-ene-3*β*-25-diol-3*β*-*trans* ferulate (**7**)
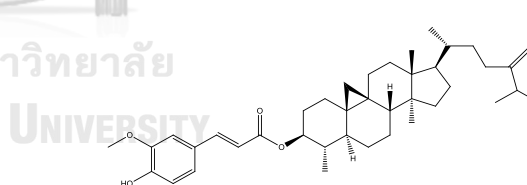
Cycloeucalenyl ferulate (**8**)
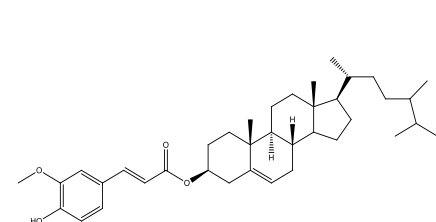
Campesteryl ferulate (**9**)
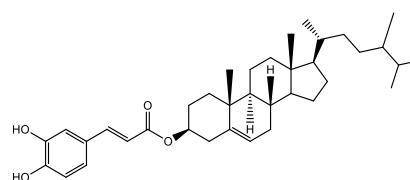
Campesteryl caffeate (**10**)
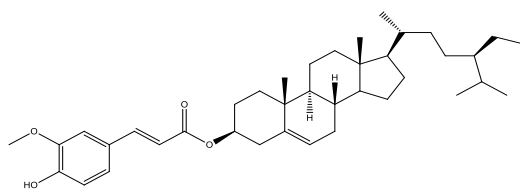
Sitosteryl ferulate (**11**)
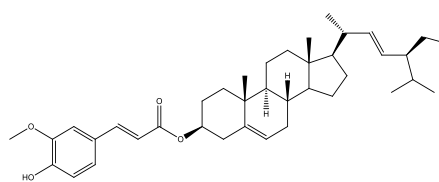
Stigmasteryl ferulate (**12**)
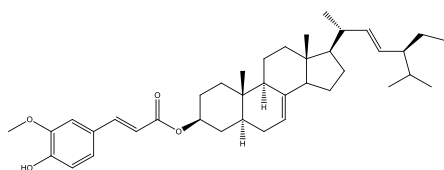
$\mathbf{\Delta}^7$-Stigmastenyl ferulate (**13**)
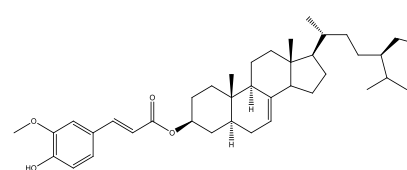
$\mathbf{\Delta}^7$-Sitostenyl ferulate (**14**)

$\mathbf{\Delta}^7$-Campestenyl ferulate (**15**)
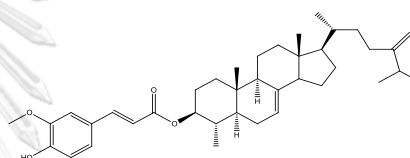
Gramisteryl ferulate (**16**)
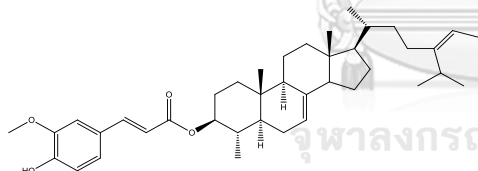
Citrostadienyl ferulate (**17**)
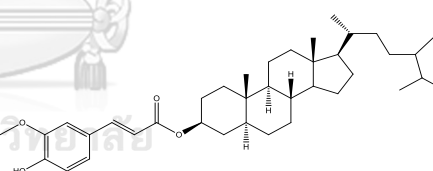
Campestanyl ferulate (**18**)
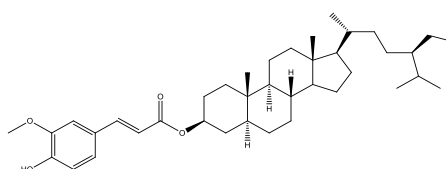
Sitostanyl ferulate (**19**)

Phytochemical constituents (**1-19**) from rice bran oil [32]

2.7.3 Properties of γ-Oryzanol

γ-Oryzanol ($C_{40}H_{58}O_4$) is an odorless white or slightly yellow crystalline powder that is stable at room temperature [33]. It has a melting point of 137.5-139.5 °C with absorption peaks in heptane at 231, 290, and 315 nm [18]. Although γ-oryzanol is insoluble in water, all its components include hydroxyl groups in the ferulate part, giving rise to a rather high polarity. As a result, it may be soluble in polar solvents like isopropanol and ethyl acetate, as well as nonpolar solvents like *n*-heptane and hexane [34].

2.7.4 Physiological and Biological Properties

Several studies over the last few decades have demonstrated the favorable physiological and biological benefits of γ-Oryzanol consumption. Because of the presence of the phenol moiety in its composition, the majority of biological research concerns the antioxidant activity of this γ-Oryzanol. Reactive oxygen species (ROS) are free radicals that, when overproduced in the body, can induce oxidative stress by oxidizing biological macromolecules such as proteins, nucleic acids, and cell membranes. Many chronic illnesses and cell aging are caused by oxidative damage. As a result, research into novel antioxidants has grown significantly in recent decades. [35]. In this respect, γ-Oryzanol has been thoroughly explored for its antioxidant qualities due to the presence of the ferulic/caffeic acid component, which facilitates electron donation and kills the action of free radicals [36].

Kim's research, for example, demonstrates that γ-Oryzanol inhibits pyrogallol autoxidation and is more efficient against hydroperoxide generation than well-known synthetic antioxidants (BHA, BHT, and TBHQ) [37]. Xu and Godber, on the other hand, were more interested in the antioxidant characteristics of the three primary γ-Oryzanol compounds (cycloartenyl ferulate, 24-methylenecycloartanyl, and campesteryl ferulate) using a linoleic acid-based per-oxidation model. Their findings suggested that these components can greatly minimize hydroperoxide formation [38]. The antioxidant properties of -oryzanol against cholesterol oxidation have also been studied [39]. Cholesterol oxidation products (COPs) produce a number of harmful atherogenic, mutagenic, and carcinogenic chemicals [40], which induce cell membrane damage and are linked to a variety of respiratory and cardiovascular disorders [41, 42]. It has been demonstrated that γ-Oryzanol may significantly inhibit COP formation, with a stronger impact than vitamin E [43]. It is worth noting that a strong link has been shown between oxidative stress and a variety of disorders, including cancer, diabetes, atherosclerosis, chronic inflammation, human immunodeficiency virus (HIV) infection, ischemia reperfusion damage, and sleep apnea [44]. Given this context, substantial research has been directed toward investigating the therapeutic effects of γ-Oryzanol against a variety of health issues and illnesses, employing a variety of models and tests.

2.7.4.1 Anti-ulcer effect

In Japan, the anti-ulcerogenic effects of γ-Oryzanol were intensively studied using rat models in the 1970s and 1980s. Nonetheless, further research is

required to determine its inhibitory impact and demonstrate its true therapeutic usefulness [32, 45]

2.7.4.2 Anti-inflammatory effect

Many studies have recently examined the ability of γ-Oryzanol to cure inflammation. In adjuvant-induced arthritis in rats, γ-Oryzanol (1-100 mg/kg) was observed to decrease the rise in swelling of the hind paw in a dose-dependent way. [46], as well as having a potent anti-inflammatory impact on sodium dextran sulfate-induced colitis [47] and ethanol-induced liver damage in mice via suppression of NF-B activity [48].

2.7.4.3 Anti-allergic effect

Oka and colleagues used the Bligh and Dyer technique to establish for the first time a probable anti-allergenic effect of γ-Oryzanol using a fraction derived from local Japanese rice. The scientists discovered a strong anti-allergic effect in rats using the passive cutaneous anaphylaxis (PCA) response paradigm, which was determined by inhibiting mast cell degranulation [49]. Furthermore, using the same methodology, they investigated the effect of major fraction components such as cycloartenyl ferulate (28.2%), 24-methylene cycloartanyl ferulate (22.4%), -Sitosteryl ferulate (12.3%), and Cyclobranyl ferulate (10%), and similar inhibition of mast cell degranulation was assisted with a higher potential for Cyclobranyl ferulate. Finally, they looked into the likely mechanism of action, hypothesizing that γ-Oryzanol can trap immunoglobulin E

(IgE), blocking it from cross-linking to the high-affinity IgE receptor (FcRI), which is implicated in allergic reactions.[50].

2.7.4.4 Anti-diabetic effect

Several studies have been carried out to investigate the possibility of γ-Oryzanol as a diabetic treatment. γ-Oryzanol was found to have an antidiabetic impact in many experiments, mostly on diabetic rats, enhancing insulin sensitivity and lowering blood glucose levels [51-53].

2.7.4.5 Anti-cancer effect

γ-Oryzanol and its constituents have been studied for anticancer potential. Yasukawa et al. discovered that the four principal components of γ-oryzanol (cycloartenyl ferulate, 24-methylene cycloartanyl ferulate, campesteryl ferulate, and Sitosteryl ferulate) had an inhibitory impact on tumor promotion in two-staged carcinogenesis in mouse skin [54]. Furthermore, Kim's latest research shows that γ-Oryzanol dramatically decreased tumor mass in mice injected with CT-26 colon cancer. Oral administration of 1% γ-oryzanol reduced tumor development by 44% in a dose-dependent manner without altering the weight of other organs [55]. Furthermore, utilizing F344 rat and B6C3F1 mouse lung carcinogenesis models, various research have been conducted to investigate the safety of γ-oryzanol's carcinogenic qualities. [56, 57]. γ-Oryzanol did have a tumor progression impact, although it was modest and only happened at large dosages [58, 59].

2.7.4.6 Anti-hyperlipidemic effect

γ-Oryzanol compounds have a structural similarity to cholesterol, another interesting study field is their capacity to reduce cholesterol levels. The first scientific investigation on this issue was conducted in people in 1970. Suzuki and Oshima in particular [60]. Within 7 days, total cholesterol (TC) was shown to be lower in the plasma of 50 healthy young women who consumed 60 g of a mixture of 70% RBO and 30% safflower oil [61]. γ-Oryzanol was studied in particular, and it was discovered that after four to eight treatments of 300 mg of this component per day in hyperlipoproteinemic subjects, there was a decrease in total cholesterol (TC), low density lipoprotein cholesterol (LDL-C), and triglyceride (TG) plasma levels, as well as an increase in high density lipoprotein cholesterol (HDL-C) concentration, with no side effects. Since then, similar findings in people have been published [62-64], rats, [65], rabbits, [66], and hamsters [67, 68]. This information is well reviewed by Cicero and Gaddi,151 with particular attention to the treatment of hyperlipoproteinemia's, indicat-ing that γ-oryzanol could be utilized as a therapeutic agent for hyperlipidemia and atherosclerosis [32, 69]

2.7.4.7 Effect on Menopause

Two studies in Japan looked at the influence of γ-oryzanol on menopausal symptoms. In the first study, conducted in the 1960s, 100 mg of γ-oryzanol was given three times a day for 38 days to 13 women who had undergone hysterectomy ("surgical menopause"). According to the data, 67% of the women

reported a substantial decrease in menopausal symptoms including hot flushes. [70].

In another study conducted in 1982, 40 women with climacteric disorders were given

300 mg of γ-oryzanol daily for 4-8 weeks. A general improvement in the decrease of

menopausal problems was reported in 90% of the patients. [71] Since then,

investigations on the effect of γ-oryzanol on menopausal problems have been

undertaken in comparison to other methods such as acupuncture. [72-74]

2.8 Computer Aided Drug Design

Drug design is both science and art, driven by the researcher's ingenuity and intuition.

Its goal is to produce concepts or theoretical models based on experimental data that

will drive research toward the identification of bioactive compounds with desired

features. Nowadays, the computational chemistry, molecular docking, and

cheminformatics methods give a variety of computational tools to aid in drug

discovery. [75].

The major difficulty of computer-aided drug design is to use these tools properly to

produce a usable result that corresponds to current demands in a fair amount of time.

Because structural information on the targets or related proteins was available,

structure-based computer-aided drug creation was mostly used in this study. The key

computational approaches used to achieve the specified aims were molecular docking,

binding free energy calculations, and virtual screening. These strategies are further

explained in depth. The visualization of molecular structures is a crucial aspect of computer-aided drug design.

2.8.1 Molecular Docking

Molecular docking is one of the most frequently used methods in structure-based drug design, due to its ability to predict the binding conformation of the small molecule ligands to the appropriate target binding site. Discovery and development of a new drug is generally known as a very complex process which takes a lot of time and resources. So computer aided drug design is used very widely to increase the efficiency of the discovery and development courses [76]. Molecular docking studies were performed using the default protocol in Autodock Vina in PyRx Software, The Scripps research institute, USA. The active site of the enzyme was set into a grid box. The protein ligand interactions were further analyzing using the Discovery Studio Visualizer (BIOVIA, San Diego, CA, USA)

2.9 Angiotensin Converting Enzyme (ACE2)

2.9.1 Discovery of ACE2

Following Tigerstedt and Bergman's key discovery of renin in 1898, the RAS has evolved into a complex network of enzymes, peptides, and receptors in Figure 3 [77, 78]. While many metallopeptidases cluster in tiny inter-related gene groups (for example, the neprilysin [NEP] family), around the turn of the century, no human homolog of the vasoactive zinc-peptidase ACE (angiotensin converting enzyme) had

been found. Almost simultaneously in 2000, two distinct methodologies looking for such ACE homologs discovered the presence of an ACE gene close cousin known as ACEH2 or ACE2 [79]. ACEH was cloned from a human cancer cDNA pool, whereas ACE2 was cloned from a human HF ventricular cDNA library, highlighting ACE2's possible relevance in cardiovascular diseases. The ACE2 gene was first shown to be expressed in the heart, kidney, and testis, but recent investigations have revealed a considerably broader distribution, including the upper airways, lungs, gut, and liver (Figure 4A. A comparison of the sequences of ACE and ACE2 indicated that ACE2, like ACE, was an integrated transmembrane protein (and ectoenzyme) with a transmembrane anchor near the C-terminus (type I membrane protein). The ACE and ACE2 genes have a strong evolutionary connection, and it was assumed that the two proteins would have comparable substrate specificities and participation in the RAS.

[80, 81].
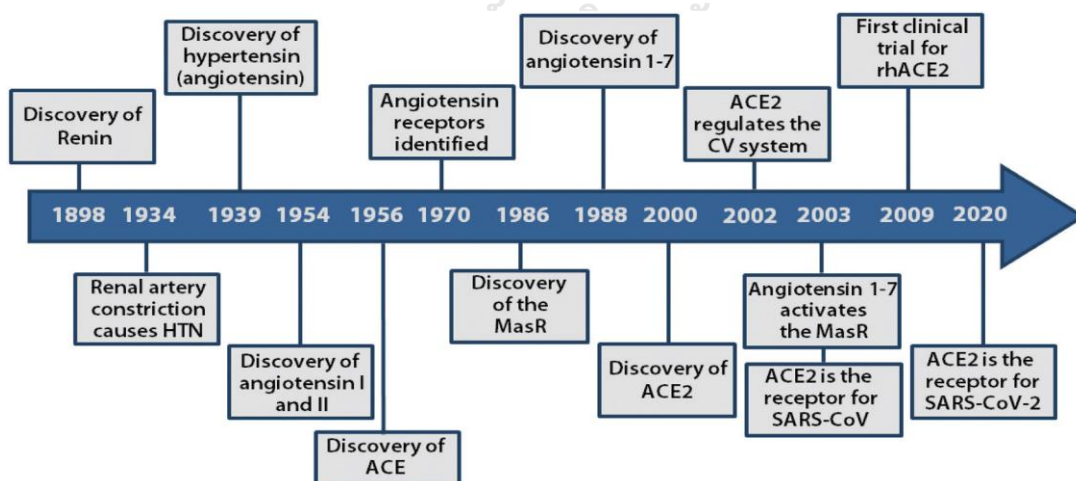
Figure 3 Historical timeline of discovery of the major renin-angiotensin system (RAS)
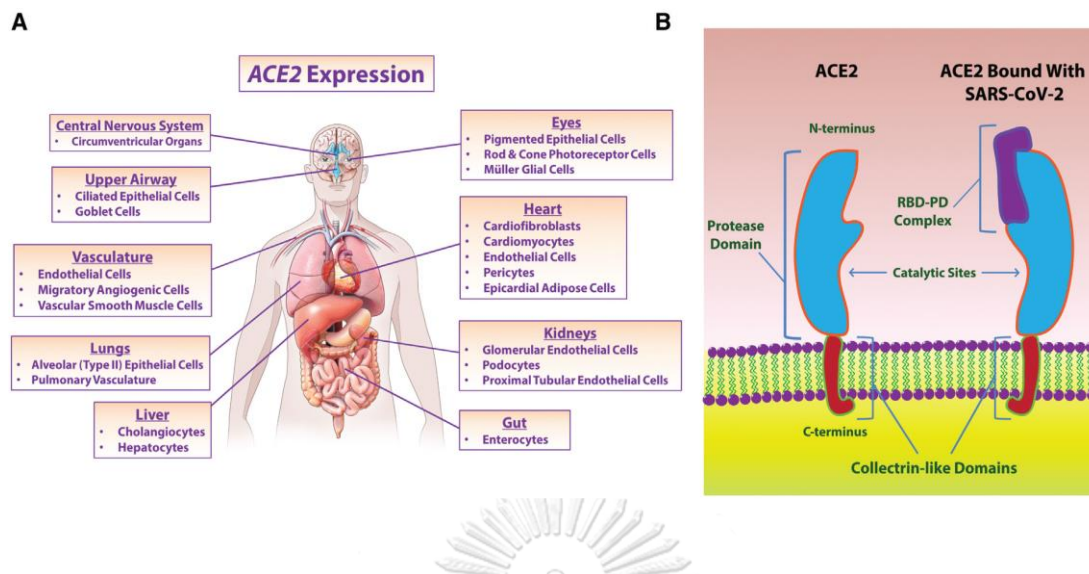
Figure 4 ACE2 (angiotensin-converting enzyme 2) expression throughout the body and schematic of ACE2 primary domain

2.9.2 The ACE2 Gene and Basic Biochemistry

Unlike the ACE gene, which is found on human chromosome 17, the 40kb ACE2 gene is found on chromosomal Xp22 and has 18 exons, the majority of which are similar to the ACE gene's exons. Unlike somatic ACE, which has two active sites, ACE2 only has one catalytic domain. Both ACE and ACE2 are zinc metallopeptidases, but their substrate specificities differ, establishing their different and opposing functions in the RAS. Whereas ACE (a peptidyl dipeptidase) cleaves C-terminal dipeptide residues from susceptible substrates, ACE2 is a simple carboxypeptidase capable of hydrolyzing Ang I to create Ang 1-9 and Ang II to form Ang 1-7 (FigURE 4B). ACE2 does not cleave bradykinin, further separating it from ACE, and it is likewise resistant to standard ACE inhibitors   [77, 81]. The C-terminal domain of ACE2, which bears no resemblance to ACE, is a homolog of collectrin, a renal protein

that controls the trafficking of amino acid transporters to the cell surface, endowing ACE2 with a variety of different physiological roles. The variety of physiological roles that ACE2 performs has allowed it to be hijacked as a receptor by SARS-CoV-2, culminating in the COVID-19 pandemic [82, 83]. Structures of the SARS-CoV and, more recently, the SARS-CoV-2 in combination with ACE2 have been identified by structural analyses (Figure 2.4B). The primary spike glycoprotein (S1) of SARS-CoV-2 interacts to the N-terminal region of ACE2. The cumulative knowledge of ACE2 biology and physiology over the last 20 years since its discovery should give a significant stimulant to understanding some of the essential processes in SARS-CoV-2 infection and eventual prevention [84, 85].

2.9.3 Role of ACE2 in Covid-19

On March 11, 2020, the World Health Organization proclaimed the SARS-CoV-2 epidemic a worldwide pandemic, citing community-scale transmissions on every continent except Antarctica. Since then, the outbreak has grown to well over a million cases and killed over 60 000 people globally by the beginning of April 2020. Prior to the emergence of SARS-CoV in 2002, coronaviruses were thought to be insignificant pathogens that circulated in nature among various host and intermediate species and occasionally infected humans, causing only mild upper respiratory tract infections and common cold symptoms [86-88]. As a result, in order to better comprehend the severity of SARS-CoV-2's global health implications and enhance therapy for infected patients, we must recognize the involvement of ACE2 in SARS-CoV-2 pathogenesis. In

addition to respiratory involvement, SARS-CoV-2 infections cause multiorgan dysfunction. [89-91]. While respiratory symptoms are predominant, acute cardiac and kidney injuries, arrhythmias, gut, and liver function abnormalities have all been documented in infected patients, suggesting myocardial, renal, enteric, and hepatic damage in COVID-19. Similarly, SARS-CoV also resulted in systemic manifestations with damage to the heart, gastrointestinal, liver, kidney, and other tissues [92, 93].
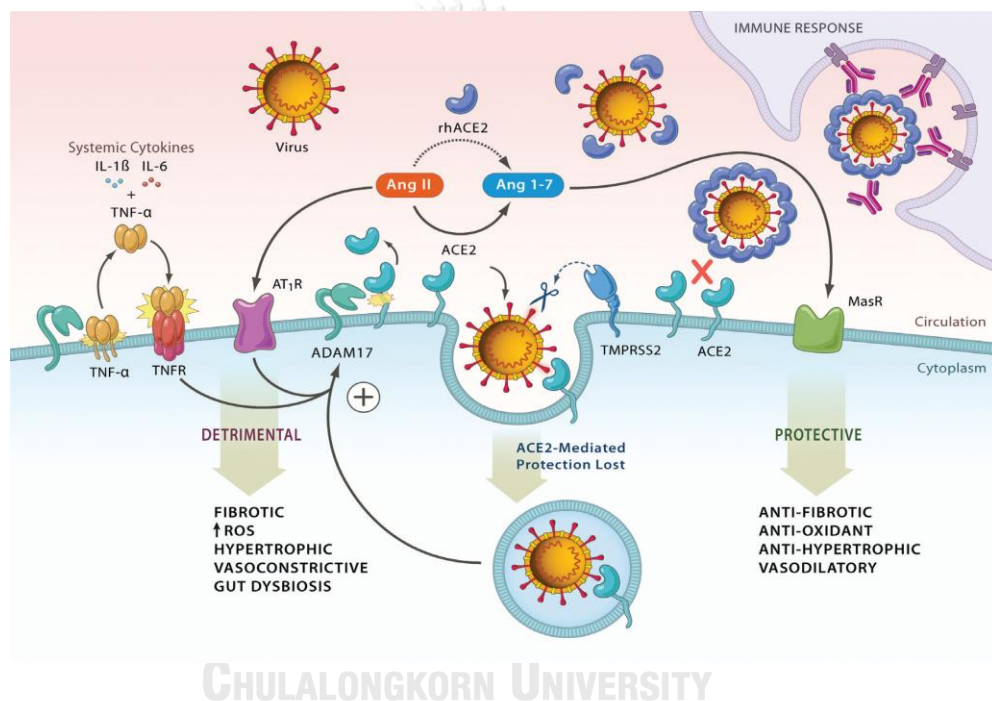
Figure 5 Role of ACE2 (angiotensin-converting enzyme 2) in the pathogenesis of coronavirus disease 2019 and the inflammatory response

2.9.4 Physiological Role of ACE2

The discovery of ACE2 led in a paradigm shift in all areas of the RAS. ACE2 is a mono-carboxypeptidase that converts Ang I to a nonapeptide (Ang 1-9), and Ang II to a heptapeptide (Ang 1-7). This unique enzymatic route for Ang I and Ang II degradation inhibits RAS activation and mitigates the detrimental effects mediated by Ang II and AT1R.1 This is especially important in pathological circumstances where the RAS is overstimulated. Ang 1-7 is a physiologically active peptide with actions that are diametrically opposed to those of Ang II [94-96]. Furthermore, ACE2 can inhibit ACE-independent Ang II production, such as from mast cell chymase [97, 98].
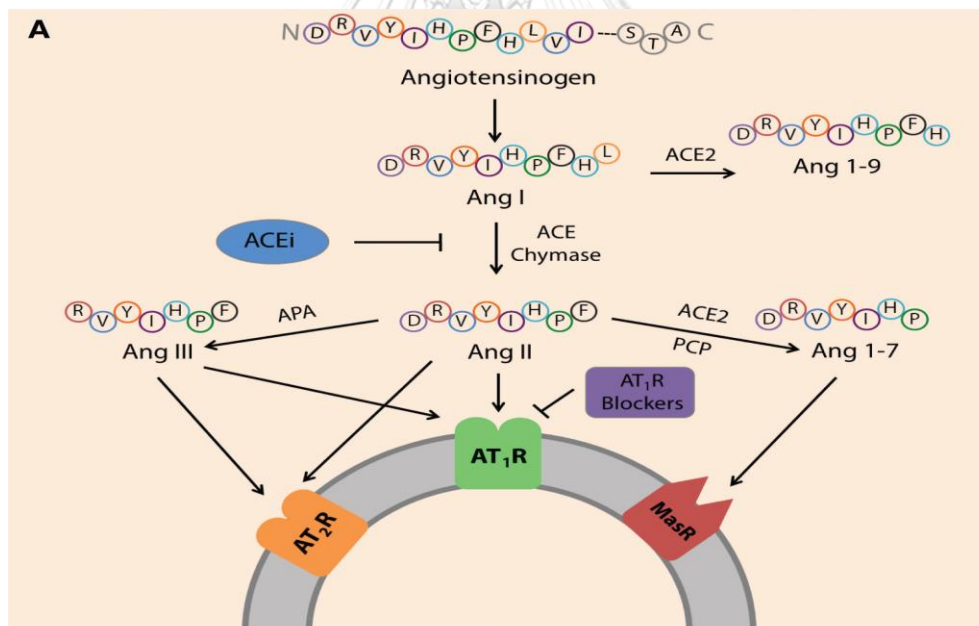
Figure 6 ACE2 (angiotensin-converting enzyme 2) role in the renin-angiotensin system peptide cascade and its interaction with the apelinergic peptide system

2.9.5 Targeting ACE2 for Therapeutics

The genesis and progression of CVD is driven by pathological neurohormonal activation of the RAS. Current pharmacotherapies try to suppress RAS at many levels using different mechanisms of action. Although ACE2 is not a direct biological target of these medicines, the RAS's complicated nature affects Ace2 gene transcription, translation, and, eventually, catalytic activity. Blocking the ACE/Ang II/AT1R axis by reducing Ang II production and activities enhances the effects of ACE2 as an endogenous RAS counter-regulator. The ARBS significantly enhanced Ace2 mRNA expression, protein levels, and catalytic activities in the heart, kidneys, and thoracic aorta, however the translation to protein levels and activity for ACE inhibitors varies between experimental models and tissues [99-103]. The combination of lisinopril and losartan therapy in normotensive Lewis rats reversed the individual increase in Ace2 mRNA levels but preserved the losartan-induced increase in ACE2 activity in the heart. Furthermore, lisinopril enhanced Ace2 mRNA in normotensive Lewis rats without changing ACE2 activity in the heart, whereas the converse was found in the kidneys [101]. These findings might be related to tissue-specific control of ACE2, since greater ACE2 protein levels were observed in the heart, while ACE2 activity was higher in the kidneys of Sprague-Dawley rats, adding to the intricacy of the tissue RAS [104]. Dual RAS inhibition with perindopril and losartan corrected disease-mediated reductions in kidney ACE2 mRNA expression and protein levels in type 1 diabetic Akita angiotensinogen-transgenic mice [105] These findings imply that Ang II buildup in diseased situations contributes to the modulatory

effects of RAS inhibition on ACE2. Ang II can influence ACE2 expression via the AT1R.

High levels of ACE2 mRNA and protein expression are seen in healthy hearts and

kidneys, while ACE1 expression is low [106]. RAS activity in CVD promotes Ang II AT1R

stimulation, increasing ERK1/2 and p38 MAPK signaling pathways to downregulate ACE2

while upregulating ACE expression. Activation of the p38 MAPK increases ADAM17

activity by posttranslational phosphorylation of the cytoplasmic domain, which leads

in shedding of surface ACE2 in a positive feedback loop, which might explain the

reported effects of ARBs on boosting ACE2 protein levels and activity [107, 108].

Table 4 Pharmacological regulation of the RAS and their effects on RAS components,

ACE2 gene expression, protein levels, and cellular activity [109].

Pharmacological Agent	Experimental Model/Subject	Tissues	Observation
ACE inhibitors			
Lisinopril	Lewis rats	Heart	Decrease in plasma Ang II, increase in plasma Ang 1–7 and ACE2 mRNA, but not cardiac ACE2 activity[179]
Enalapril	Coronary artery ligation in Sprague Dawley rats	Heart	Increased plasma and cardiac ACE2 activity, and cardiac *Ace2* mRNA levels 8 wk post-surgery[183]
Lisinopril	Transgenic Ren2 rats	Heart/Kidney	Decrease in plasma Ang II, increase in plasma Ang 1—7, cardiac and renal ACE2 mRNA and activity[182]

Lisinopril	Lewis rats	Kidney	No change in kidney ACE2 mRNA but increased ACE2 activity[180]
Angiotensin receptor blockers			
Losartan/ Olmesartan	Coronary artery ligation in Lewis rats	Heart	Increase in plasma Ang II, Ang 1–7 and ACE2 mRNA 28 days post surgery[178]
Losartan	Lewis rats	Heart	Increase in plasma Ang II, Ang 1–7 levels, ACE2 mRNA and cardiac ACE2 activity[179]
Irbesartan	C57BL/6 mice	Heart	Increase in cardiac ACE2 mRNA, Irbesartan prevented Ang II-induced decrease in ACE2 protein levels[77]
Losartan	Transgenic Ren2 rats	Heart/ Kidney	Increase in plasma Ang II, Ang 1—7, cardiac and renal ACE2 mRNA and activity[182]
Telmisartan	C57BLKS/J mice	Kidney	Following 2 wk administration, increased ACE2 protein levels, and ACE2 mRNA expression[184]
Irbesartan	C57BL/6 mice	Aorta	Treatment with irbesartan significantly augmented ACE2 protein levels and ACE2 mRNA expression[185]
Olmesartan	Spontaneously hypertensive rats	Aorta	Increased plasma Ang II and Ang 1–7 levels, ACE2 mRNA expression and ACE2 protein levels[181]
Mineralocorticoid receptor blockers			
Spironolactone	Patients with heart failure	Monocyte-derived macrop	Increase in ACE2 activity and ACE2 mRNA expression 1-month post-therapy[188]

		hage	
Eplerenone	Balb/C mice	Heart/ Kidney	Increase in cardiac ACE2 activity and ACE2 mRNA expression but nonsignificant increase in the kidneys[188]
Eplerenone	Wistar rats	Heart	Prevented aldosterone induced reduction in cardiac *Ace2* mRNA expression[189]
Eplerenone	Dahl salt–sensitive hypertensive rats	Heart	No effect on cardiac ACE2 mRNA expression and protein levels observed in DS rats[190]

จุฬาลงกรณ์มหาวิทยาลัย
CHULALONGKORN UNIVERSITY

CHAPTER III EXPERIMENTAL

3.1 *In silico* Approach (ACE2 Inhibition Assay)

3.1.1 Ligand Preparation

In silico approaches aims to investigate the binding affinity of the bioactive
phytochemicals from the *γ-Oryzanol* to the ACE2 enzyme. The 2D structure of the
nineteen bioactive phytochemicals were downloaded from PubChem website
(https://pubchem.ncbi.nlm.nih.gov/) in SDF file and by using Open babel software to
convert all the ligands into PDB format. The structures were optimized by semi-
empirical AM1 method using the PyRx software and then converted files for all
compounds to PDBQT format for docking investigations.

3.1.2 Protein Preparation

The crystal structures of the target proteins were downloaded from the PDB
(www.pdb.org). The protein structures were refined by deleting the existing ligand using
Autodock software and were used to prepare the PDBQT file by adding polar hydrogens
and partial charges to the protein molecule. PDB codes 1R42 were used for the crystal
structures of ACE2.

3.1.3 Drug-Likeness Prediction

The structures of bioactive phytochemicals in the rice bran acid fraction (RBAF) were
obtained from PubChem database as SMILE files. SwissADME
(http://www.swissadme.ch/) was used to evaluate drug-likeness according to the

Lipinski's rule of five to predict their pharmacokinetic distinctive features such as the Absorption, Distribution, Metabolism, and Excretion (ADME).

3.2 Rice Bran Acid Fraction

Rice bran acid fraction (RBAF) was obtained from the Thai Edible Oil Co. Ltd., Samutprakarn, Thailand.

3.3 General Experimental Procedures

3.3.1 Thin-Layer Chromatography (TLC)

TLC analysis using Silicycle's aluminium sheet (Merck) coated with 0.2 mm silica gel 60 F254, 20 × 20 cm was used to monitor the separation processes. The TLC reverse phase analysis was performed on Merck's aluminium sheets coated with silica gel 60 RP-18 F254s. TLC was visualized under UV light at wavelengths of 254 and 365 nm and by staining with *p*-anisaldehyde and ferric chloride in methanol (1% ferric chloride in 50% methanol).

3.3.2 Column Chromatography

Column chromatography (CC) was performed using Silica gel 60H (Merck code No. 7734 and No. 9385) as packing materials. Reverse-phase C18 (RP-18) 17 chromatography was performed using Silica gel C-18 (Wako code No. 237-01555) as packing materials.

3.3.3 Nuclear Magnetic Resonance Spectroscopy (NMR)

The NMR spectra were recorded on a JEOL (500 MHz for ^{1}H NMR, and ^{13}C NMR) using tetramethylsilane (TMS) as an internal standard. The chemical shifts (δ) were reported in parts per million (ppm) and the coupling constants (J) in Hertz (Hz). Mestrelab Research – MestReNova NMR software version 14.1.1-24571 was used to analyze the spectral data. Chloroform-d (CDCl$_3$) were used in NMR experiments and chemical shifts were referenced to the signals of the residual solvent for CDCl$_3$ at δH 7.26 ppm.

3.3.4 Microplate Spectrophotometer

UV data of chromogenic methods were obtained from Power Wave XS2 (Biotek Instruments Inc, USA) microplate reader.

3.4 Chemicals

All commercial-grade solvents used in the present study, such as methanol (MeOH), ethyl acetate (EtOAc), and *n*-hexane, were distilled prior to use. The reagent grade (AR) and HPLC grade solvents were purchased from Sigma-Aldrich, Burdick & Jackson, and Merck® (Germany) used for thin layer chromatography, crystallization and HPLC experiments.

3.5 *In vitro* ACE2 Inhibition assay

The catalytic activity of ACE2 was monitored using the substrate Mca-APK(Dnp), in which Mca fluorescence is quenched by Dnp until cleavage at Pro-Lys separates them. Fluorescence intensity was measured in black 96-well at 320 nm excitation

and 405 nm emission, with shaking using a microplate reader (EnSight, PerkinElmer, Inc, USA). The assay buffer used in the ACE2 activity assay had 0.05 M 2-morpholino ethane-sulfonic acid (MES), 0.3 M NaCl, and 10 μM ZnCl$_2$, pH 6.8. it was stored at 4 °C when not in use. The ACE2 enzyme, the Mca- APK(Dnp) substrate, and DX600 (sigma Aldrich, Supelco, Singapore) were diluted in the assay buffer. The γ-oryzanol were first dissolved in 1.0% tween80 and a concentration of 2mg/ml as stock solutions. For inhibition, assays consisted of 40 μl of the enzyme solution (100 U/ml final concentration), 40 μl of the Mca-APK(Dnp) substrate (4.5 μM final concentration), and 20 μl sample (50-0.01 μg/ml final concentration). Background controls consisted of 20 μl of the sample, 40 μl of the Mca-APK(Dnp) substrate, and 40 μl assay buffer. Background substrate controls 40 μl of assay buffer with 60 μl of the substrate. ACE2 activity consisted of 40 μl of the enzyme solution, 40 μl of the Mca-APK(Dnp) substrate, 20 μl assay buffer. The mixture was incubated at 37 °C for 16 min, and the fluorescence. Inhibitors were included in background control samples. The inhibition (%) was calculated by comparing the fluorescence with the maximum fluorescence as

$$\%ACE2 \text{ activity} = [(A\text{-}B) / (C\text{-}D)] \times 100$$

where A is the fluorescence in the presence of the inhibitor, B is the background control (inhibitor and substrate) fluorescence, C is the ACE2 activity fluorescence

(ACE2 + substrate), D is the background substrate control fluorescence (only substrate) [110].

3.6 Isolation of Rice Bran Acid Fraction

The rice bran acid fraction (53 g) was chromatographed to CC over silica gel 60 with gradient n-hexane, n-hexane: EtOAc (20:1, 15:1, 10:1, and 5:1) and EtOAc. The mobile phase 15:1 n-hexane: EtOAc to give fractions 1-10 and mobile phase 10:1 n-hexane: EtOAc to give fractions 1-16. The **γ**-oryzanol in fractions 7 to 8 from eluting with 15:1 n-hexane: EtOAc and fractions 11-13 and 14-16 eluting with 10:1 n-hexane: EtOAc was monitored by TLC analysis and those fractions were combined. After evaporation of the solvent, the residue was diluted in ethyl acetate and formed a solid and liquid phase. The precipitated solids were filtered through filter paper and purity of **γ**-oryzanol of the precipitation product was analyzed by TLC and ^{1}H NMR of metabolites **1-3**.

CHAPTER IV RESULTS AND DISCUSSION

4.1 *In silico* Approach (ACE2 Inhibition Assay)

4.1.1 *In Silico* Study of Phytochemicals of **γ**-Oryzanol as ACE2 Inhibitors

The crystal structure of ACE2 (PDB ID: 1R42) native human angiotensin converting enzyme-related carboxypeptidase was obtained from RCSB Protein Data Bank. The protein was prepared for docking studies by removing water molecules and the native ligand to provide stable conformation.
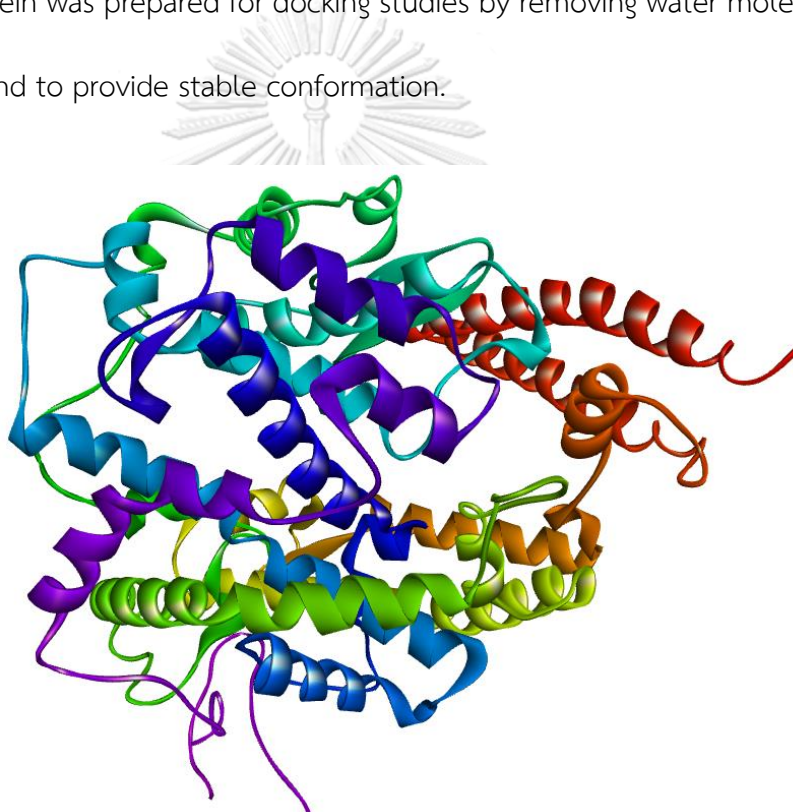
Figure 7 Structure of 1R42 protein

Chain A is the proposed active site pocket, and the ligands docked make polar contact with the amino acid residues. The calculated binding energy is presented in Table 1 below.

Table 5 Calculated free binding energy (kcal/mol) of the phytochemicals (**1-19**) from rice bran oil against ACE2 (PDB ID: 1R42)

Phytochemicals	Binding energy (kcal/mol)	Phytochemicals	Binding energy (kcal/mol)
Δ^7-Stigmastenyl ferulate (**1**)	-10.2	24-Methylenecycloartanyl ferulate (**11**)	-9.3
Cycloart-23-*Z*-ene-3β-25-diol-3β-*trans* ferulate (**2**)	-9.9	Cycloeucalenyl ferulate (**12**)	-9.3
Cyclobranyl ferulate (**3**)	-9.8	Campesteryl ferulate (**13**)	-9.3
Cycloartenyl ferulate (**4**)	-9.7	Δ^7-Campestenyl ferulate (**14**)	-9.0
Cycloartanyl ferulate (**5**)	-9.5	Stigmasteryl ferulate (**15**)	-9
Gramisteryl ferulate (**6**)	-9.5	Cycloartenyl caffeate (**16**)	-8.9
(24)-cycloart-25-ene-3β-24-diol-3β-*trans* ferulate (**7**)	-9.4	Sitostanyl ferulate (**17**)	-8.8
Citrostadienyl ferulate (**8**)	-9.4	Sitosteryl ferulate (**18**)	-8.7
Campesteryl caffeate (**9**)	-9.4	Δ^7-Sitostenyl ferulate (**19**)	-8.5
Campestanyl ferulate (**10**)	-9.4		

All 19 phytochemicals of **γ**-oryzanol exhibited a high binding score against ACE2 enzyme. For three major phytochemicals of **γ**-oryzanol, 24-methylenecycloartanyl ferulate, campesteryl ferulate, and cycloartenyl ferulate showed -9.3, -9.3, and -9.7

kcal/mol, respectively. The minor phytochemical of **γ**-oryzanol, **Δ**^{7}-Stigmastenyl ferulate (**1**), and cycloart-23-Z-ene-3**β**, 25-diol-3**β**-trans ferulate showed the highest binding score with -10.2 and -9.9 kcal/mol, respectively but the LD_{50} value of both compounds (Table 8) was 1000 mg/kg belonging to the toxicity class 4 level, which was extremely hazardous and ingested. The 3D structures of the 19 compounds from **γ**-oryzanol (**1-19**) in the active site of ACE2 (PDB ID: 1R42) were shown in Fig 8.

Δ7-Campestenyl ferulate

Δ7-Sitostenyl ferulate

Δ7-Stigmastenyl ferulate

24-Methylenecycloartanyl ferulate
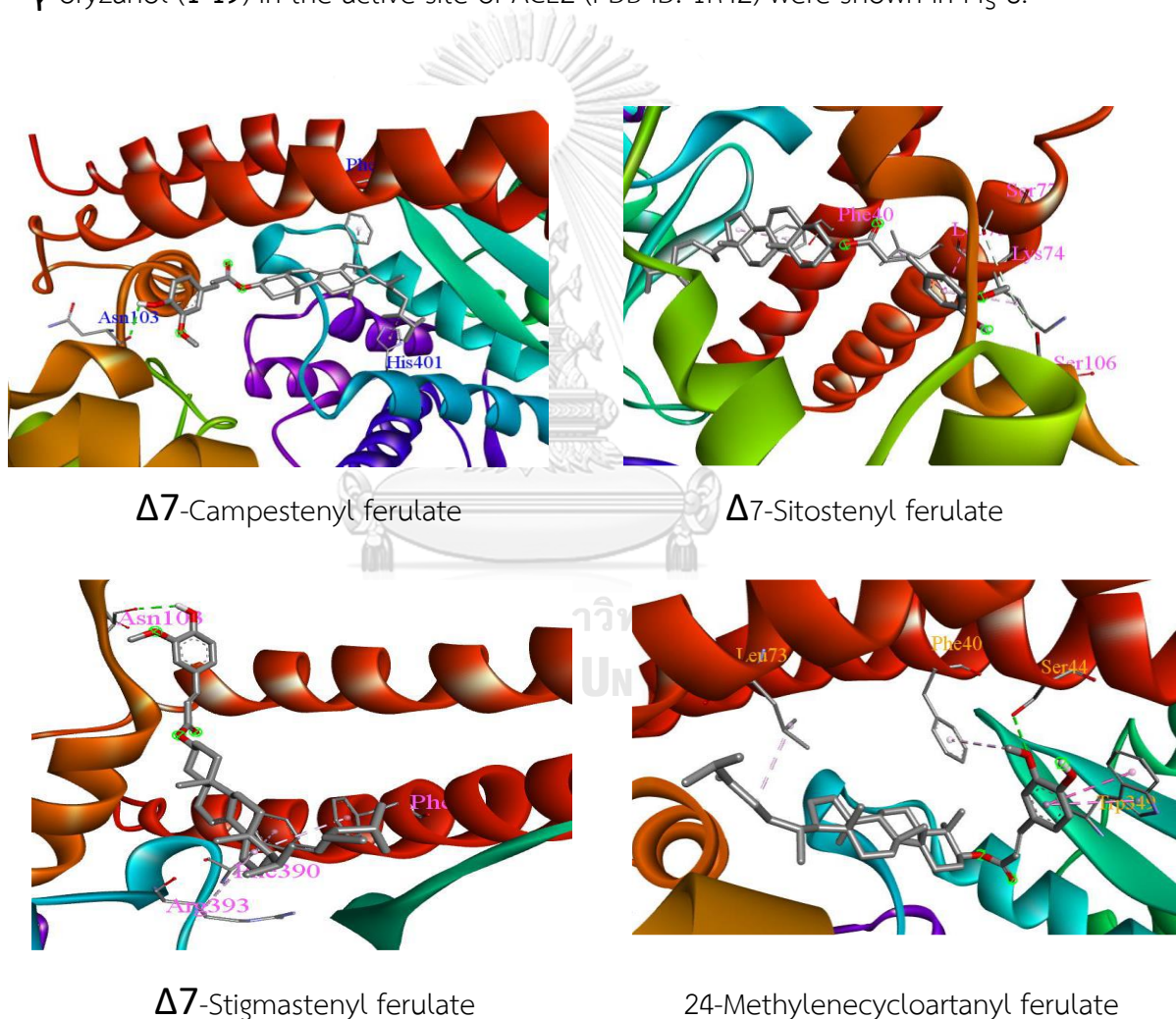
Figure 8 3D structure of 19 **γ**-Oryzanol bound into the active site of ACE2 (PDB ID: 1R42)
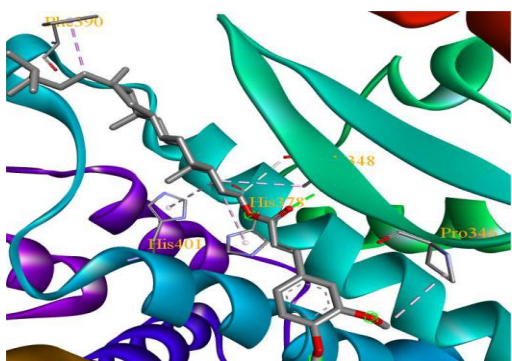
Campestanyl ferulate
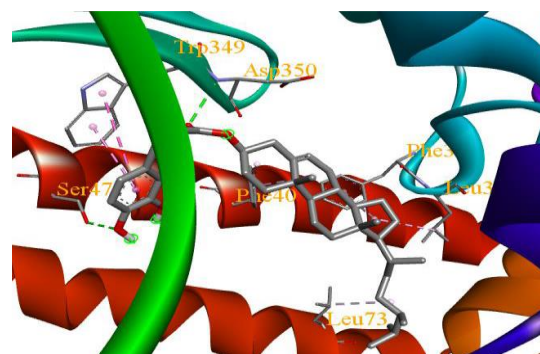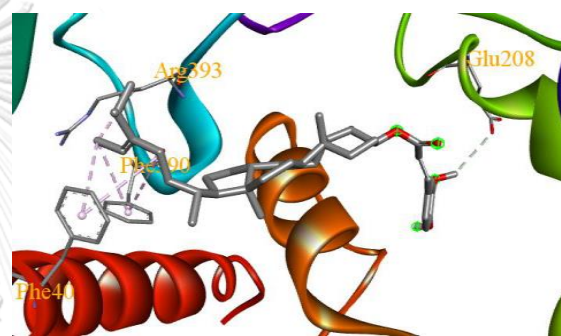
Campesteryl caffeate

Campesteryl ferulate

Citrostadienyl ferulate
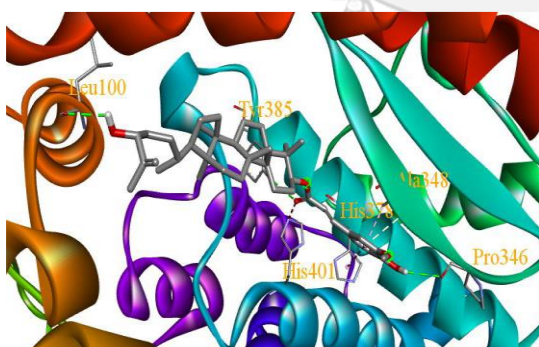
Cycloart-23-Z-ene-3β-25-diol-3β-*trans* ferulate
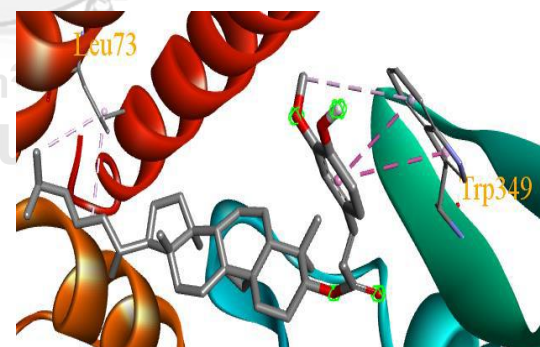
Cycloartanyl ferulate
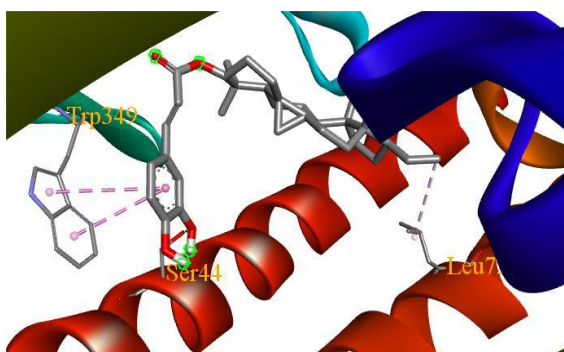
Figure 8 (Continue)

Cycloartenyl caffeate
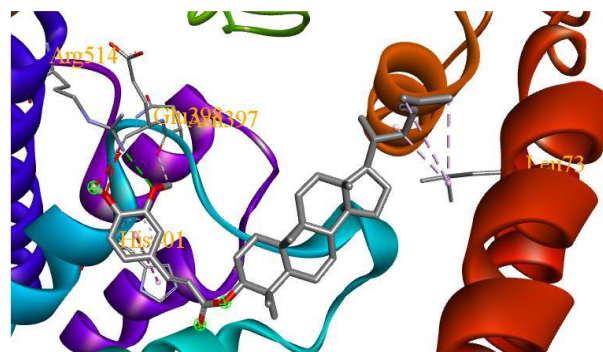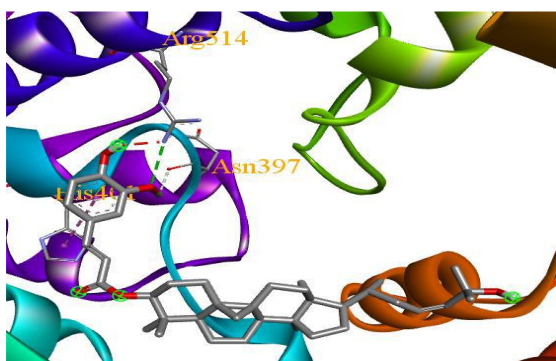
Cycloartenyl ferulate

(24)-cycloart-25-ene-3β-24-diol-3β-*trans* ferulate
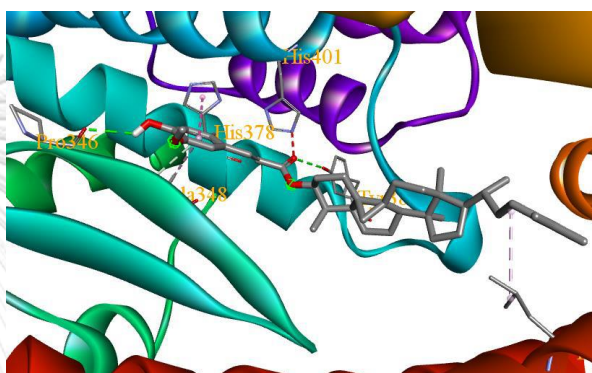
Cyclobranyl ferulate
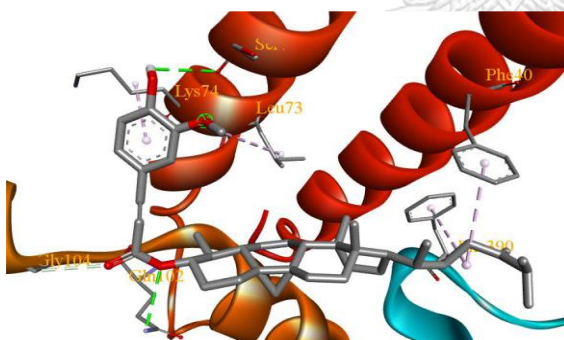
Cycloeucalenyl ferulate
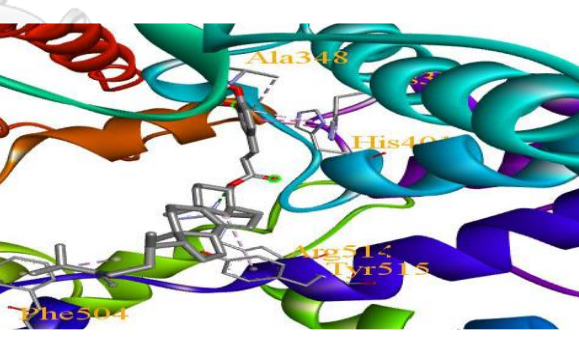
Gramisteryl ferulate

Figure 8 (Continue)
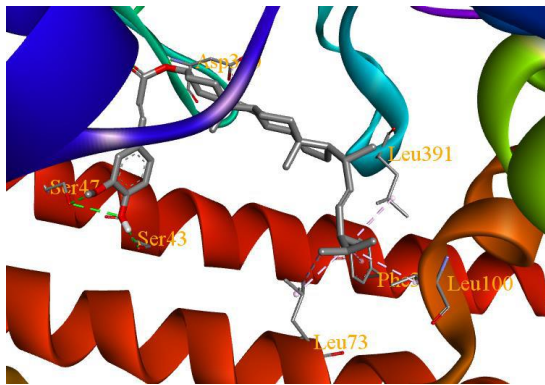
Sitosteryl ferulate
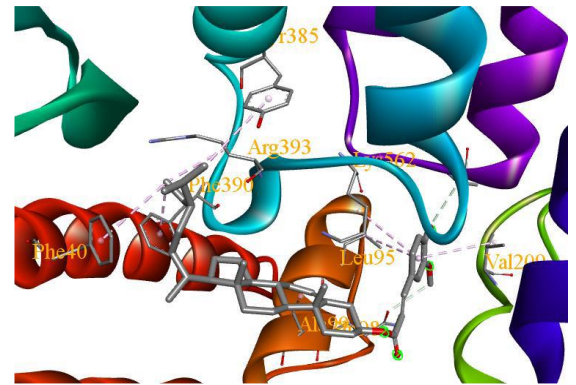
Sitostanyl ferulate
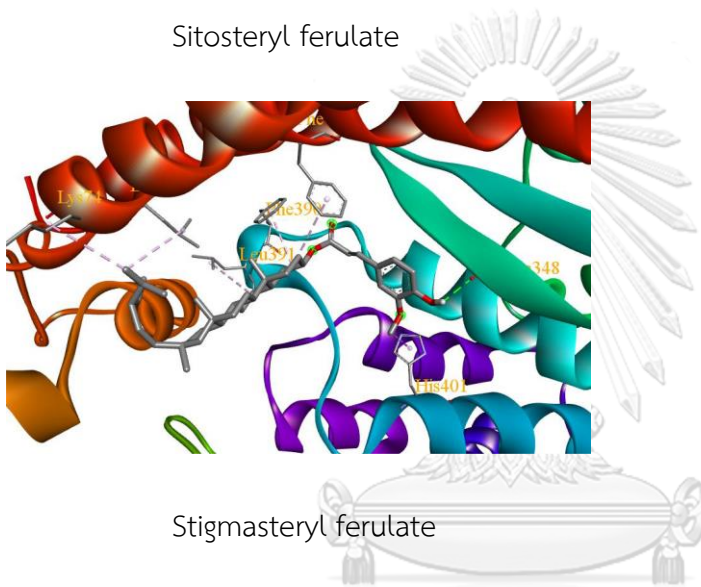
Stigmasteryl ferulate

Figure 8 3D representation of the phytochemicals from gamma-oryzanol in the active site of ACE2 (PDB ID: 1R42)

Figure 9 3D molecular amino acid interactions of the phytochemicals of gamma-oryzanol in the binding site of ACE2 (PDB ID: 1R42)
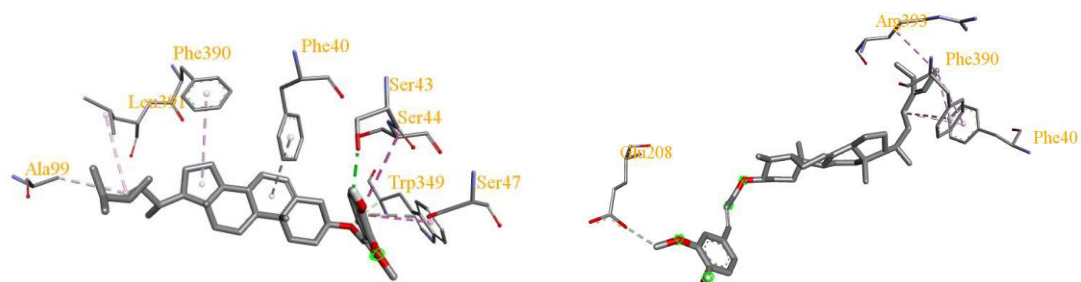
(24)-cycloart-25-ene-3β-24-diol-3β-*trans* ferulate

Δ7-Sitostenyl ferulate

Δ7-Stigmastenyl ferulate

24-Methylenecycloartanyl ferulate

Campestanyl ferulate

Campesteryl caffeate

Figure 9 (Continue)

Campesteryl ferulate
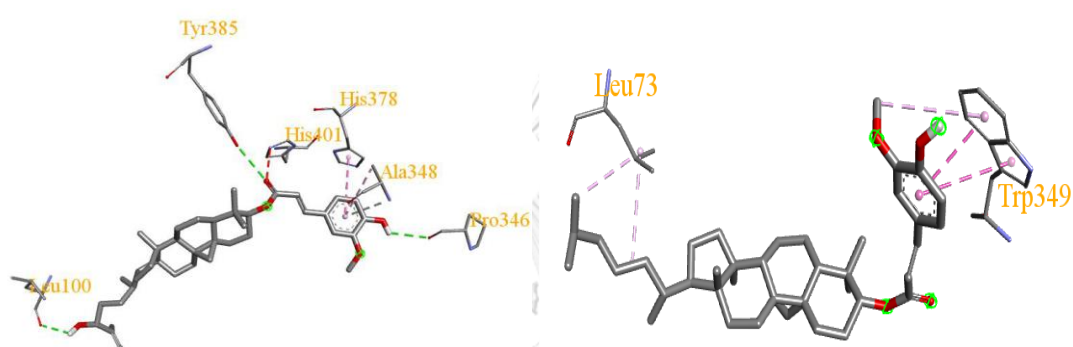
Citrostadienyl ferulate

Cycloart-23-*Z*-ene-3β-25-diol-3β-*trans* ferulate

Cycloartanyl ferulate
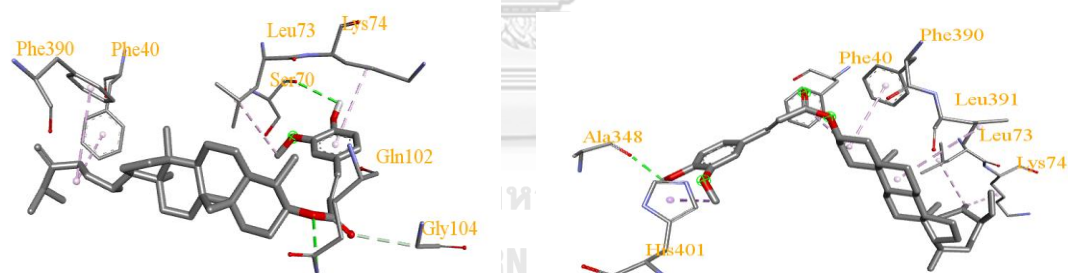
Cycloartenyl caffeate

Cyclobranyl ferulate
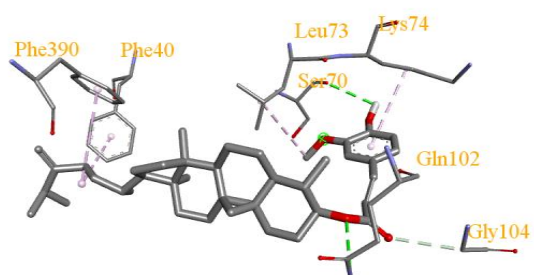
Figure 9 (Continue)

Cycloeucalenyl ferulate
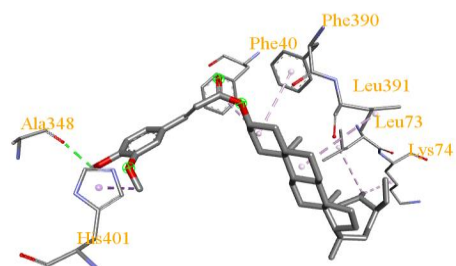
Sitostanyl ferulate
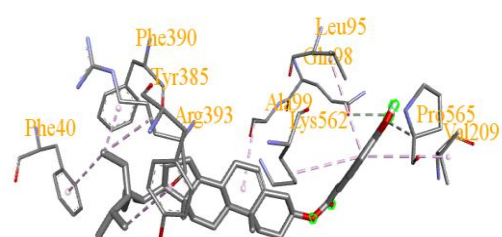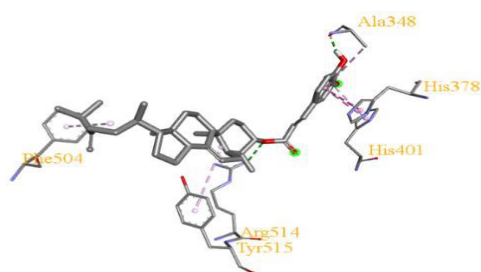
Sitosteryl ferulate

Stigmasteryl ferulate

Gramisteryl ferulate

Δ7-Campestenyl ferulate

Cycloartenyl ferulate

Figure 9 (Continue)

Δ7-Campestenyl ferulate   Δ7-Sitostenyl ferulate

Δ7-Stigmastenyl ferulate   24-Methylenecycloartanyl ferulate
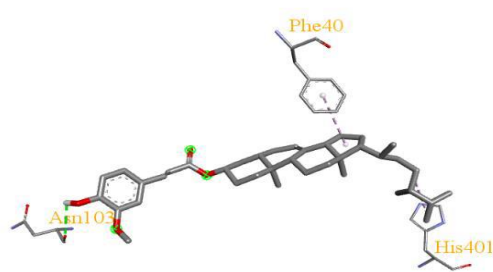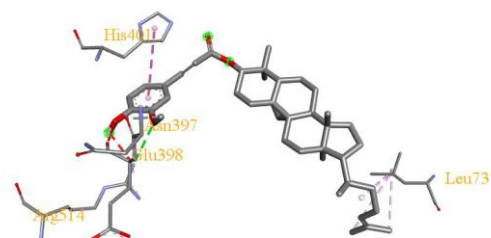
Campestanyl ferulate   Campesteryl caffeate
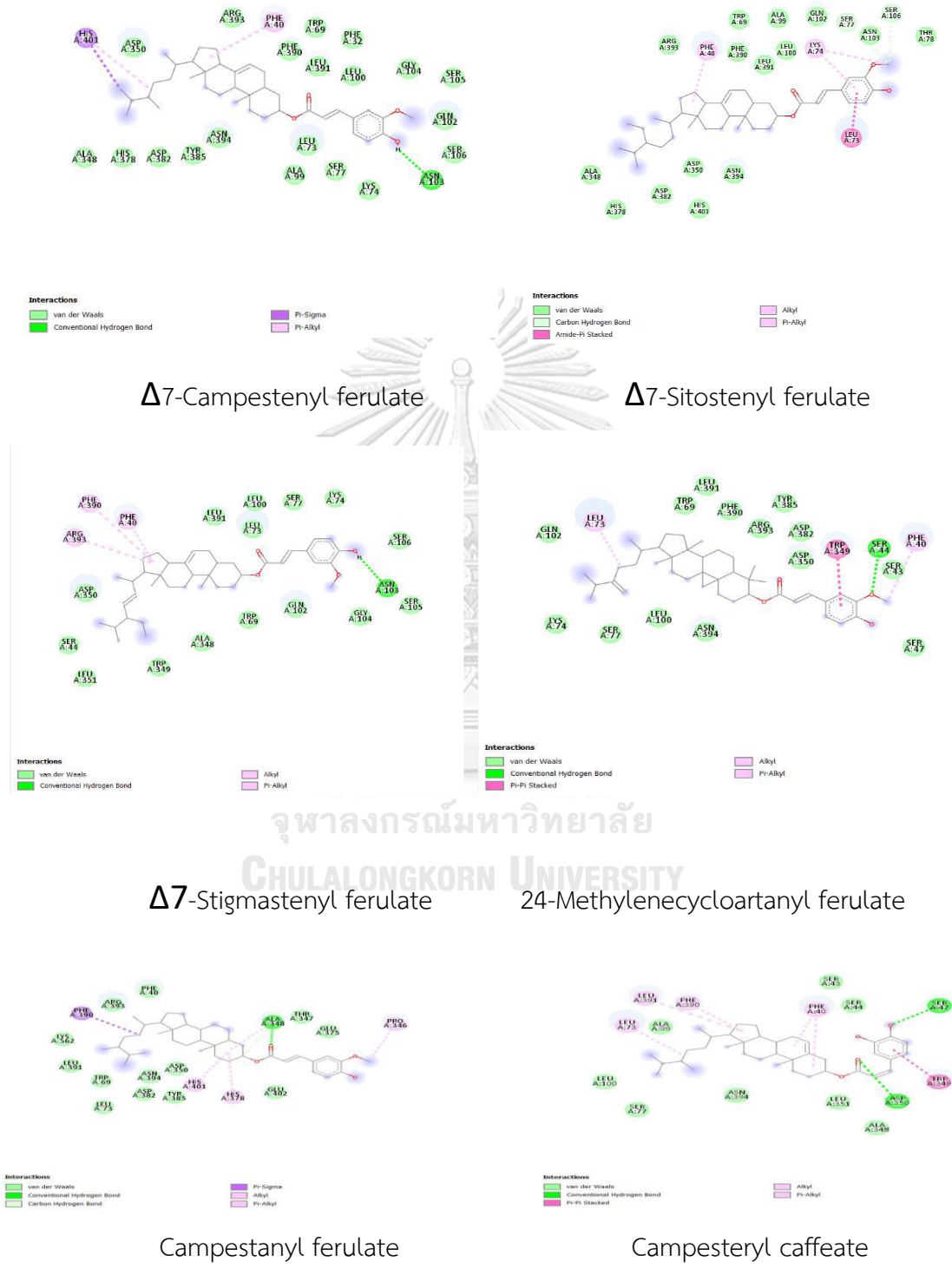
Figure 10 Depicted the amino acid residual and its interaction types.

Campesteryl ferulate

Citrostadienyl ferulate

Cycloart-23-*Z*-ene-3β-25-diol-3β-*trans* ferulate

Cycloartanyl ferulate

Cycloartenyl caffeate

Cycloartenyl ferulate

Figure 10 (Continue)

(24)-cycloart-25-ene-3β-24-diol-3β-*trans* ferulate

Cyclobranyl ferulate

Cycloeucalenyl ferulate

Gramisteryl ferulate

Sitostanyl ferulate

Sitosteryl ferulate
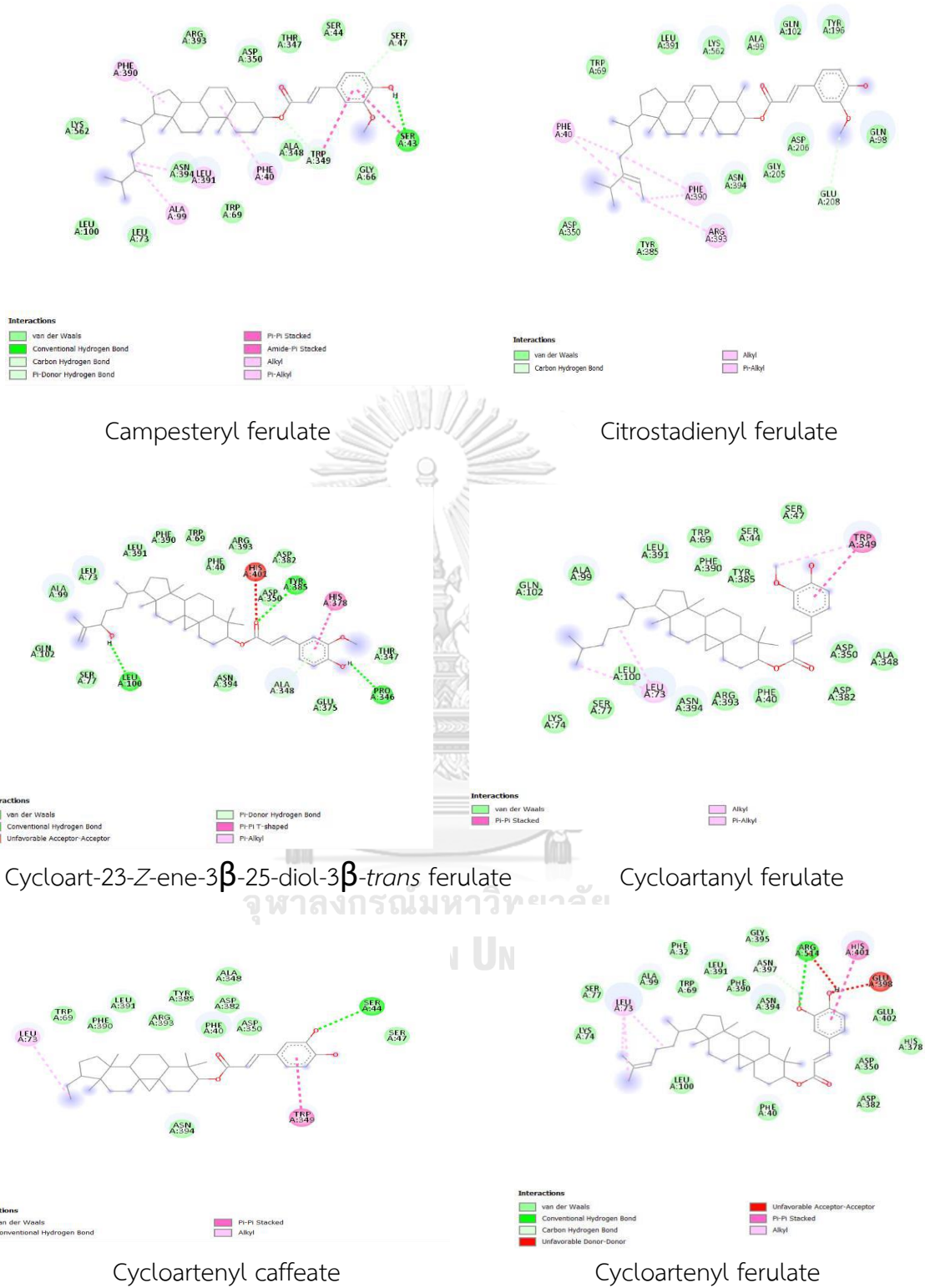
Stigmasteryl ferulate
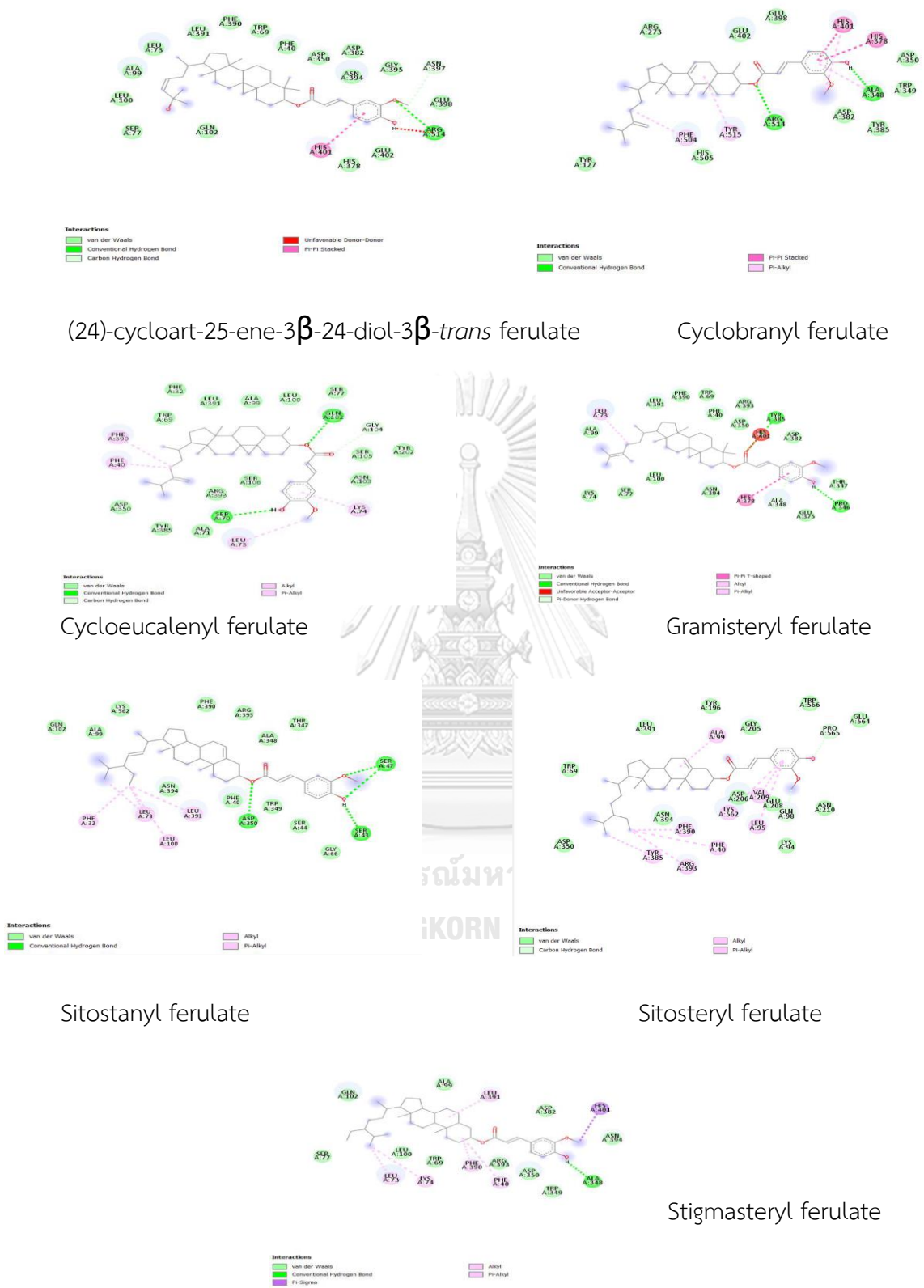
Figure 10 Amino acids residual interactions of the interacting pocket between ACE2 (PDB ID:1R42) and ligands

Table 6 List all the amino acids residue into 3 types of interaction (Conventional hydrogen bond, pi-pi/pi-alkyl interaction, and van der waals force) with the active site of ACE2 (PDB ID:1R42)

Compound	Conventional Hydrogen Bond	Pi-Pi / Alkyl interaction	Van der Waals
Δ^7-Campestenyl ferulate	ASN103	HIS401, PHE40	ASP350, ARG393, PHE390, TRP69, LEU391, PHE32, LEU100, GLY104, SER105, GLN102, SER106, LYS74, SER77, ALA99, LEU73, ASN394, TYR385, ASP382, HIS378, ALA348
Δ^7-Sitostenyl ferulate	SER106, SER77	PHE40, LYS74, LEU74	ARG393, PHE390, TRP69, LEU391, LEU100, ALA99, GLN102, ASN103, THR78, ASN394, ASP350, HIS401, ASP382, HIS378, ALA348
Δ^7-Stigmastenyl ferulate	ASN103	ARG393, PHE390, PHE40	ASP350, SER44, LEU351, TRP349, ALA348, TRP69, GLN102, GLY104, SER105, SER106, LYS74, SER77, LEU73, LEU100, LEU391
24-Methylenecycloartanyl ferulate	SER44	LEU73, TRP39, PHE40	GLN102, LYS74, SER77, LEU100, ASN394, SER47, SER43, ASP350, ASP382, TYR385, ARG393, PHE390, LEU391, TRP69
Campestanyl ferulate	ALA348	PHE390, HIS401, HIS378, PRO346	ARG393, PHE40, THR347, GLU375, GLU402, TYR385, ASP350, ASN394, ASP382, LEU73, TRP69, LEU391, LYS562

Compound	Conventional Hydrogen Bond	Pi-Pi / Alkyl interaction	Van der Waals
Campesteryl caffeate	ASP350, SER47	TRP349, PHE40, PHE390, LEU391, LEU73	ALA99, LEU100, SER77, ASN394, LEU351, ALA348, SER44, SER43
Campesteryl ferulate	SER43, SER47, TRP349	PHE390, ALA99, LEU391, PHE40	LYS562, LEU100, LEU73, ASN39, TRP69, ALA348, GLY66, SER44, THR347, ASP350, ARG393
Citrostadienyl ferulate	GLU208	PHE40, PHE390, ARG393	TRP69, LEU391, LYS562, ALA99, GLN102, TYR196, GLN98, ASP206, GLY205, ASN394, TYR385, ASP350
Cycloart-23-Z-ene-3β-25-diol-3β-trans ferulate	TYR385, PRO346, LEU100, ALA348	HIS378	ALA99, LEU73, LEU391, PHE390, TRP69, PHE40, ARG393, ASP382, ASP350, THR347, GLU375, ASN394, SER77, GLN102
Cycloartanyl ferulate	-	TRP349, LEU73	GLN102, ALA99, LEU391, TRP69, PHE390, TYR385, SER44, SER47, ASP350, ALA348, ASP382, PHE40, ARG393, ASN394, LEU100, SER77, LYS74
Cycloartenyl caffeate	SER44	TRP349, LEU73	TRP69, PHE390, LEU391, ARG393, TYR385, PHE40, ASP382, ALA348, ASP350, SER47, ASN394

Compound	Conventional Hydrogen Bond	Pi-Pi / Alkyl interaction	Van der Waals
Cycloartenyl ferulate	ARG514, ASN397	HIS401, LEU73	LYS74, SER77, ALA99, PHE32, TRP69, LEU391, PHE390, ASN394, GLY395, GLU402, HIS378, ASP350, ASP382, PHE40, LEU100
(24)-cycloart-25-ene-3β-24-diol-3β-*trans* ferulate	ARG514, ASN397	HIS401	GLN102, SER77, LEU100, ALA99, LEU73, LEU391, PHE390, TRP69, PHE40, ASP350, ASP382, ASN394, GLY395, GLU398, GLU402, HIS378,
Cyclobranyl ferulate	PRO346, TYP385, ALA348	HIS378, LEU73	LEU391, PHE390, TRP69, PHE40, ARG393, ASP350, ASP382, THR347, GLU375, ASN394, LEU100, SER77, LYS74, ALA99
Cycloeucalenyl ferulate	GLN102, SER70, GLY104	LYS74, LEU73, PHE40, PHE390	TRP69, PHE32, LEU391, ALA99, LEU100, SER77, SER105, TYR202, ASN103, ALA71, ARG393, SER106, TYR385, ASP350
Gramisteryl ferulate	ALA348, ARG514	HIS401, HIS378, TYR515, PHE504	ARG273, GLU402, GLU398, ASP350, TRP349, TYR385, ASP382, HIS505, TYR127
Sitostanyl ferulate	ALA348	HIS401, LEU391, LEU73, LYS74, PHE390, PHE40	GLN102, ALA99, ASP382, ASN394, TRP349, ASP350, ARG393, TRP69, LEU100, SER77

Sitosteryl ferulate	-	ALA99, TYR385, ARG393, PHE40, PHE390, LYS562, LEU95, VAL209	TRP69, GLY205, GLU564, GLU208, ASP350	LEU391, TRP566, ASN210, ASP206,	TYR196, PRO565, GLN98, LYS94, ASN394,
Stigmasteryl ferulate	SER47, SER43, ASP350	PHE32, LEU73, LEU100, LEU391	GLN102, PHE390, THR347, GLY66, PHE40, ASN394	ALA99, ARG393, SER44, TRP349,	LYS562, ALA348,

24-Methylenecycloartanyl ferulate docked with ACE2 protein (PDB ID: 1R42) revealed the docking and binding energy score of -9.3 kcal/mol. Besides, it is formed one hydrogen bond interaction with one amino acid is SER44. These hydrogen bond interactions indeed enhance the binding affinity of the complex by stabilizing the ligand at the active site of the target and thereby help in increasing the biological activity of the complex. The other interaction includes pi-pi interaction with TRP39, pi-alkyl with LEU73, PHE40 and van der Waals interaction with GLN102, LYS74, SER77, LEU100, ASN394, SER47, SER43, ASP350, ASP382, TYR385, ARG393, PHE390, LEU391, TRP69.

The cycloartenyl ferulate docked with ACE2 protein (PDB ID: 1R42) revealed the docking and binding energy score of -9.7 kcal/mol. Besides, it formed two hydrogen

bond interaction with two amino acids is ARG514, ASN397. The other interaction includes pi-pi interaction with HIS401, alkyl interaction with LEU73 and van der waals interaction with LYS74, SER77, ALA99, PHE32, TRP69, LEU391, PHE390, ASN394, GLY395, GLU402, HIS378, ASP350, ASP382, PHE40, LEU100.

Campesteryl ferulate docked with ACE2 protein (PDB ID: 1R42) revealed the docking and binding energy score of -9.3 kcal/mol. Besides, it formed three hydrogen bond interactions with three amino acids is SER43, SER47, TRP349. The other interactions include pi-pi interaction with SER43, amide pi-stacked with TRP349, pi-alkyl interaction with PHE390, ALA99, LEU391, PHE40 and van der waals interaction with LYS562, LEU100, LEU73, ASN39, TRP69, ALA348, GLY66, SER44, THR347, ASP350, ARG393.

4.1.2 The Physiochemical Properties of Phytochemicals from **γ**-Oryzanol Based on Lipinski's Rule of Five.

The 19 phytochemicals of **γ**-oryzanol were investigated for the drug-like properties using the ADME (Adsorption, Distribution, Metabolism, and Excretion). In the examination of the structures of orally administered drugs, and potential pharmaceuticals using Lipinski's rule of five highlights, the significance of molecular weight (MW), number of hydrogen bond donor, and number of hydrogen bond acceptors, GI absorption, BBB permeant and Lipinski's, the test compounds must meet certain requirements, such as the molecular weight (MW) < 500 g/mol, the number of

hydrogen bond acceptors ≤ 10, the number of hydrogen donors ≤ 5, and a maximum

of 1 violations [111, 112].

Table 7 The physiochemical properties of the phytochemicals from gamma-oryzanol
based on Lipinski's tule of five.

Compound	Molecular weight (g/mol) (≤ 500)	Hydrogen bond acceptors (≤ 10)	Hydrogen bond donor (≤ 5)	GI Absorption	BBB permeant	Lipinski's	Log $P_{o/w}$
Δ^7-Campestenyl ferulate	586.96	4	1	Low	No	2	-3.70
Δ^7-Sitostenyl ferulate	600.95	4	1	Low	No	2	-4.84
Δ^7-Stigmastenyl ferulate	600.95	4	1	Low	No	2	-4.84
24-Methylenecyclo-artanyl ferulate	616.91	4	1	Low	No	2	-3.42
Campestanyl ferulate	587.94	4	1	Low	No	2	-3.70
Campesteryl caffeate	562.82	4	2	Low	No	2	-25.5
Campesteryl ferulate	576.85	4	1	Low	No	2	-3.70
Citrostadienyl ferulate	614.98	4	1	Low	No	2	-4.43

Compound	Molecular weight (g/mol) (≤ 500)	Hydrogen bond acceptors (≤ 10)	Hydrogen bond donor (≤ 5)	GI Absorption	BBB permeant	Lipinski's	Log $P_{o/w}$
Cycloart-23-*Z*-ene-3**β**-25-diol-3**β**-*trans* ferulate	628.96	5	2	Low	No	2	-4.26
Cycloartanyl ferulate	602.89	4	1	Low	No	2	-3.37
Cycloartenyl caffeate	516.8	4	2	Low	No	2	-26.2
Cycloartenyl ferulate	602.89	4	1	Low	No	2	-3.41
(24)-cycloart-25-ene-3**β**-24-diol-3**β**-*trans* ferulate	628.96	5	2	Low	No	2	-3.84
Cyclobranyl ferulate	624.98	4	1	Low	No	2	-16.0
Cycloeucalenyl ferulate	612.97	4	1	Low	No	2	-15.9
Gramisteryl ferulate	600.95	4	1	Low	No	2	-4.64
Sitostanyl ferulate	592.89	4	1	Low	No	2	-4.22
Sitosteryl ferulate	590.88	4	1	Low	No	2	-16.1
Stigmasteryl ferulate	588.86	4	1	Low	No	2	-4.84

Almost all 19 phytochemicals have molecular weight more than 500 g/mol. Two from the 19 have hydrogen bond acceptors more than 4 which are cycloart-23-*Z*-ene-3β, 25-diol-3β-*trans* ferulate and (24)-cycloart-25-ene-3β, 24-diol-3β-trans ferulate. Four out of 19 phytochemicals (campesteryl caffeate, cycloart-23-*Z*-ene-3β-25-diol-3β-*trans* ferulate, (24)-cycloart-25-ene-3β-24-diol-3β-*trans* ferulate and cycloartenyl caffeate) have hydrogen bond donor more than 1. HBA and HBD total hydrogen bond counts are significant indictors for high oral bioavailability [113]. The gastrointestinal absorption (GI absorption) of all 19 phytochemicals was low. This parameter is under the category of pharmacokinetics. The Blood-brain barrier (BBB permeant) is selective permeable to drugs and plays an important role in determining the brain distribution of CNS drugs. According to the results all 19 phytochemicals show no BBB permeant. In conclusion, all 19 phytochemicals of γ-oryzanol violate Lipinski's rule of five more than 1 because the molecular weight of all 19 phytochemicals of γ-oryzanol is more than 500 g/mol. The $P_{o/w}$ of all 19 phytochemicals of γ-oryzanol are negative.

4.1.3 Toxicity of the Phytochemicals of γ-Oryzanol

The toxicity of the phytochemicals was calculated by ProTox-II web server. The toxicity prediction was demonstrated in Table 8. The ProTox-II differentiated the classification system of toxicity into oral toxicity, organ toxicity (hepatotoxicity), toxicological endpoints (such as mutagenicity, carcinogenicity, cytotoxicity, and immunotoxicity), toxicological pathways (AOPs) and toxicity target. The rule that identifies the

compound's acute toxicity (rodent) was based on the analysis of the two-dimensional (2D) similarity with known LD_{50} value and identification of fragments over-represented in toxic compound. The hepatotoxicity was based on Random Forest with SMOTE TC (Synthetic Minority Over-Sampling-using Tanimoto Coefficient) sampling. The carcinogenicity, mutagenicity and cytotoxicity were based on machine learning with over sampling, while immunotoxicity was based on the Multinomial Naïve Bayes.

Table 8 Toxicity of the phytochemicals of gamma-oryzanol

Compound	LD_{50} value (mg/kg)	Toxicity class	Hepato-toxicity	Carcino-genicity	Immun-toxicity	Mutage-nicity	Cyto-toxicity
Δ^7-Campestenyl ferulate	9600	6	I; 0.72	I; 0.69	A; 0.99	I; 0.94	I; 0.79
Δ^7-Sitostenyl ferulate	9600	6	I; 0.72	I; 0.73	A; 0.99	I; 0.88	I; 0.80
Δ^7-Stigmastenyl ferulate	1000	4	I; 0.70	I; 0.67	A; 0.99	I; 0.85	I; 0.79
24-Methylenecyclo-artanyl ferulate	25000	6	I; 0.70	I; 0.76	A; 0.99	I; 0.91	I; 0.58

Compound	LD$_{50}$ value (mg/kg)	Toxicity class	Hepato- toxicity	Carcino- genicity	Immun- toxicity	Mutage- nicity	Cyto- toxicity
Campestanyl ferulate	9600	6	I; 0.70	I; 0.73	A; 0.99	I; 0.89	I; 0.83
Campesteryl caffeate	9960	6	I; 0.74	I; 0.55	A; 0.99	I; 0.91	I; 0.78
Campesteryl ferulate	9600	6	I; 0.72	I; 0.65	A; 0.99	I; 0.94	I; 0.79
Citrostadienyl ferulate	1000	4	I; 0.70	I; 0.67	A; 0.99	I; 0.85	I; 0.79
Cycloart-23-Z-ene-3β-25-diol-3β-$trans$ ferulate	1000	4	I; 0.67	I; 0.68	A; 0.99	I; 0.71	I; 0.70
Cycloartanyl ferulate	9600	6	I; 0.70	I; 0.75	A; 0.99	I; 0.88	I; 0.62
Cycloartenyl caffeate	5000	5	I; 0.61	I; 0.66	A; 0.88	I; 0.66	I; 0.74
Cycloartenyl ferulate	25000	6	I; 0.71	I; 0.77	A; 0.99	I; 0.91	I; 0.60
(24)-cycloart-25-ene-3β-24-diol-3β-$trans$ ferulate	1000	4	I; 0.65	I; 0.66	A; 0.99	I; 0.67	I; 0.68
Cyclobranyl ferulate	1000	4	I; 0.70	I; 0.65	A; 0.99	I; 0.76	I; 0.70

Compound	LD$_{50}$ value (mg/kg)	Toxicity class	Hepato-toxicity	Carcino-genicity	Immun-toxicity	Mutage-nicity	Cyto-toxicity
Cycloeucalenyl ferulate	1000	4	I; 0.67	I; 0.68	A; 0.99	I; 0.75	I; 0.70
Gramisteryl ferulate	1000	4	I; 0.67	I; 0.67	A; 0.99	I; 0.84	I; 0.82
Sitostanyl ferulate	9600	6	I; 0.72	I; 0.73	A; 0.99	I; 0.88	I; 0.80
Sitosteryl ferulate	9600	6	I; 0.74	I; 0.66	A; 0.99	I; 0.93	I; 0.79
Stigmasteryl ferulate	9600	6	I; 0.74	I; 0.66	A; 0.99	I; 0.93	I; 0.79

LD$_{50}$: Median lethal dose; I: Inactive; A: Active

The GHS guidelines classify the substance into six groups, with the highest group having the low likelihood of being dangerous or harmful. Class 1 (LD$_{50}$ ≤ 5) and class 2 (5 < LD$_{50}$ ≤ 50) signifies that the compound is lethal and almost certainly will result in death. Class 3 (50 < LD$_{50}$ ≤ 300), indicates potential toxicity hazards, from oral exposure. Class 4 (300 < LD$_{50}$ ≤ 2000) classifies substance that are most likely to be dangerous when consumed. Seven phytochemicals including fall in class 4 such as Δ^7-stigmastenyl ferulate, citrostadienyl ferulate, cycloart-23-*Z*-ene-3β-25-diol-3β-*trans* ferulate, (24)-cycloart-25-ene-3β-24-diol-3β-*trans* ferulate, cyclobranyl ferulate, cycloeucalenyl ferulate, and gramisteryl ferulate. Compounds that are less likely to be hazardous after oral consumption are included under class 5 (2000 < LD$_{50}$ ≤ 5000).

Among only one phytochemical such as cycloartenyl caffeate were classified in class

5. Finally, class 6 (LD$_{50}$ **>** 5000) reflects the non-toxic compounds. Eleven

phytochemical falls in class 6 such as **Δ**^{7}-campestenyl ferulate, **Δ**^{7}-sitostenyl ferulate,

campestanyl ferulate, campesteryl caffeate, campesteryl ferulate, cycloartanyl

ferulate, sitostanyl ferulate, sitosteryl ferulate, stigmasteryl ferulate, and the major

compounds of **γ**-oryzanol, 24-methylenecycloartanyl ferulate and cycloartenyl

ferulate is (LD*50* 25000 mg/kg).

Overall, eleven phytochemicals of **γ**-Oryzanol (**Δ**^{7}-campestenyl ferulate, **Δ**^{7}-sitostenyl

ferulate, campestanyl ferulate, campesteryl caffeate, campesteryl ferulate,

cycloartanyl ferulate, sitostanyl ferulate, sitosteryl ferulate, stigmasteryl ferulate, 24-

methylenecycloartanyl ferulate, and cycloartenyl ferulate) out of 19 were calculated

as non-toxic phytochemicals of **γ**-oryzanol.

Based on the *in-silico* study, the major compounds of **γ**-Oryzanol show ADME

calculation, and toxicity predictions, (24-methylenecycloartanyl ferulate, cycloartenyl

ferulate, and campesteryl ferulate) were potential to be developed as novel inhibitors

for ACE2.

4.2 Isolation of target compound

Isolation of **γ**-oryzanol from crude rice bran acid fraction (RBAF) was carried out

chromatographic and precipitation techniques. RBAF (53 g) was subjected to silica gel

column chromatography (310 g of silica gel in column with 13 cm diameter and 16 cm

length), eluting with hexanes, hexanes: EtOAc (20:1, 15:1, 10:1, and 5:1) and EtOAc in stepwise fashion. For eluting with hexane there was no indication of γ-oryzanol according to TLC and NMR analysis. Those fractions contained fatty acid and triglycerides as a liquid. For eluting with 20:1 (n-hexane: EtOAc) there was no indication of γ-oryzanol. Using 15:1 n-hexane: EtOAc as eluent. The total 10 combined were obtained. According to TLC and NMR analysis, γ-oryzanol was obtained in fractions 7, 8, 9, and 10. By staining with $FeCl_3$ in MeOH, γ-oryzanol of the fractions 7 and 8 showed R_f value of 0.5 on TLC developed by 8:2 as a mobile phase while γ-oryzanol of the fractions 9 and 10 showed the R_f value of 0.3 on TLC developed by the same mobile phase 8:2. After evaporation of the solvent and kept the residue at room temperature white or yellow solids were precipitated in the combined fractions of 7 and 8 and of 9 and 10. By NMR analysis, the liquid from the precipitation comprised of γ-Oryzanol and fatty acid (triglycerides). The precipitated solids were separated from the combined fractions by using vacuum filtration. The residue on filter paper was washed with 1 ml of cold hexane to afford the white and yellow solid. The precipitated solid was analyzed by TLC and ^{1}H NMR. Based on NMR result, the white and yellow solid were mainly γ-oryzanol and the filtrate, obtained as liquid after removal of the solvent was triglyceride. The NMR analysis was also used to confirm the existence of γ-oryzanol in the product. The % purity of γ-oryzanol and % yield of γ-oryzanol were calculated by:

% yield of **γ**-oryzanol product =

$$\frac{Amount\ of\ \gamma-orzanol\ product\ from\ precipation\ (mg)}{Amount\ of\ RBAF\ (mg)} \times 100 \quad \text{Eq. (1)}$$

% purity of **γ**-oryzanol = $\dfrac{I\gamma/3}{\left(\frac{I\gamma}{3}+\frac{I\alpha}{2}\right)} \times 100$ Eq. (2)

Whereas I_γ is integral of the methoxy protons of **γ**-oryzanol and I_α is integral of triplet signal for **α**-proton of the fatty acid moiety. The purity of **γ**-oryzanol of the white or yellow solid product were estimated by NMR analysis (E.q 2) is **>** 90%. The **γ**-Oryzanol obtained from fractions 7 and 8 were mainly pure (see Fig 11) while the **γ**-Oryzanol from fractions 9 and 10 contained small amount of triglycerides (see Fig).

Further eluting with the mobile phase hexane: EtOAc 10:1, the 16 combined fractions were obtained. According to TLC analysis the fractions 11-16 comprised of **γ**-oryzanol. Because fractions 11-13 showed similar TLC profile, these fractions were combined. By staining with $FeCl_3$ in MeOH, **γ**-Oryzanol of the fractions 11-13 showed R_f value of 0.5 on TLC developed by 8:2 as a mobile phase. while **γ**-oryzanol of the fractions 14-16 showed the R_f 0.3 on TLC developed by the same mobile phase 8:2. After, evaporation of the solvent the residue was kept at room temperature and white or yellow solids were precipitated in the fraction 11-13. By NMR analysis, the liquid from the precipitation comprised of **γ**-oryzanol and fatty acid (triglycerides). The precipitation and isolation of **γ**-oryzanol from the fractions 11-13 and 14-16 was performed in similar manner as described above. The purity of **γ**-oryzanol in both fractions 11-13 and 14-16 was **>** 90% (calculated by equation 2).

For further isolation eluting with the mobile phase 5:1 n-hexane: EtOAc, there was no indication of **γ**-oryzanol in each fraction according to TLC and NMR analysis. The results eluting with 5:1 n-hexane: EtOAc were totally triglyceride and the last combined fractions from elution with EtOAc was fatty acid and without **γ**-oryzanol.

4.3 Structure Elucidation of Isolated Compounds

For 19 structures of **γ**-oryzanol obtained from the rice bran oil, 8 structures are cycloartenyl type **γ**-oryzanol including 24-methylenecycloartanyl ferulate, cycloartenyl ferulate, cycloartenyl caffeate, cycloartanyl ferulate, cyclobranyl ferulate, (24)-cycloart-25-ene-3β, 24-diol-3β-trans ferulate, cycloart-23-Z-ene-3β, 25-diol-3β-trans ferulate, and cycloeucalenyl ferulate and 11 structures are phytosterols type **γ**-oryzanol including campesteryl that consist of campesteryl ferulate, campesteryl caffeate, sitosteryl ferulate, stigmasteryl ferulate, Δ^7-stigmastenyl ferulate, Δ^7-sitostenyl ferulate, Δ^7-campestenyl ferulate, gramisteryl ferulate, citrostadienyl ferulate, campestanyl ferulate, and sitostanyl ferulate.

4.3.1 Structure Elucidation of Isolated Fractions 1, 2, and 3.
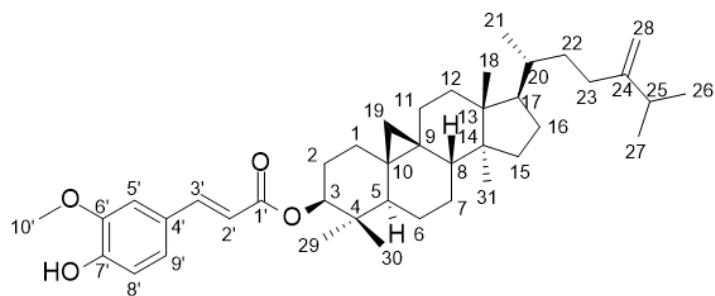
Figure 11 Structure of 24-Methylenecycloartenyl Ferulate
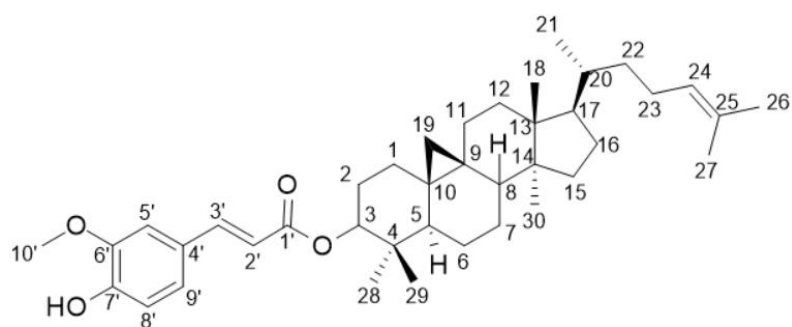
Figure 12 Structure of Cycloartenyl Ferulate
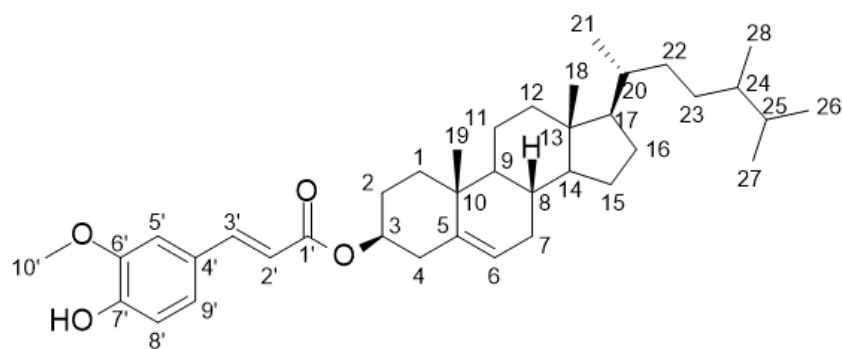
Figure 13 Structure of Campesteryl Ferulate
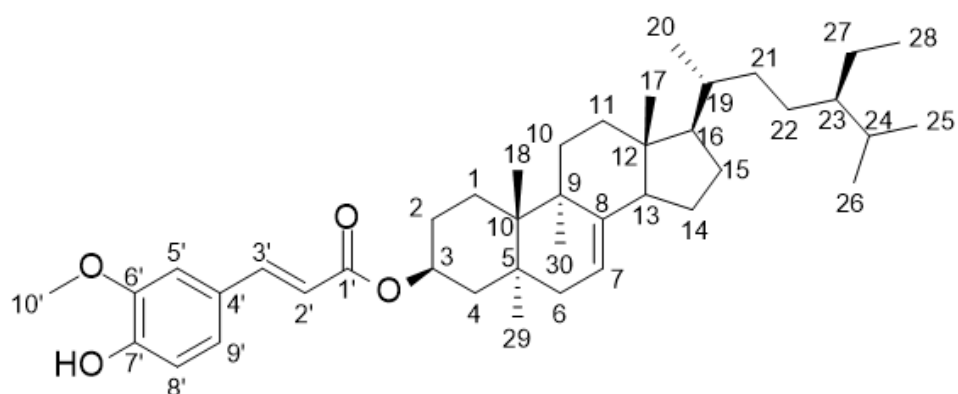
Figure 14 Structure of Sitostenyl Ferulate
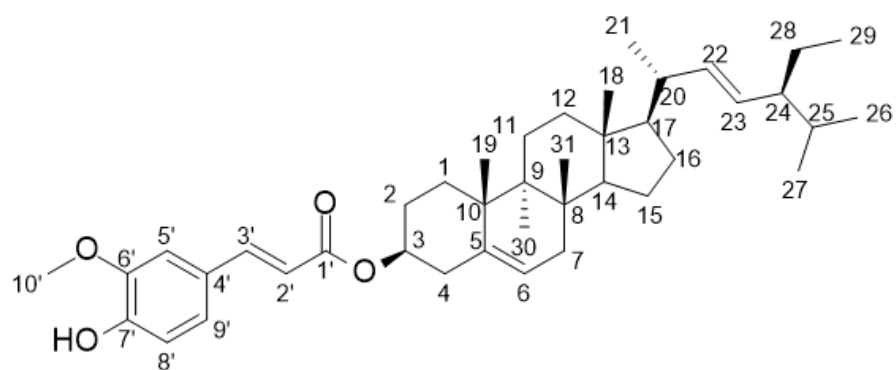
Figure 15 Structure of Stigmasteryl ferulate
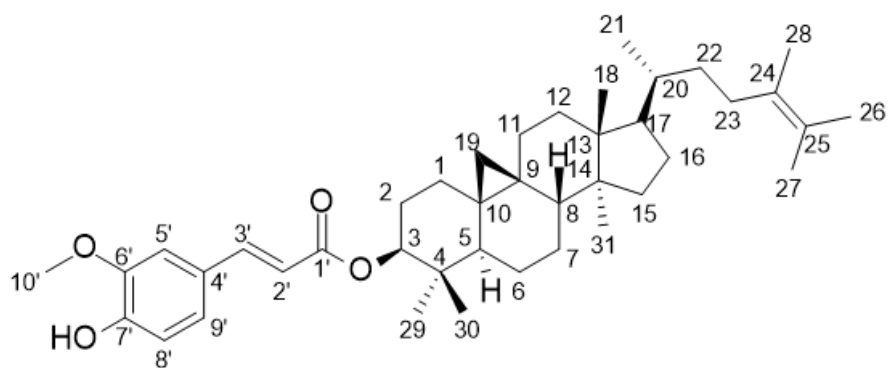
Figure 16 Structure of Cyclobranyl ferulate
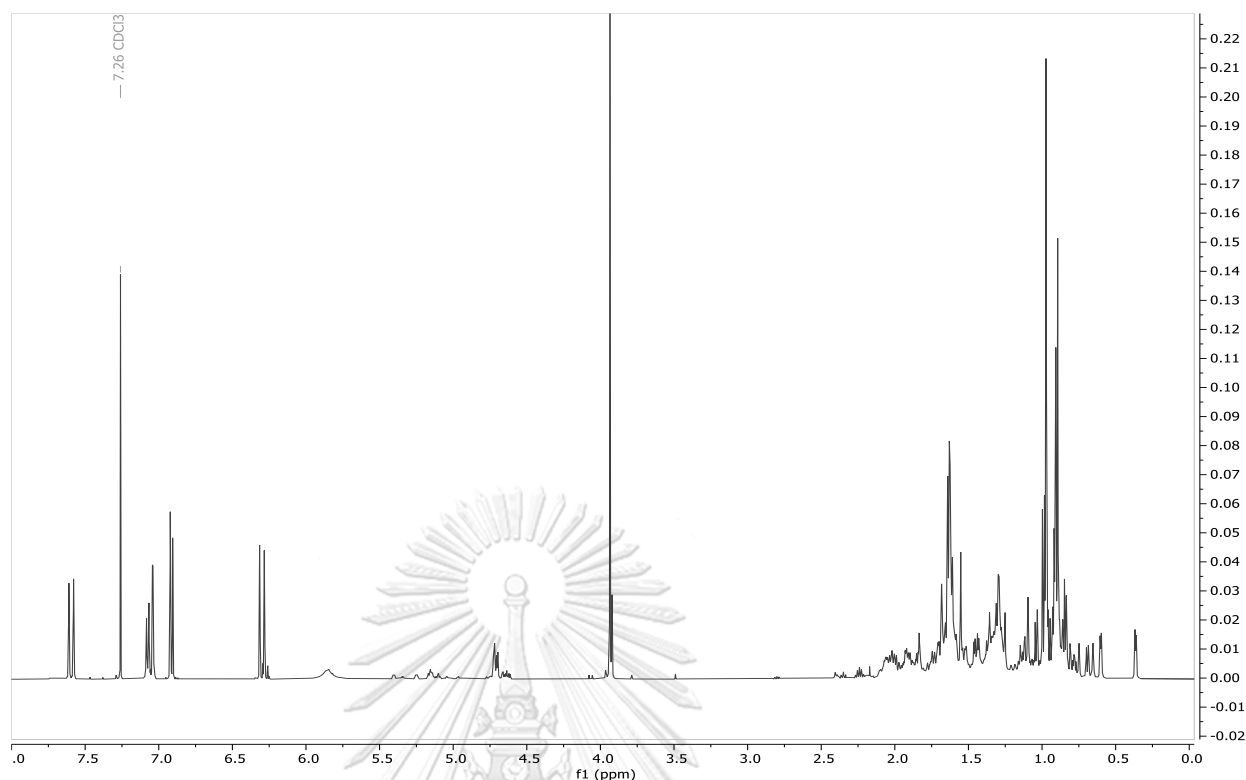
Figure 17 ^{1}H NMR spectrum of isolated fraction 1

Isolated fraction 1 was obtained as a white and yellow solid from the fractions 7 and 8 eluted with 15:1 (Hexane: EtOAc). Based on NMR analysis, it was a mixture of different structures of γ-Oryzanol. Although 24-methylenecycloartanyl ferulate is a major compound of γ-Oryzanol in rice bran oil. According to ^{1}H NMR (Figure 17) and ^{13}C NMR (Figure 18) spectra of the isolated fraction 1 showed no signals of olefinic protons of 24-methylenecycloartenyl ferulate at δ_H 4.72 and 4.67 ppm (br,s) for H_2-28 and at δ_C 105 ppm for C-28. Compared to ^{1}H and ^{13}C NMR data of cycloartenyl ferulate in the (Table 9 and 10, Figure 12), stigmasteryl ferulate (Figure 16), campesteryl ferulate (Figure 13), sitostenyl ferulate (Figure 14) and cycloartenyl ferulate was the major

component of the γ-Oryzanol fraction 1. Thus isolated fraction 1 was a mixture of cycloartenyl ferulate as a major component, cyclobranyl ferulate, and small amount of campesteryl ferulate.
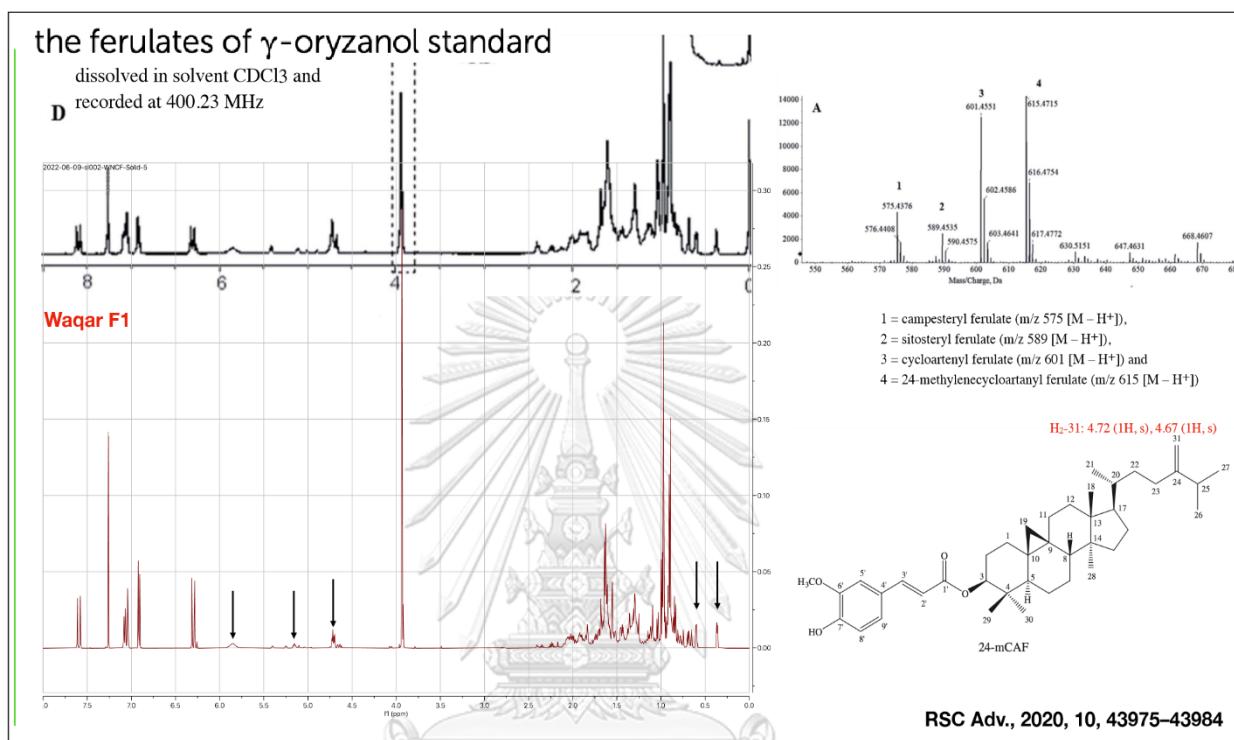
Figure 18 Comparison NMR data of Isolated fraction 1

Compared to the NMR spectra with the previous data as shown in Figure 18 the isolated fraction 1, was a mixture of cycloartenyl ferulate (CAF), as a major component of γ-oryzanol, cyclobranyl ferulate (CBF), and small amounts of campesteryl ferulate (CPF).

Figure 19 Compare NMR of cycloartenyl ferulate, cyclobranyl ferulate and campesteryl ferulate.

In Figure 19, it was obvious that cycloartenyl ferulate was a major component in mainly

structures of γ-oryzanol fraction 1 together with cyclobranyl ferulate and a small

amount of campesteryl ferulate.
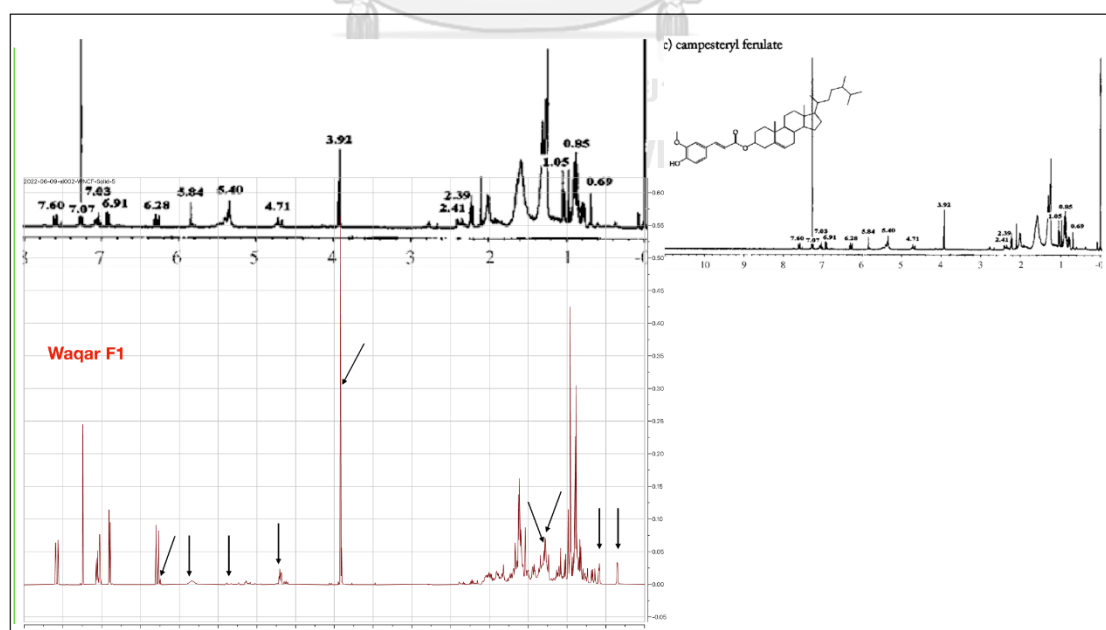
Figure 20 Comparison NMR spectrum of campesteryl ferulate

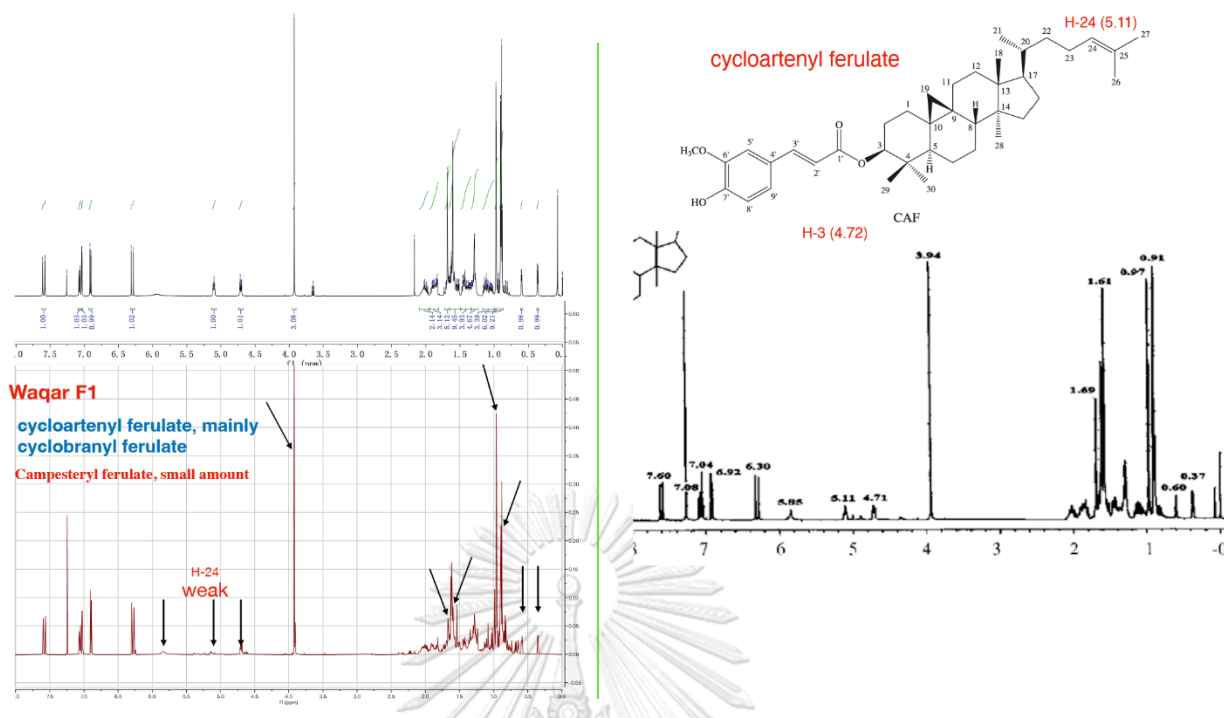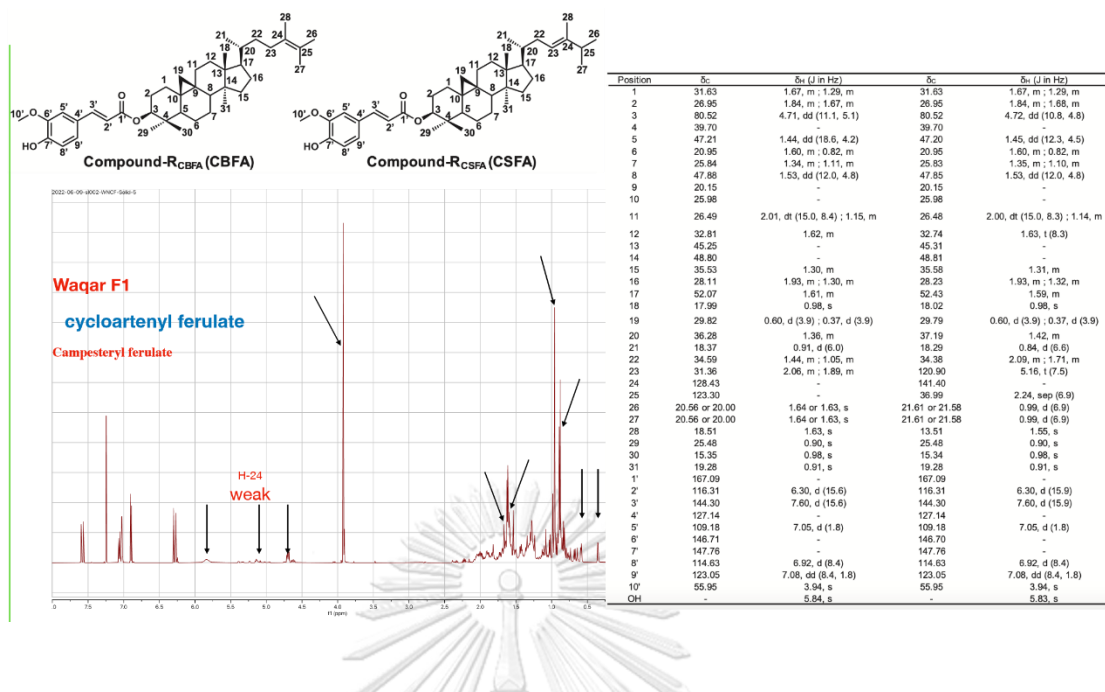| Position	δc	δH (J in Hz)	δc	δH (J in Hz)
1	31.63	1.67, m ; 1.29, m	31.63	1.67, m ; 1.29, m
2	26.95	1.84, m ; 1.67, m	26.95	1.84, m ; 1.88, m
3	80.52	4.71, dd (11.1, 5.1)	80.52	4.72, dd (10.8, 4.8)
4	39.70	-	39.70	-
5	47.21	1.44, dd (18.6, 4.2)	47.20	1.45, dd (12.3, 4.5)
6	20.95	1.60, m ; 0.82, m	20.95	1.60, m ; 0.82, m
7	25.84	1.34, m ; 1.11, m	25.83	1.35, m ; 1.10, m
8	47.88	1.53, dd (12.0, 4.8)	47.85	1.53, dd (12.0, 4.8)
9	20.15	-	20.15	-
10	25.98	-	25.98	-
11	26.49	2.01, dt (15.0, 8.4) ; 1.15, m	26.48	2.00, dt (15.0, 8.3) ; 1.14, m
12	32.81	1.62, m	32.74	1.63, t (8.3)
13	45.25	-	45.31	-
14	48.80	-	48.81	-
15	35.53	1.30, m	35.58	1.31, m
16	28.11	1.93, m ; 1.30, m	28.23	1.93, m ; 1.32, m
17	52.07	1.61, m	52.43	1.59, m
18	17.99	0.98, s	18.02	0.98, s
19	29.82	0.60, d (3.9) ; 0.37, d (3.9)	29.79	0.60, d (3.9) ; 0.37, d (3.9)
20	36.28	1.36, m	37.19	1.42, m
21	18.37	0.91, d (6.0)	18.29	0.84, d (6.6)
22	34.59	1.44, m ; 1.05, m	34.38	2.09, m ; 1.71, m
23	31.36	2.06, m ; 1.89, m	120.90	5.16, t (7.5)
24	128.43	-	141.40	-
25	123.30	-	36.99	2.24, sep (6.9)
26	20.56 or 20.00	1.64 or 1.63, s	21.61 or 21.58	0.99, d (6.9)
27	20.56 or 20.00	1.64 or 1.63, s	21.61 or 21.58	0.99, d (6.9)
28	18.51	1.63, s	13.51	1.55, s
29	25.48	0.90, s	25.48	0.90, s
30	15.35	0.98, s	15.34	0.98, s
31	19.28	0.91, s	19.28	0.91, s
1'	167.09	-	167.09	-
2'	116.31	6.30, d (15.6)	116.31	6.30, d (15.9)
3'	144.30	7.60, d (15.6)	144.30	7.60, d (15.9)
4'	127.14	-	127.14	-
5'	109.18	7.05, d (1.8)	109.18	7.05, d (1.8)
6'	146.71	-	146.70	-
7'	147.76	-	147.76	-
8'	114.63	6.92, d (8.4)	114.63	6.92, d (8.4)
9'	123.05	7.08, dd (8.4, 1.8)	123.05	7.08, dd (8.4, 1.8)
10'	55.95	3.94, s	55.95	3.94, s
OH	-	5.84, s	-	5.83, s

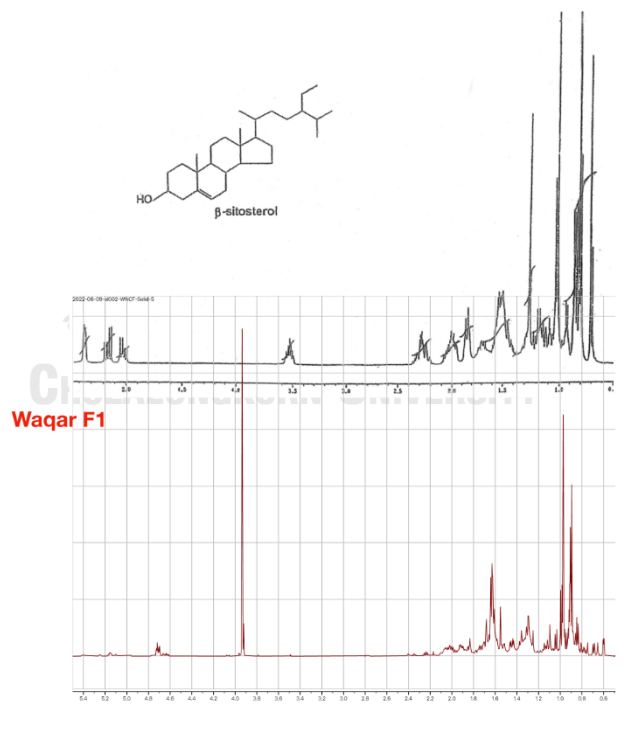**Figure 21** Comparison NMR data of cyclobranyl ferulate and cycloartenyl ferulate

Figure 22 Compare the NMR spectrum of sitosterol (phytosterol) with isolated fraction 1.
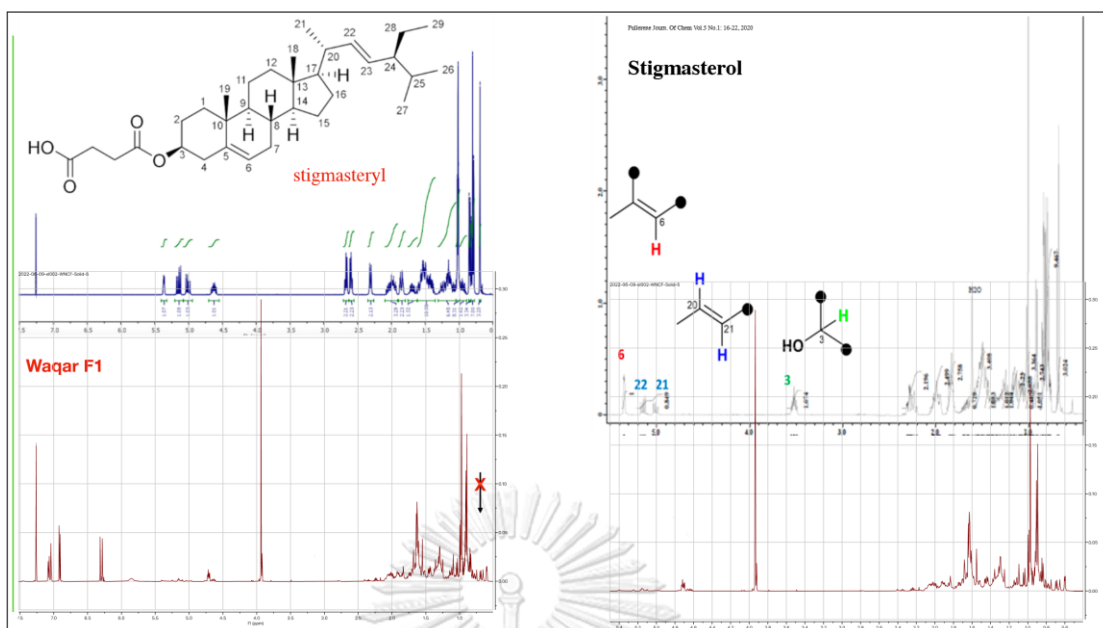
Figure 23 Compare the NMR spectrum of stigmasteryl with isolated fraction 1
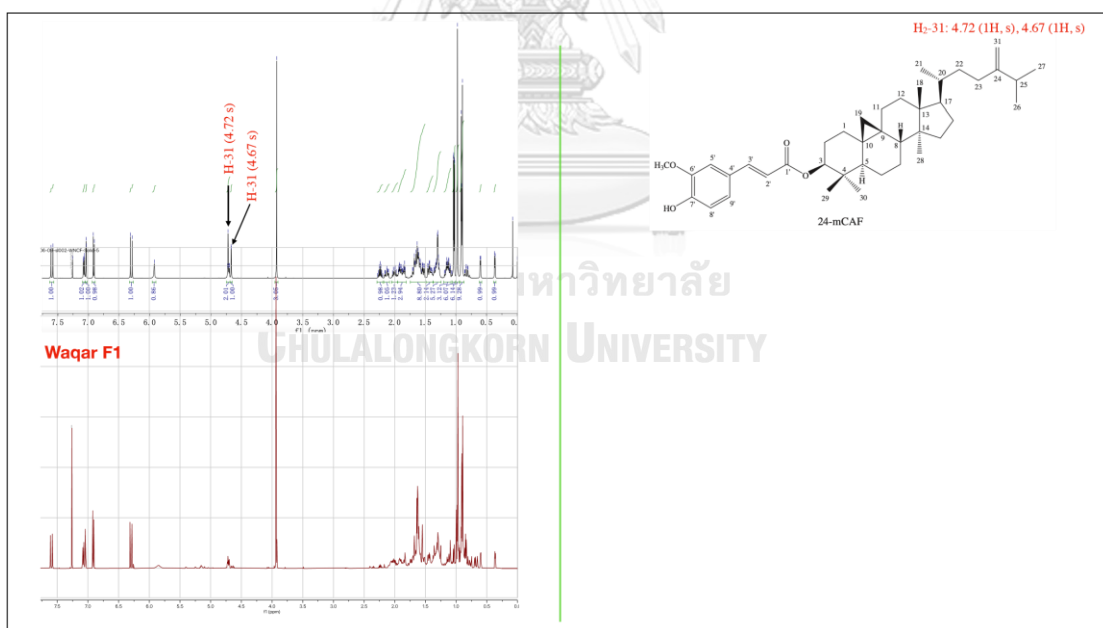
Figure 24 Compare the NMR spectrum of 24-methylenecycloartenyl ferulate

In figure 24, C-28 of 24-methylenecycloartenyl ferulate is a terminal of olefinic double bond. In comparison of the isolated fraction 1 with the previous data there was no show olefinic signal of H_2-28.
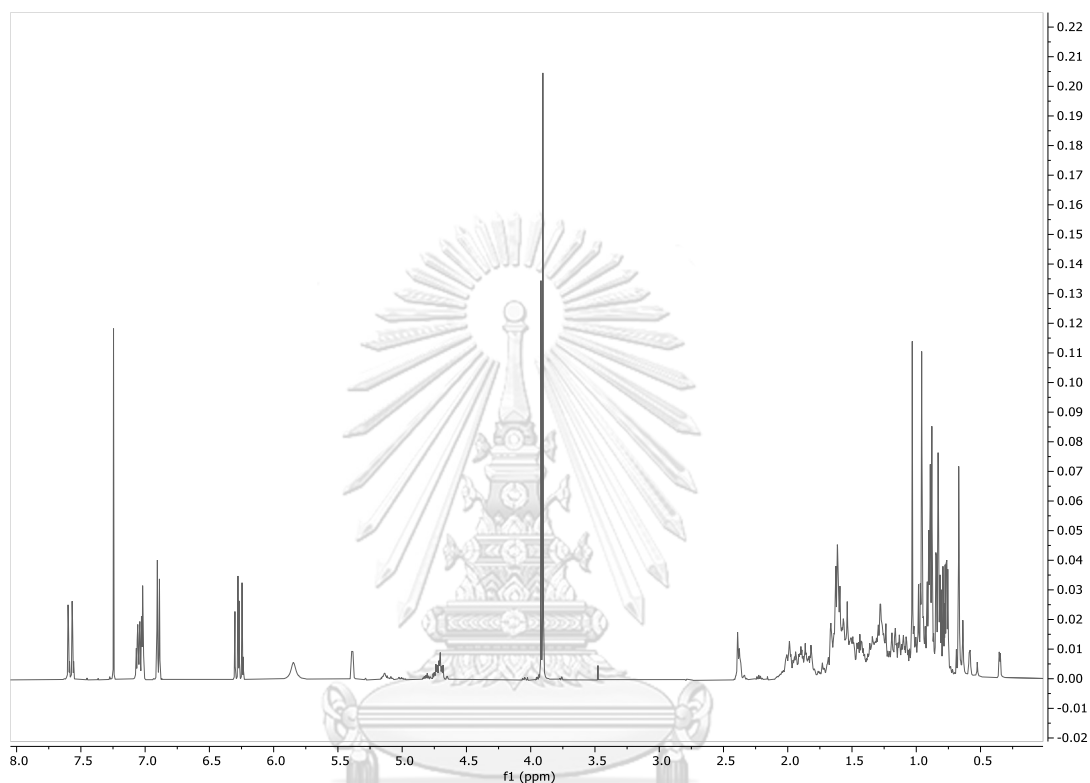
Figure 25 ^{1}H NMR spectrum of isolated fraction 2 (CDCl$_3$, 500 MHz)

Isolated fraction 2 was obtained as a white and yellow solid from fraction 11 and 13 eluted with 10:1 (Hexane: EtOAc). Based on NMR analysis, it was a mixture of different structures of γ-oryzanol. The isolated fraction 2 was a mixture of campesteryl ferulate (CPF), sitosteryl ferulate (STF), stigmasteryl ferulate (SMF), and cycloartenyl ferulate (CAF).

Figure 26 Compare ¹H NMR spectrum of isolated fraction 2.

Figure 27 ¹H NMR spectrum mixture of isolated fraction 2

Figure 28 ^{1}H NMR spectrum of campesteryl ferulate compare with isolated fraction 2.
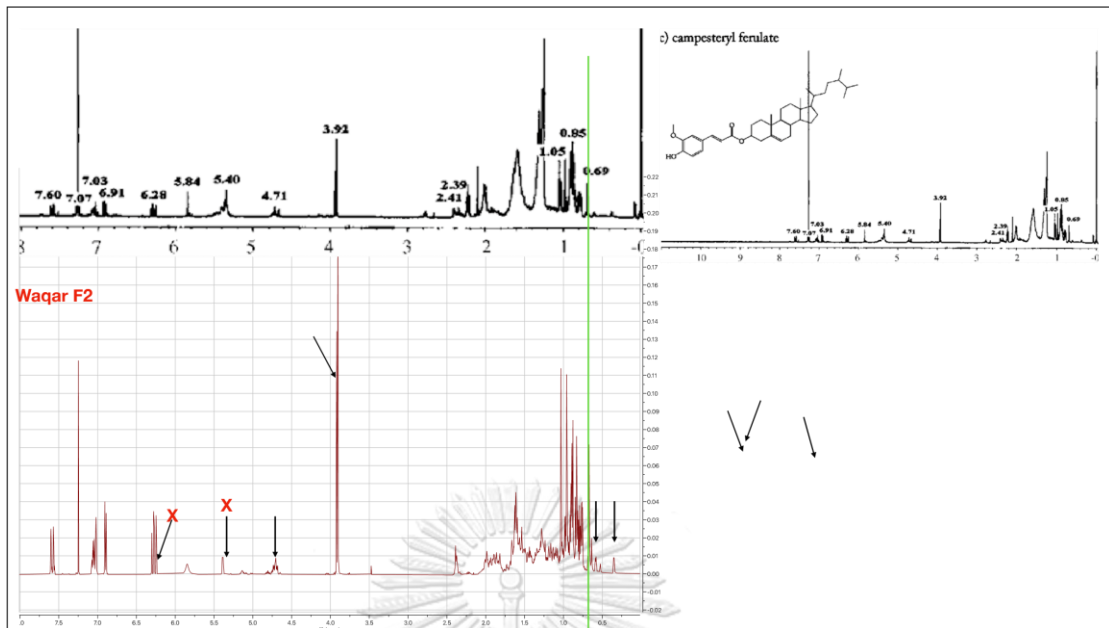

Position	δc	δH (J in Hz)	δc	δH (J in Hz)
1	31.63	1.67, m ; 1.29, m	31.63	1.67, m ; 1.29, m
2	26.95	1.84, m ; 1.67, m	26.95	1.84, m ; 1.68, m
3	80.52	4.71, dd (11.1, 5.1)	80.52	4.72, dd (10.8, 4.8)
4	39.70	-	39.70	-
5	47.21	1.44, dd (18.6, 4.2)	47.20	1.45, dd (12.3, 4.5)
6	20.95	1.60, m ; 0.82, m	20.95	1.60, m ; 0.82, m
7	25.84	1.34, m ; 1.11, m	25.83	1.35, m ; 1.10, m
8	47.88	1.53, dd (12.0, 4.8)	47.85	1.53, dd (12.0, 4.8)
9	20.15	-	20.15	-
10	25.98	-	25.98	-
11	26.49	2.01, dt (15.0, 8.4) ; 1.15, m	26.48	2.00, dt (15.0, 8.3) ; 1.14, m
12	32.81	1.62, m	32.74	1.63, t (8.3)
13	45.25	-	45.31	-
14	48.80	-	48.81	-
15	35.53	1.30, m	35.58	1.31, m
16	28.11	1.93, m ; 1.30, m	28.23	1.93, m ; 1.32, m
17	52.07	1.61, m	52.43	1.59, m
18	17.99	0.98, s	18.02	0.98, s
19	29.82	0.60, d (3.9) ; 0.37, d (3.9)	29.79	0.60, d (3.9) ; 0.37, d (3.9)
20	36.28	1.36, m	37.19	1.42, m
21	18.37	0.91, d (6.0)	18.29	0.84, d (6.6)
22	34.59	1.44, m ; 1.05, m	34.38	2.09, m ; 1.71, m
23	31.36	2.06, m ; 1.89, m	120.90	5.16, t (7.5)
24	128.43	-	141.40	-
25	123.30	-	36.99	2.24, sep (6.9)
26	20.56 or 20.00	1.64 or 1.63, s	21.61 or 21.58	0.99, d (6.9)
27	20.56 or 20.00	1.64 or 1.63, s	21.61 or 21.58	0.99, d (6.9)
28	18.51	1.63, s	13.51	1.55, s
29	25.48	0.90, s	25.48	0.90, s
30	15.35	0.98, s	15.34	0.98, s
31	19.28	0.91, s	19.28	0.91, s
1'	167.09	-	167.09	-
2'	116.31	6.30, d (15.6)	116.31	6.30, d (15.9)
3'	144.30	7.60, d (15.6)	144.30	7.60, d (15.9)
4'	127.14	-	127.14	-
5'	109.18	7.05, d (1.8)	109.18	7.05, d (1.8)
6'	146.71	-	146.70	-
7'	147.76	-	147.76	-
8'	114.63	6.92, d (8.4)	114.63	6.92, d (8.4)
9'	123.05	7.08, dd (8.4, 1.8)	123.05	7.08, dd (8.4, 1.8)
10'	55.95	3.94, s	55.95	3.94, s
OH	-	5.84, s	-	5.83, s

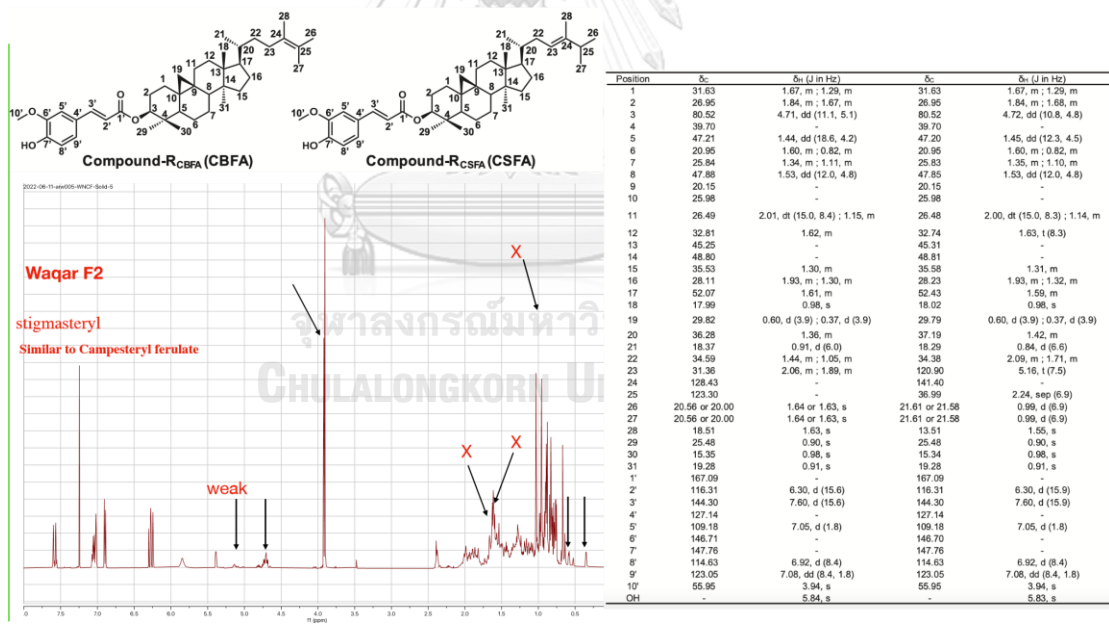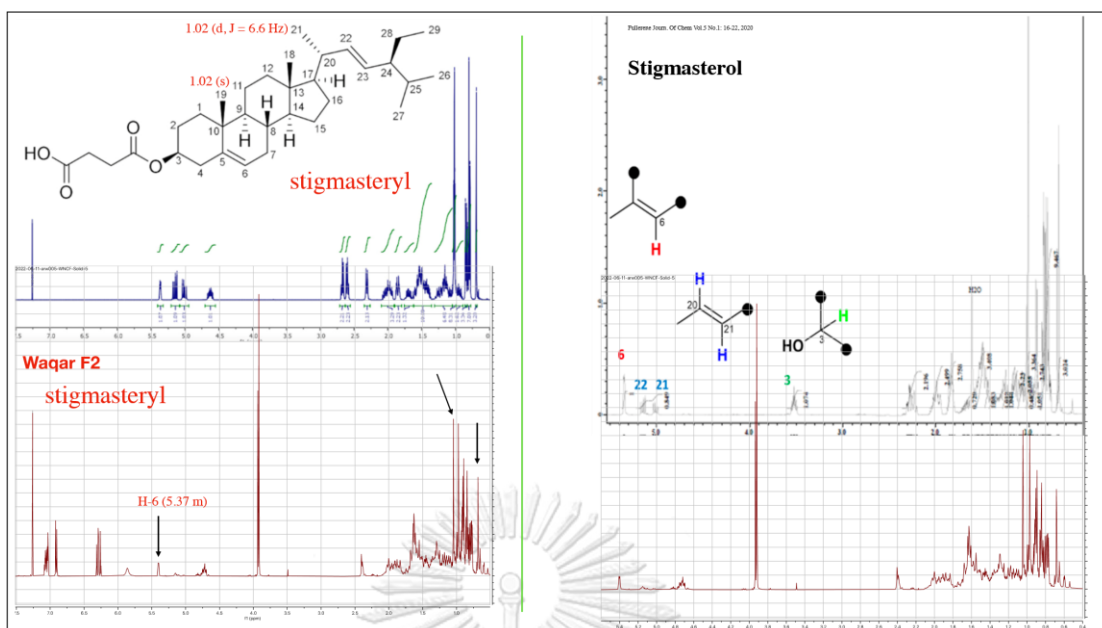**Figure 29** ^{1}H NMR spectrum of stigmasteryl ferulate with isolated fraction 2

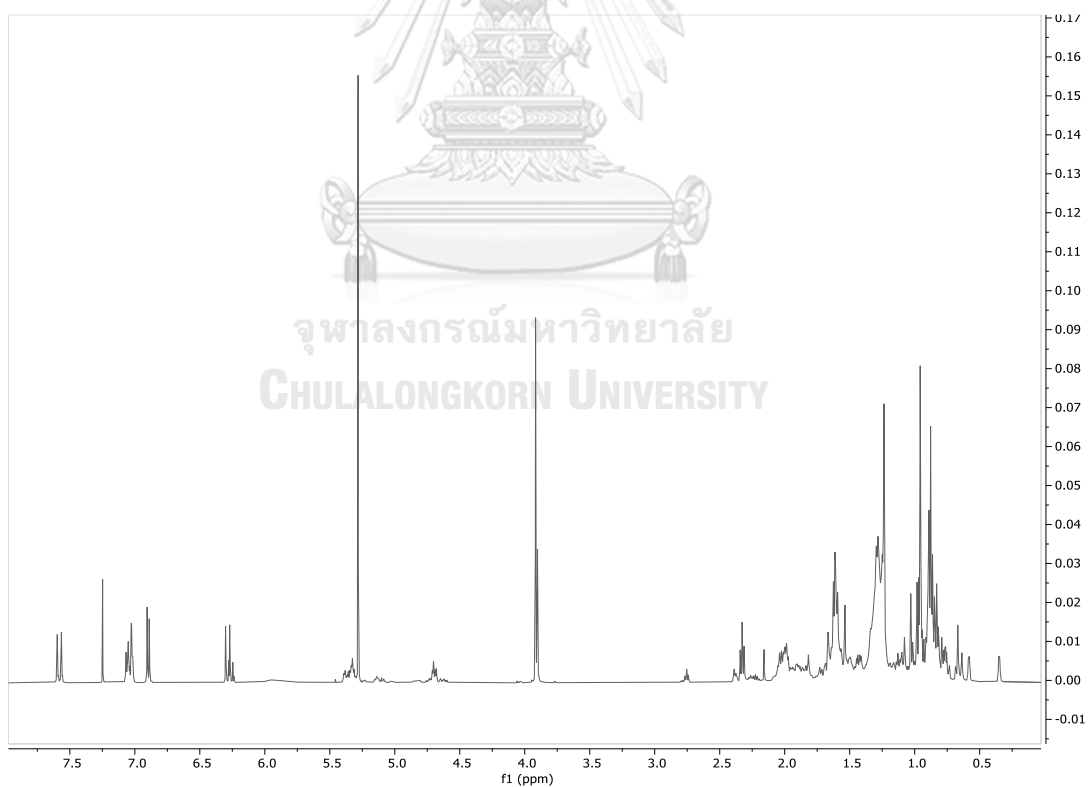**Figure 30** ^{1}H NMR spectrum of stigmasteryl compare with previous data.

Figure 31 ^{1}H NMR spectrum of isolated fraction 3

Isolated fraction 3 was obtained as a white and yellow solid from fraction 14 and 16 eluted with 10:1 (Hexane: EtOAc). Based on NMR analysis, it was a mixture of different structures of γ-Oryzanol. The isolated fraction 3 was a mixture of campesteryl ferulate (CPF) as a major component, together with small amount of cycloartenyl ferulate (CAF), and cyclobranyl ferulate (CBF).
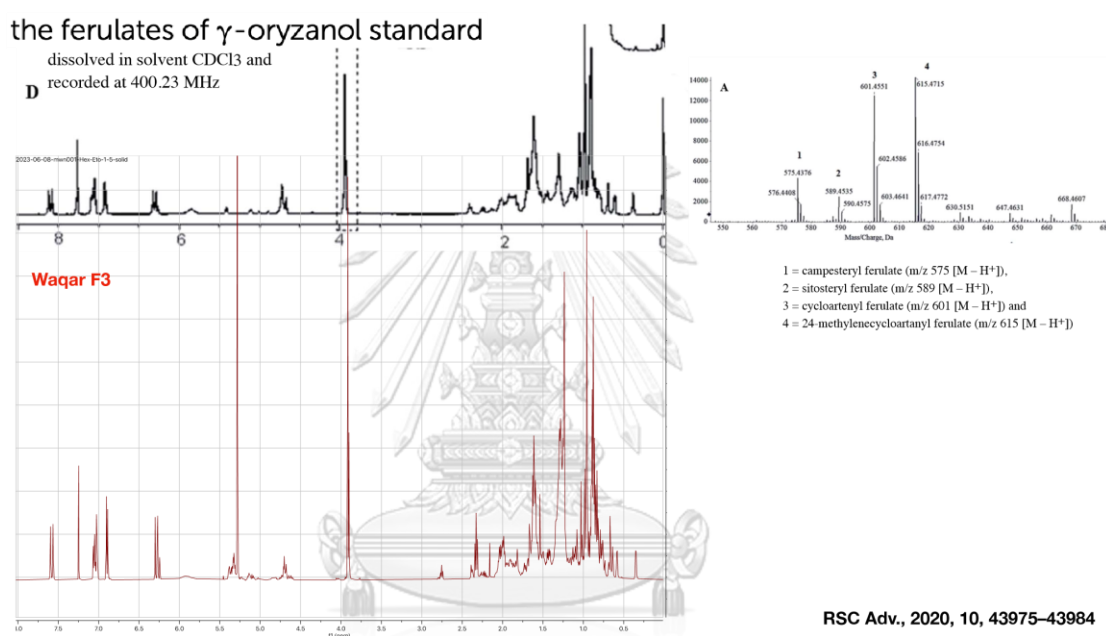
Figure 32 Compare ^{1}H NMR spectrum of isolated fraction 3 with previous data.
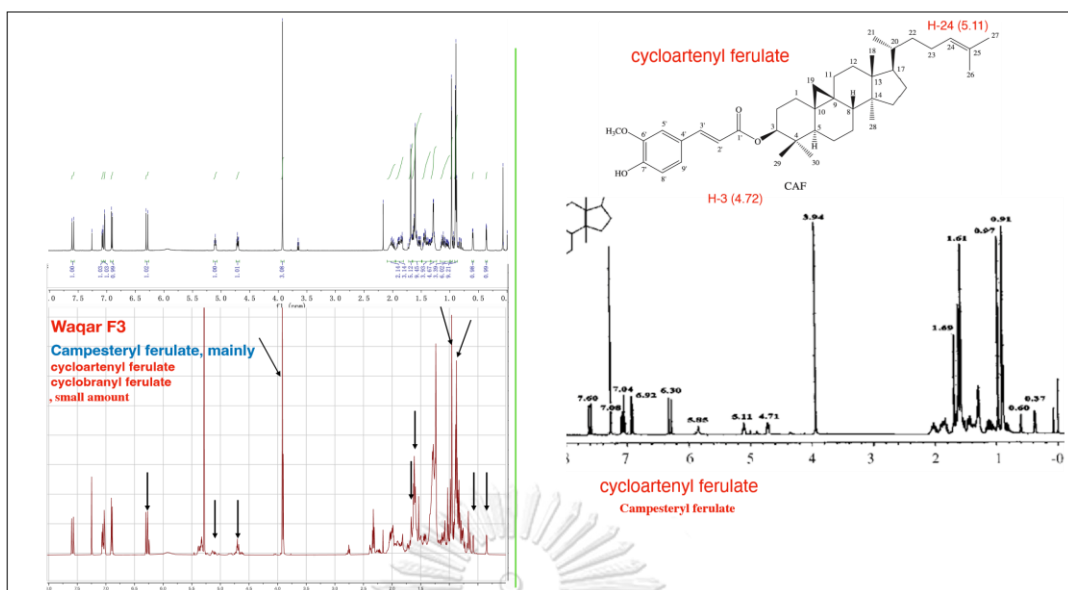
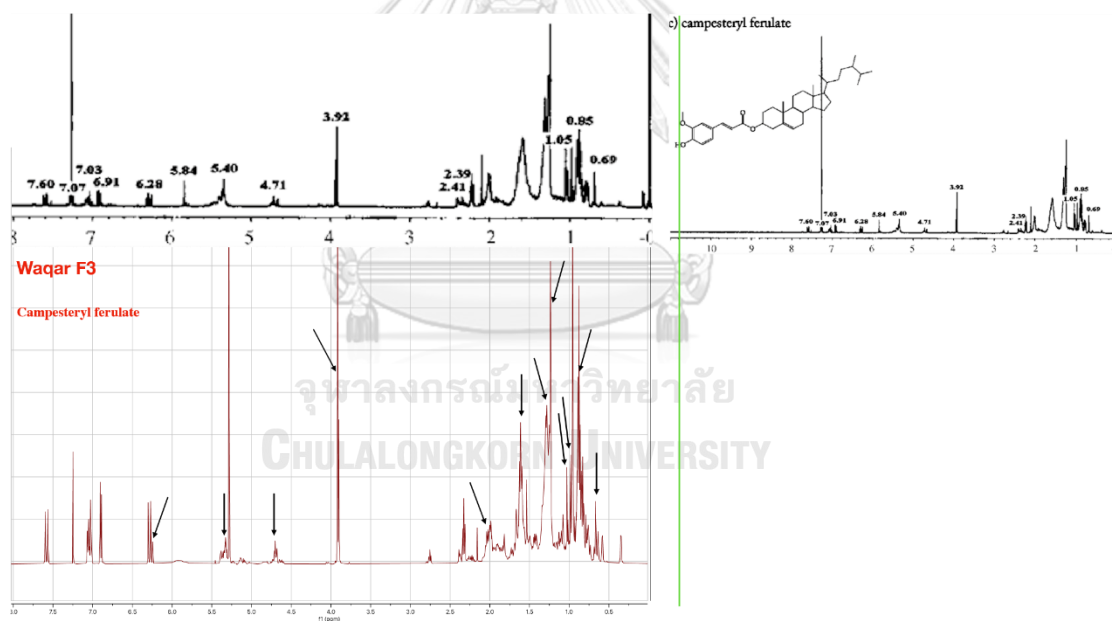**Figure 33** ^{1}H NMR spectrum of cycloartenyl ferulate compare with isolated fraction 3.

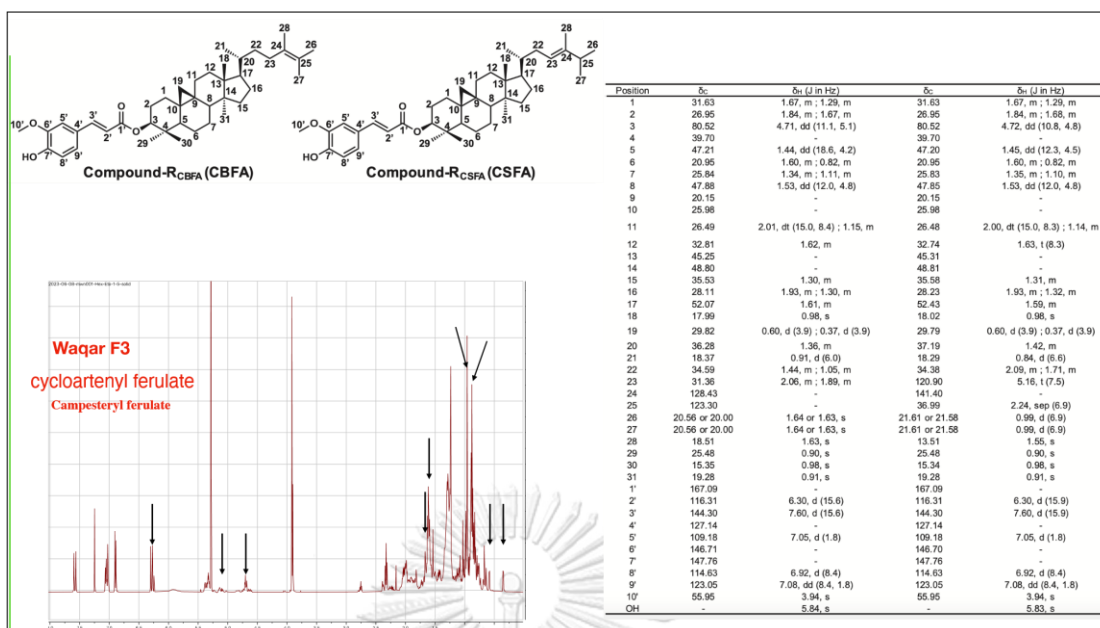**Figure 34** ^{1}H NMR spectrum of campesteryl ferulate compare with isolated fraction 3.

Position	δc	δH (J in Hz)	δc	δH (J in Hz)
1	31.63	1.67, m ; 1.29, m	31.63	1.67, m ; 1.29, m
2	26.95	1.84, m ; 1.67, m	26.95	1.84, m ; 1.68, m
3	80.52	4.71, dd (11.1, 5.1)	80.52	4.72, dd (10.8, 4.8)
4	39.70	-	39.70	-
5	47.21	1.44, dd (18.6, 4.2)	47.20	1.45, dd (12.3, 4.5)
6	20.95	1.60, m ; 0.82, m	20.95	1.60, m ; 0.82, m
7	25.84	1.34, m ; 1.11, m	25.83	1.35, m ; 1.10, m
8	47.88	1.53, dd (12.0, 4.8)	47.85	1.53, dd (12.0, 4.8)
9	20.15	-	20.15	-
10	25.98	-	25.98	-
11	26.49	2.01, dt (15.0, 8.4) ; 1.15, m	26.48	2.00, dt (15.0, 8.3) ; 1.14, m
12	32.81	1.62, m	32.74	1.63, t (8.3)
13	45.25	-	45.31	-
14	48.80	-	48.81	-
15	35.53	1.30, m	35.58	1.31, m
16	28.11	1.93, m ; 1.30, m	28.23	1.93, m ; 1.32, m
17	52.07	1.61, m	52.43	1.59, m
18	17.99	0.98, s	18.02	0.98, s
19	29.82	0.60, d (3.9) ; 0.37, d (3.9)	29.79	0.60, d (3.9) ; 0.37, d (3.9)
20	36.28	1.36, m	37.19	1.42, m
21	18.37	0.91, d (6.0)	18.29	0.84, d (6.6)
22	34.59	1.44, m ; 1.05, m	34.38	2.09, m ; 1.71, m
23	31.38	2.06, m ; 1.89, m	120.90	5.16, t (7.5)
24	128.43	-	141.40	-
25	123.30	-	36.99	2.24, sep (6.9)
26	20.56 or 20.00	1.64 or 1.63, s	21.61 or 21.58	0.99, d (6.9)
27	20.56 or 20.00	1.64 or 1.63, s	21.61 or 21.58	0.99, d (6.9)
28	18.51	1.63, s	13.51	1.55, s
29	25.48	0.90, s	25.48	0.90, s
30	15.35	0.98, s	15.34	0.98, s
31	19.28	0.91, s	19.28	0.91, s
1'	167.09	-	167.09	-
2'	116.31	6.30, d (15.6)	116.31	6.30, d (15.9)
3'	144.30	7.60, d (15.6)	144.30	7.60, d (15.9)
4'	127.14	-	127.14	-
5'	109.18	7.05, d (1.8)	109.18	7.05, d (1.8)
6'	146.71	-	146.70	-
7'	147.76	-	147.76	-
8'	114.63	6.92, d (8.4)	114.63	6.92, d (8.4)
9'	123.05	7.08, dd (8.4, 1.8)	123.05	7.08, dd (8.4, 1.8)
10'	55.95	3.94, s	55.95	3.94, s
OH	-	5.84, s	-	5.83, s

Figure 35 Compare ^{1}H NMR data of cycloartenyl ferulate and campesteryl ferulate of isolated fraction 3 with the previous data.

4.63 (m, H-3)
5.01 (dd, J = 15.2 and 8.7 Hz, 1H, H-23),
5.15 (dd, J = 15.2 and 8.6 Hz, 1H, H-22)
5.37 (m, H-6)
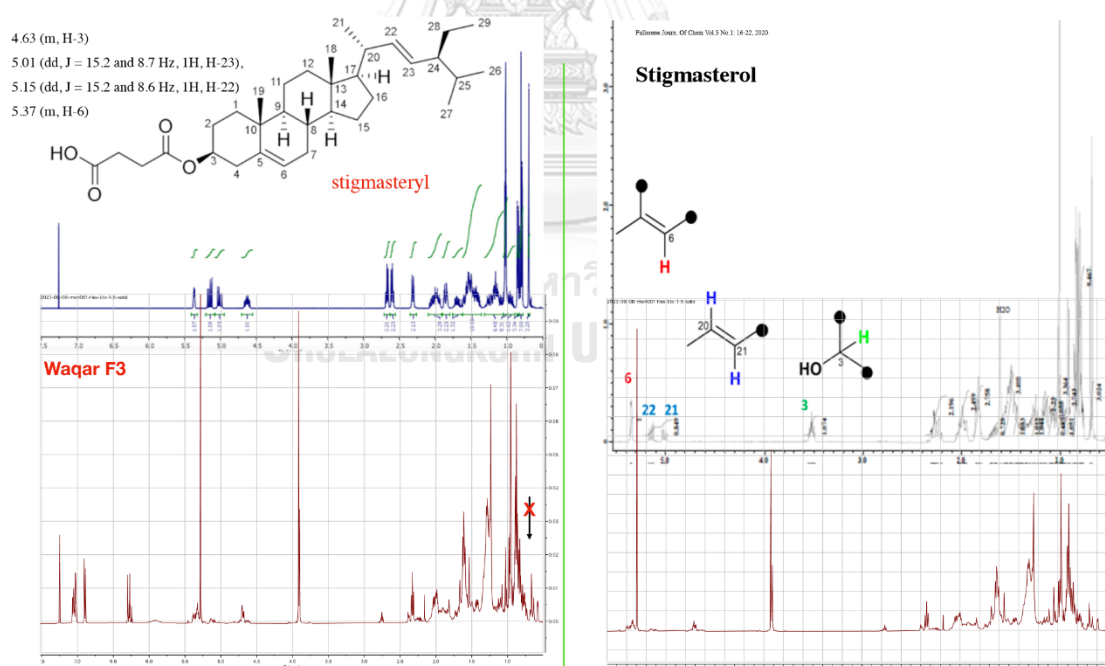
Figure 36 ^{1}H NMR spectrum of stigmasteryl of isolated fraction 3

Table 9 ^{1}H NMR data of cycloartenyl ferulate (CDCl$_3$, 500 MHz)

Position	Reference	δ_H (ppm), J in Hz	Position	Reference	δ_H (ppm), J in Hz
1	1.27, m	1.28, m	6	1.44, d (12.40, 4.35)	1.45, d (12.40, 4.35)
2	1.65, m	1.66, m	7	1.30, m	1.28, m
3	4.71, m	4.71, m	8	1.53, dd (12.15, 3.70)	1.54, dd (12.15, 3.70)
4	-	-	9	-	-
5	1.44, d (12.40, 4.35)	1.45, d (12.40, 4.35)	10	-	-
11	1.15, m	1.17, m	25	-	-
12	1.30, m	1.28, m	26, 27	1.68, s ; 1.61, s	1.68, s ; 1.61, s
13	-	-	28	0.97, s	0.96, s
14	-	-	29	0.90, s	0.90, s
15	1.63, m	1.64, m	30	0.97, s	0.96, s
16	1.11, m	1.15, m	1`	-	-
17	1.63, m	1.64, m	2`	6.29, d (15.90)	6.29, d (15.90)

18	0.91, s	0.89, s	3`	7.59, d (15.85)	7.60, d (15.85)
19	0.36, d (3.95) ; 0.60, d (3.90)	0.35, d (3.95) ; 0.58, d (3.90)	4`	-	-
20	1.40, m	1.41, m	5`	7.07, dd (8.15, 1.55)	7.06, dd (8.15, 1.55)
21	0.90, s	0.89, s	6`	6.91, d (8.15)	6.91, d (8.15)
22	1.15, m	1.17, m	7`	5.85, s	5.85, s
23	2.03, m	2.02, m	8`	6.92, d (8.4)	6.91, d (8.4)
24	5.10, t (6.75)	5.11, t (6.75)	9`	7.03, d (1.50)	7.03, d (1.50)
			10`	3.92, s	3.91, s
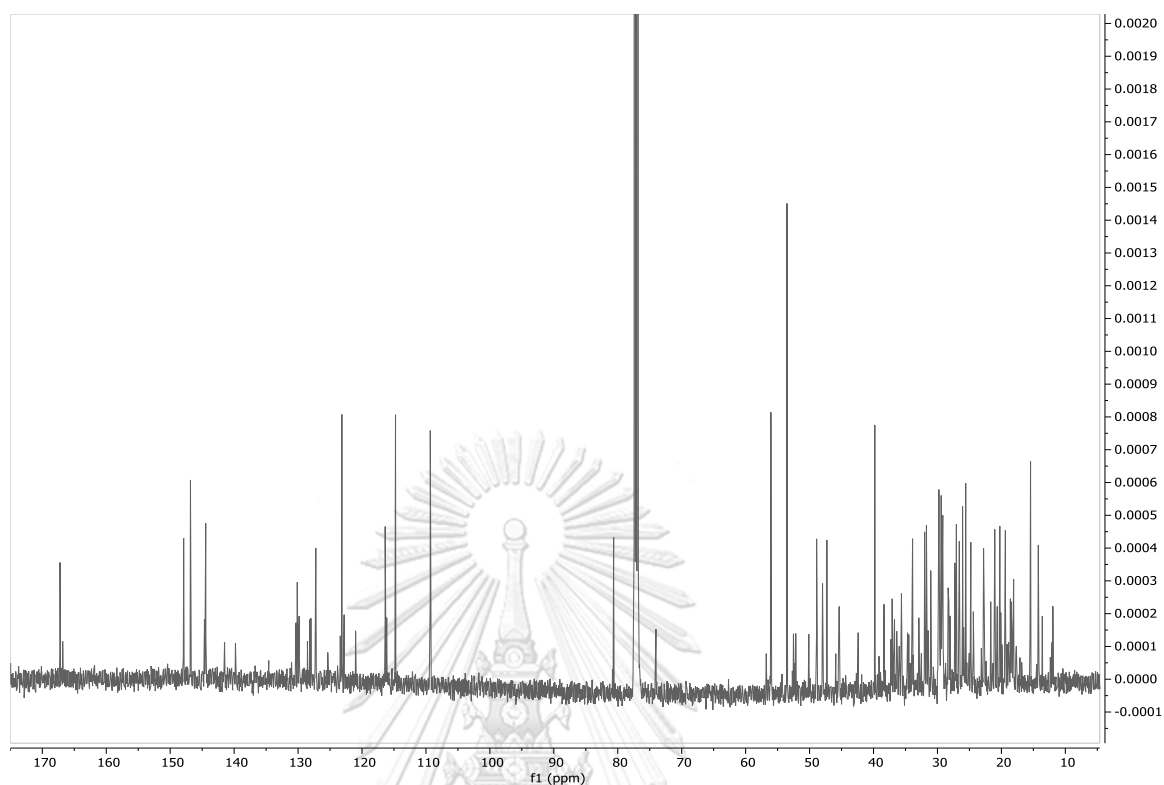
Figure 37 13C NMR spectrum of isolated fraction 1

Table 10 ^{13}C NMR data of cycloartenyl ferulate (CDCl$_3$, 500 MHz)

Position	Reference	δ_C (ppm)	Position	Reference	δ_C (ppm)
1	31.8	32.0	6	21.1	20.9
2	27.1	27.1	7	28.3	28.2
3	80.7	80.7	8	48.0	47.9
4	39.8	40.0	9	20.3	21.0
5	47.3	47.5	10	26.1	26.0
11	26.0	26.0	25	131.0	131.0

12	35.7	35.7	26, 27	17.8 ; 25.9	178 ; 25.9
13	45.3	45.4	28	19.4	20.0
14	48.9	49.0	29	25.6	25.6
15	33.0	33.0	30	15.5	16.0
16	26.6	27.0	1'	167.2	167.3
17	52.4	52.4	2'	116.4	116.5
18	18.1	18.0	3'	144.5	144.5
19	29.9	30.0	4'	127.3	127.3
20	36.0	36.0	5'	109.4	109.4
21	18.4	15.5	6'	146.9	146.9
22	36.5	36.6	7'	148.0	148.0
23	25.1	25.0	8'	114.8	114.7
24	125.4	125.6	9'	123.1	123
			10'	56.1	56.0

Cyclobranyl ferulate was another structure of cycloartenyl that are present in the mixture. It is molecular formula $C_{41}H_{60}O_4$, and its ^1H NMR data were shown in table 13. The structure of cyclobranyl ferulate was established as shown in figure 15 [114].
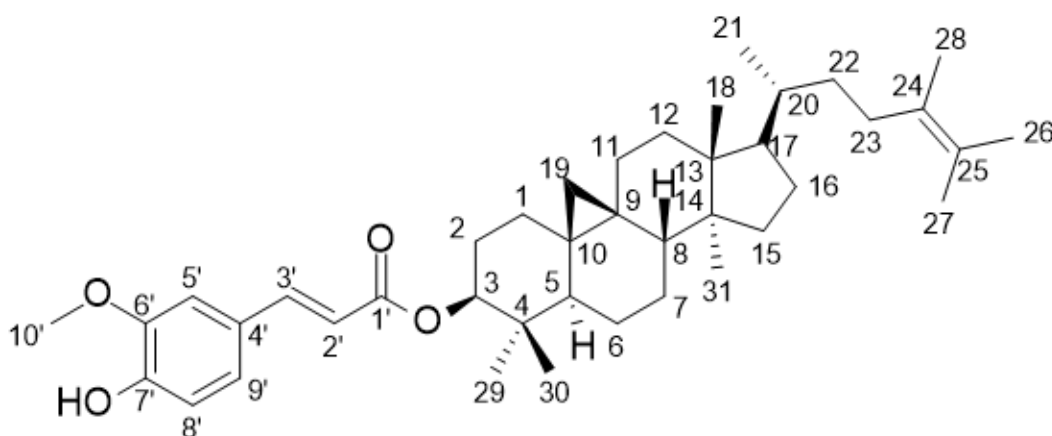
Figure 38 Structure of cyclobranyl ferulate

Table 11 ^1H NMR data of cyclobranyl ferulate (CDCl$_3$, 500 MHz)

Position	Reference	δ_H (ppm), J in Hz	Position	Reference	δ_H (ppm), J in Hz
1	1.67, m ; 1.29, m	1.68, m ; 1.30, m	6	1.60, m ; 0.82, m	1.60, m ; 0.90, m
2	1.84, m ; 1.67, m	1.85, m ; 1.68, m	7	1.34, m ; 1.11, m	1.32, m ; 1.10, m
3	4.71, dd (11.1, 5.1)	4.71, dd (11.1, 5.1)	8	1.53, dd (12.0, 4.8)	1.55, dd (12.0, 4.8)
4	-	-	9	-	-
5	1.44, dd (18.6, 4.2)	1.44. dd (18.6, 4.2)	10	-	-

Position	Reference	δ_H (ppm), J in Hz	Position	Reference	δ_H (ppm), J in Hz
11	2.01, dt (15.0, 8.4) ; 1.15, m	2.01, dt (15.0, 8.4) ; 1.13, m	25	-	-
12	1.62, m	1.62, m	26, 27	1.64, s ; 1.64, s	1.64, s ; 1.64, s
13	-	-	28	1.63, s	1.62, s
14	-	-	29	0.90, s	0.90, s
15	1.30, m	1.29, m	30	0.98, s	0.97, s
16	1.93, m ; 1.30, m	1.93, m ; 1.29, m	31	0.91, s	0.90, s
17	1.61, m	1.61, m	1`	-	-
18	0.96, s	0.96, s	2`	6.30, d (15.6)	6.29, d (15.6)
19	0.60, d (3.9) ; 0.37, d (3.9)	0.58, d (3.9) ; 0.35, d (3.9)	3`	7.60, d (15.6)	7.59, d (15.6)
20	1.36, m	1.36, m	4`	-	-
21	0.91, d (6.0)	0.90, d (6.0)	5`	7.05, d (1.8)	7.04, d (1.8)
22	1.44, m ; 1.05, m	1.44, m ; 1.05, m	6`	-	-
23	2.06, m ; 1.89, m	2.05, m ; 1.89, m	7`	-	-
24	-		8`	6.92, d (8.4)	6.90, d (8.4)
9'	7.08, dd (8.4, 1.8)	7.07, dd (8.4, 1.8)	10`	3.94, s	3.92, s

Table 12 $_{13}$C NMR data of cyclobranyl ferulate (CDCl3, 500 MHz)

Position	Reference	δ_C (ppm)	Position	Reference	δ_C (ppm)
1	31.63	32.0	6	20.95	21.0
2	26.95	27.1	7	25.84	25.83
3	80.52	80.7	8	47.86	47.9
4	39.70	40.0	9	20.15	20.1
5	47.21	47.5	10	25.98	25.92
11	26.49	26.0	21	18.37	18.37
12	32.81	35.7	22	34.59	34.60
13	45.25	45.4	23	31.36	31.40
14	48.80	49.0	24	128.43	128.5
15	35.53	33.0	25	123.30	123.25
16	28.11	27.0	26	20.56	21.00
17	52.07	52.4	27	20.56	21.00
18	17.99	18.0	28	18.51	18.75
19	29.82	30.0	29	25.48	25.55
20	36.28	36.0	30	15.35	15.90
31	19.28	19.38	6`	146.71	146.7

Position	Reference	δ_C (ppm)	Position	Reference	δ_C (ppm)
1`	167.09	167.0	7`	147.76	147.7
2`	116.31	116.3	8`	114.63	114.6
3`	144.30	144.3	9`	123.05	123.0
4`	127.14	126.9	10`	55.95	56.0
5`	109.18	109.18			

The other three structures of cycloartenyl are (24)-cycloart-25-ene-3β-24-diol-3β-trans ferulate, cycloart-23-*Z*-ene-3β-25-diol-3β-trans ferulate, and cycloeucalenyl ferulate have olefinic double bond in their structure. There is no peak of olefinic double bond in the ^{1}H and ^{13}C NMR spectrum. So, we can say these structures are not present in the mixture of compounds.

จุฬาลงกรณ์มหาวิทยาลัย

CHULALONGKORN UNIVERSITY

4.4 *In vitro* ACE2 Inhibition Assay
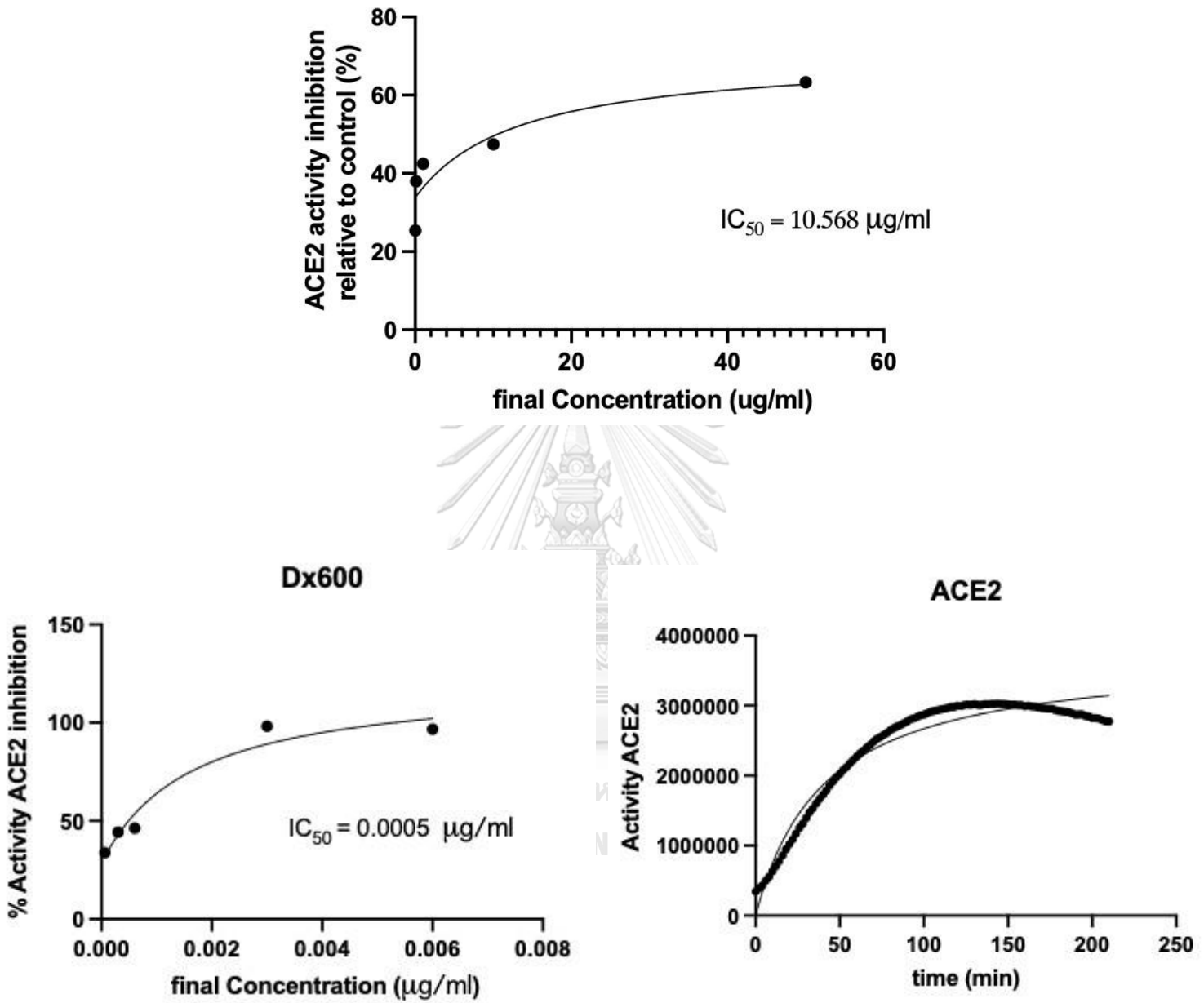
Figure 39 ACE2 inhibition assay

Compound	IC$_{50}$ value of inhibition, concentration in μg/ml
Isolated fraction 1 (Cycloartenyl ferulate, cycloartenyl caffeate, cycloartanyl ferulate, and cyclobranyl ferulate)	10.57
Positive control Dx600	0.0005

Table 13 IC 50 value of ACE2 inhibition assay

The isolated fraction 1 as a mixture of cycloartenyl ferulate, cycloartenyl caffeate, cycloartanyl ferulate, and cyclobranyl ferulate of γ-oryzanol was tested on ACE2 activity. The IC$_{50}$ value of the isolated γ-Oryzanol was 10.57 μg/ml. These results showed that the isolated γ-oryzanol showed potentials for ACE2 inhibitor.

CHAPTER V CONCLUSION

In conclusion, purification of γ-oryzanol from the crude rice bran acid fraction to get the three isolated fraction of γ-oryzanol containing cycloartenyl ferulate, campesteryl ferulate, sitosteryl ferulate, stigmasteryl ferulate, and cyclobranyl ferulate. The cycloartenyl ferulate and campesteryl ferulate as major components of γ-oryzanol showed good ACE2 inhibitory activity with the IC_{50} 10.57 μg/ml. Furthermore, the 19 structures of γ-oryzanol were also studied for their interaction against ACE2 through molecular docking. Based on the *in-silico* study, ADME investigation, and toxicity prediction, cycloartenyl ferulate and campesteryl ferulate out of 19 were potential to be developed as novel inhibitor for ACE2. This result demonstrated that the isolated γ-oryzanol from the crude acid fraction had the potential to be ACE2 inhibitor and its significant ACE2 inhibitory activity could serve as leads for the development of novel therapeutics targeting COVID-19.

REFERENCES

[1]   Sarker, S.D. and Nahar, L. Hyphenated techniques and their applications in natural products analysis. Natural Products Isolation (2012): 301-340.

[2]   Dias, D.A., Urban, S., and Roessner, U. A historical overview of natural products in drug discovery. Metabolites 2(2) (2012): 303-336.

[3]   Shao, Z. and Zhao, H. Manipulating natural product biosynthetic pathways via DNA assembler. Current protocols in chemical biology 6(2) (2014): 65-100.

[4]   Ram, M., Davari, M., and Sharma, S. Organic farming of rice (Oryza sativa L.)-wheat (Triticum aestivum L.) cropping system: a review. International Journal of Agronomy and Plant Production 2(3) (2011): 114-134.

[5]   Kochhar, S.P. 11 Minor and Speciality Oils. Vegetable oils in food technology: composition, properties and uses (2011): 291.

[6]   Islam, S., et al. Biological abilities of rice bran-derived antioxidant phytochemicals for medical therapy. Current Topics in Medicinal Chemistry 11(14) (2011): 1847-1853.

[7]   B Ghatak, S. and J Panchal, S. Gamma-oryzanol-A multi-purpose steryl ferulate. Current Nutrition & Food Science 7(1) (2011): 10-20.

[8]   Tan, Z. and Shahidi, F. Chemoenzymatic synthesis of phytosteryl ferulates and evaluation of their antioxidant activity. Journal of agricultural and food chemistry 59(23) (2011): 12375-12383.

[9]   Organization, W.H. Evaluation of certain contaminants in food: ninety-third report of the Joint FAO/WHO Expert Committee on Food Additives. (2023).

[10]   Orthoefer, F.T. and Eastman, J. Rice bran oil. <u>Bailey's industrial oil and fat products</u> 2(7) (2005): 465-489.

[11]   Webb, B., Bollich, C., Carnahan, H., Kuenzel, K., and McKenzie, K. Utilization characteristics and qualities of United States rice. <u>Rice grain quality and marketing. IRRI, Manila, Philippines</u> (1985): 25-35.

[12]   Kiritsakis, A. Flavor components of olive oil—A review. <u>Journal of the American Oil Chemists' Society</u> 75(6) (1998): 673-681.

[13]   Devi, R., Veliveli, V.L., and Devi, S.S. Nutritional composition of rice bran and its potentials in the development of nutraceuticals rich products. <u>Journal of Pharmacognosy and Phytochemistry</u> 10(2) (2021): 470-473.

[14]   Mohapatra, P.K., Sahu, B.B., Mohapatra, P.K., and Sahu, B.B. Fertilization and Seed Development in Rice. <u>Panicle Architecture of Rice and its Relationship with Grain Filling</u> (2022): 63-86.

[15]   Saunders, R. Rice bran: Composition and potential food uses. <u>Food Reviews International</u> 1(3) (1985): 465-495.

[16]   Miller, D.D. Minerals. in <u>Fennema's food chemistry</u>, pp. 627-679: CRC Press, 2017.

[17]   Punia, S., Kumar, M., Siroha, A.K., and Purewal, S.S. Rice bran oil: Emerging trends in extraction, health benefit, and its industrial application. <u>Rice science</u> 28(3) (2021): 217-232.

[18] WANGDEE, M.K. UTILIZATION OF SOAPSTOCK FROM RICE BRAN OIL PRODUCTION. International journal of food science and technology 38 (2003): 95-102.

[19] Punia, S., Kumar, M., Sandhu, K.S., and Whiteside, W.S. Rice-bran oil: An emerging source of functional oil. Journal of Food Processing and Preservation 45(4) (2021): e15318.

[20] Lai, O.-M., Jacoby, J.J., Leong, W.-F., and Lai, W.-T. Nutritional studies of rice bran oil. Rice bran and rice bran oil (2019): 19-54.

[21] Ghosh, M. Review on recent trends in rice bran oil processing. Journal of the American oil chemists' society 84 (2007): 315-324.

[22] Patel, M. and Naik, S. Gamma-oryzanol from rice bran oil–A review. (2004).

[23] Seetharamaiah, G. and Prabhakar, J. Oryzanol content of Indian rice bran oil and its extraction from soap stock. Journal of Food Science and Technology, India 23(5) (1986): 270-273.

[24] Song, G., Zhang, M., Peng, X., Yu, X., Dai, Z., and Shen, Q. Effect of deodorization method on the chemical and nutritional properties of fish oil during refining. LWT 96 (2018): 560-567.

[25] De, B. and Bhattacharyya, D. Physical refining of rice bran oil in relation to degumming and dewaxing. Journal of the American Oil Chemists' Society 75(11) (1998): 1683-1686.

[26]   Li, D., Liu, P., Wang, W., Wang, X., Yang, B., and Wang, Y. An innovative deacidification approach for producing partial glycerides-free rice bran oil. Food and Bioprocess Technology 10 (2017): 1154-1161.

[27]   Van Hoed, V., Vila Ayala, J., Czarnowska, M., De Greyt, W., and Verhé, R. Optimization of physical refining to produce rice bran oil with light color and high oryzanol content. Journal of the American Oil Chemists' Society 87 (2010): 1227-1234.

[28]   Xu, Z. and Godber, J.S. Purification and identification of components of γ-oryzanol in rice bran oil. Journal of agricultural and food chemistry 47(7) (1999): 2724-2728.

[29]   Manasa, V., Chaudhari, S.R., and Tumaney, A.W. Spice fixed oils as a new source of γ-oryzanol: Nutraceutical characterization of fixed oils from selected spices. RSC advances 10(72) (2020): 43975-43984.

[30]   Sawada, K., et al. Absorption and metabolism of γ-oryzanol, a characteristic functional ingredient in rice bran. Journal of nutritional science and vitaminology 65(Supplement) (2019): S180-S184.

[31]   Lerma-García, M., Herrero-Martínez, J., Simó-Alfonso, E., Mendonça, C.R., and Ramis-Ramos, G. Composition, industrial processing and applications of rice bran γ-oryzanol. Food Chemistry 115(2) (2009): 389-404.

[32]   Lemus, C., Angelis, A., Halabalaki, M., and Skaltsounis, A.L. γ-Oryzanol: An attractive bioactive component from rice bran. in Wheat and rice in disease prevention and health, pp. 409-430: Elsevier, 2014.

[33]   Singanusong, R. and Garba, U. Micronutrients in rice bran oil. in Rice bran and rice bran oil, pp. 125-158: Elsevier, 2019.

[34]   Cheetangdee, N. Rice phenolics: extraction, characterization, and utilization in foods. in Polyphenols in plants, pp. 217-242: Elsevier, 2019.

[35]   Wen, T.X. Extraction and Analysis of Antioxidant Capacity in Rice Bran Extracts from Different Sarawak Local Rice Varieties. Malaysia: Swinburne University of Technology (2015).

[36]   Wang, T., Hicks, K.B., and Moreau, R. Antioxidant activity of phytosterols, oryzanol, and other phytosterol conjugates. Journal of the American Oil Chemists' Society 79(12) (2002): 1201-1206.

[37]   Kim, J.-S. Antioxidant activity of γ-oryzanol and synthetic phenolic compounds in an oil/water (O/W) emulsion system. Journal of Food Science and Nutrition 12(3) (2007): 173-176.

[38]   Xu, Z. and Godber, J.S. Antioxidant activities of major components of γ-oryzanol from rice bran using a linoleic acid model. Journal of the American Oil Chemists' Society 78(6) (2001): 645.

[39]   Kim, J.-S., Godber, J., King, J., and Prinyawiwatkul, W. Inhibition of cholesterol autoxidation by the nonsaponifiable fraction in rice bran in an aqueous model system. Journal of the American Oil Chemists' Society 78(7) (2001): 685-689.

[40]   Woods, J. and O'Brien, N. Investigation of the potential genotoxidty of cholesterol oxidation products in two mammalian fibroblast cell lines. (1998).

[41]   Ansari, G., Walker, R., Smart, V., and Smith, L. Further investigations of mutagenic cholesterol preparations. Food and Chemical Toxicology 20(1) (1982): 35-41.

[42]   Kumar, N. and Singhal, O. Cholesterol oxides and atherosclerosis: a review. Journal of the Science of Food and Agriculture 55(4) (1991): 497-510.

[43]   Xu, Z., Hua, N., and Godber, J.S. Antioxidant activity of tocopherols, tocotrienols, and γ-oryzanol components from rice bran against cholesterol oxidation accelerated by 2, 2 '-azobis (2-methylpropionamidine) dihydrochloride. Journal of agricultural and food chemistry 49(4) (2001): 2077-2081.

[44]   Droge, W. Free radicals in the physiological control of cell function. Physiological reviews 82(1) (2002): 47-95.

[45]   Ichimaru, Y., Moriyama, M., Ichimaru, M., and Gomita, Y. Effects of gamma-oryzanol on gastric lesions and small intestinal propulsive activity in mice. Nihon Yakurigaku zasshi. Folia Pharmacologica Japonica 84(6) (1984): 537-542.

[46] Akihisa, T. and Yasukawa, K. Anti-inflammatory and antiallergic properties of triterpenoids from plants. in Biomaterials from Aquatic and Terrestrial Organisms, pp. 75-126: CRC Press, 2006.

[47] Cordaro, M., et al. Effect of N-palmitoylethanolamine-oxazoline on comorbid neuropsychiatric disturbance associated with inflammatory bowel disease. The FASEB Journal 34(3) (2020): 4085-4106.

[48] Chotimarkorn, C. and Ushio, H. The effect of trans-ferulic acid and gamma-oryzanol on ethanol-induced liver injury in C57BL mouse. Phytomedicine 15(11) (2008): 951-958.

[49] Oka, T., Fujimoto, M., Nagasaka, R., Ushio, H., Hori, M., and Ozaki, H. Cycloartenyl ferulate, a component of rice bran oil-derived γ-oryzanol, attenuates mast cell degranulation. Phytomedicine 17(2) (2010): 152-156.

[50] Sulaiman, A., Sulaiman, A., Sert, M., Khan, M.S.A., and Khan, M.A. Functional and Therapeutic Potential of γ-Oryzanol. in Functional Foods-Phytochemicals and Health Promoting Potential: IntechOpen, 2021.

[51] Ghatak, S.B. and Panchal, S.S. Anti-diabetic activity of oryzanol and its relationship with the anti-oxidant property. International Journal of Diabetes in Developing Countries 32 (2012): 185-192.

[52] Cheng, H.-H., Ma, C.-Y., Chou, T.-W., Chen, Y.-Y., and Lai, M.-H. Gamma-oryzanol ameliorates insulin resistance and hyperlipidemia in rats with

streptozotocin/nicotinami-de-induced type 2 diabetes. <u>Int. J. Vitam. Nutr. Res</u> 80(1) (2010): 45-53.

[53]   Ghatak, S.B. and Panchal, S.S. Protective effect of oryzanol isolated from crude rice bran oil in experimental model of diabetic neuropathy. <u>Revista Brasileira de Farmacognosia</u> 22 (2012): 1092-1103.

[54]   Yasukawa, K., Akihisa, T., Kimura, Y., TAMURA, T., and TAKIDO, M. Inhibitory effect of cycloartenol ferulate, a component of rice bran, on tumor promotion in two-stage carcinogenesis in mouse skin. <u>Biological and Pharmaceutical Bulletin</u> 21(10) (1998): 1072-1076.

[55]   Kim, S.P., Kang, M.Y., Nam, S.H., and Friedman, M. Dietary rice bran component γ-oryzanol inhibits tumor growth in tumor-bearing mice. <u>Molecular nutrition & food research</u> 56(6) (2012): 935-944.

[56]   Tamagawa, M., Otaki, Y., Takahashi, T., Otaka, T., Kimura, S., and Miwa, T. Carcinogenicity study of γ-oryzanol in B6C3F1 mice. <u>Food and chemical toxicology</u> 30(1) (1992): 49-56.

[57]   Tamagawa, M., et al. Carcinogenicity study of γ-oryzanol in F344 rats. <u>Food and chemical toxicology</u> 30(1) (1992): 41-48.

[58]   Hirose, M., Ozaki, K., Takaba, K., Fukushima, S., Shirai, T., and Nobuyuki, I. Modifying effects of the naturally occurring antioxidants γ-oryzanol, phytic acid,

tannic acid and n-tritriacontane-16, 18-dione in a rat wide-spectrum organ carcinogenesis model. <u>Carcinogenesis</u> 12(10) (1991): 1917-1921.

[59]   Hirose, M., Fukushima, S., Imaida, K., Ito, N., and Shirai, T. Modifying effects of phytic acid and gamma-oryzanol on the promotion stage of rat carcinogenesis. <u>Anticancer research</u> 19(5A) (1999): 3665-3670.

[60]   Suzuki, S. and Oshima, S. Influence of Blending of Edible Fats and Oils on Human Serum Cholesterol Level (Part 1) Blending of Rice Bran Oil and Safflower Oil. <u>The Japanese Journal of Nutrition and Dietetics</u> 28(1) (1970): 3-6.

[61]   Ishihara, M. Effect of γ-Oryzanol on Serum Lipid Peroxide Level and Clinical Symptoms of Patients with Climacteric Disturbances. <u>Asia-Oceania Journal of Obstetrics and Gynaecology</u> 10(3) (1984): 317-323.

[62]   Yoshino, G., Kazumi, T., Amano, M., Tateiwa, M., Yamasaki, T., and Takashima, S. Effects of gamma-oryzanol and probucol on hyperlipidemia. <u>Current therapeutic research</u> 45(6) (1989): 975-982.

[63]   Sasaki, J., et al. Effects of gamma-oryzanol on serum lipids and apolipoproteins in dyslipidemic schizophrenics receiving major tranquilizers. <u>Clinical therapeutics</u> 12(3) (1990): 263-268.

[64]   Berger, A., et al. Similar cholesterol–lowering properties of rice bran oil, with varied γ–oryzanol, in mildly hypercholesterolemic men. <u>European Journal of Nutrition</u> 44 (2005): 163-173.

[65]   Ghatak, S.B. and Panchal, S.J. Anti-hyperlipidemic activity of oryzanol, isolated from crude rice bran oil, on Triton WR-1339-induced acute hyperlipidemia in rats. Revista brasileira de farmacognosia 22 (2012): 642-648.

[66]   Hiramatsu, K., Tani, T., Kimura, Y., Izumi, S.-i., and Nakane, P.K. Effect of gamma-oryzanol on atheroma formation in hypercholesterolemic rabbits. The Tokai Journal of Experimental and Clinical Medicine 15(4) (1990): 299-305.

[67]   Negm, C. and Silliman, K. The effects of rice bran oil and oryzanol on plasma levels of total cholesterol and hdl-cholesterol in male golden hamsters. Journal of the American Dietetic Association 95(9) (1995): A29.

[68]   Rong, N., Ausman, L.M., and Nicolosi, R.J. Oryzanol decreases cholesterol absorption and aortic fatty streaks in hamsters. Lipids 32(3) (1997): 303-309.

[69]   Shahidi, F., et al. Wheat and Rice beyond Phenolic Acids: Genetics, Identification Database, Antioxidant Properties, and Potential Health Effects. Plants 11(23) (2022): 3283.

[70]   Murase, Y. and Iishima, H. Clinical studies of oral administration of gamma-oryzanol on climacteric complaints and its syndrome. Obstet Gynecol Prac 12(3) (1963).

[71]   Ishihara, M., et al. Clinical effect of gamma-oryzanol on climacteric disturbance-on serum lipid peroxides (author's transl). Nihon Sanka Fujinka Gakkai Zasshi 34(2) (1982): 243-251.

[72] Borud, E., Grimsgaard, S., and White, A. Menopausal problems and acupuncture. Autonomic Neuroscience 157(1-2) (2010): 57-62.

[73] Cho, S.-H. and Whang, W.-W. Acupuncture for vasomotor menopausal symptoms: a systematic review. Menopause 16(5) (2009): 1065-1073.

[74] Ma, X.-p., Wu, F.-d., and Shan, Q.-h. Clinical observation on treating menopause syndrome with acupuncture therapy. Journal of Acupuncture and Tuina Science 7 (2009): 51-54.

[75] Mannhold, R., Kubinyi, H., and Folkers, G. Virtual screening: principles, challenges, and practical guidelines. John Wiley & Sons, 2011.

[76] Meng, X.-Y., Zhang, H.-X., Mezei, M., and Cui, M. Molecular docking: a powerful approach for structure-based drug discovery. Current computer-aided drug design 7(2) (2011): 146-157.

[77] Tipnis, S.R., Hooper, N.M., Hyde, R., Karran, E., Christie, G., and Turner, A.J. A human homolog of angiotensin-converting enzyme: cloning and functional expression as a captopril-insensitive carboxypeptidase. Journal of Biological Chemistry 275(43) (2000): 33238-33243.

[78] Burrell, L.M., Harrap, S.B., Velkoska, E., and Patel, S.K. The ACE2 gene: its potential as a functional candidate for cardiovascular disease. Clinical science 124(2) (2013): 65-76.

[79]   Donoghue, M., et al. A novel angiotensin-converting enzyme–related carboxypeptidase (ACE2) converts angiotensin I to angiotensin 1-9. Circulation research 87(5) (2000): e1-e9.

[80]   Lane, T., et al. Natural history, quality of life, and outcome in cardiac transthyretin amyloidosis. Circulation 140(1) (2019): 16-26.

[81]   Rice, G.I., Thomas, D.A., Grant, P.J., Turner, A.J., and Hooper, N.M. Evaluation of angiotensin-converting enzyme (ACE), its homologue ACE2 and neprilysin in angiotensin peptide metabolism. Biochemical Journal 383(1) (2004): 45-51.

[82]   Walls, A.C., Park, Y.-J., Tortorici, M.A., Wall, A., McGuire, A.T., and Veesler, D. Structure, function, and antigenicity of the SARS-CoV-2 spike glycoprotein. Cell 181(2) (2020): 281-292. e6.

[83]   Yan, R., Zhang, Y., Guo, Y., Xia, L., and Zhou, Q. Structural basis for the recognition of the 2019-nCoV by human ACE2. BioRxiv (2020): 2020.02. 19.956946.

[84]   Li, F., Li, W., Farzan, M., and Harrison, S.C. Structure of SARS coronavirus spike receptor-binding domain complexed with receptor. Science 309(5742) (2005): 1864-1868.

[85]   Wrapp, D., et al. Cryo-EM structure of the 2019-nCoV spike in the prefusion conformation. Science 367(6483) (2020): 1260-1263.

[86]   Perlman, S. and Netland, J. Coronaviruses post-SARS: update on replication and pathogenesis. Nature reviews microbiology 7(6) (2009): 439-450.

[87]   Künkel, F. and Herrler, G. Structural and functional analysis of the surface protein of human coronavirus OC43. Virology 195(1) (1993): 195-202.

[88]   McIntosh, K., Dees, J.H., Becker, W.B., Kapikian, A.Z., and Chanock, R.M. Recovery in tracheal organ cultures of novel viruses from patients with respiratory disease. Proceedings of the National Academy of Sciences 57(4) (1967): 933-940.

[89]   Ngandu, T., et al. A 2 year multidomain intervention of diet, exercise, cognitive training, and vascular risk monitoring versus control to prevent cognitive decline in at-risk elderly people (FINGER): a randomised controlled trial. The Lancet 385(9984) (2015): 2255-2263.

[90]   Wang, D., et al. Clinical characteristics of 138 hospitalized patients with 2019 novel coronavirus–infected pneumonia in Wuhan, China. jama 323(11) (2020): 1061-1069.

[91]   Yang, X., et al. Clinical course and outcomes of critically ill patients with SARS-CoV-2 pneumonia in Wuhan, China: a single-centered, retrospective, observational study. The lancet respiratory medicine 8(5) (2020): 475-481.

[92]   Ding, Y., et al. Organ distribution of severe acute respiratory syndrome (SARS) associated coronavirus (SARS-CoV) in SARS patients: implications for pathogenesis and virus transmission pathways. The Journal of Pathology: A Journal of the Pathological Society of Great Britain and Ireland 203(2) (2004): 622-630.

[93]   Gu, J., et al. Multiple organ infection and the pathogenesis of SARS. <u>The Journal of experimental medicine</u> 202(3) (2005): 415-424.

[94]   Al-Kuraishy, H.M., et al. 5-HT/CGRP pathway and Sumatriptan role in Covid-19. <u>Biotechnology and Genetic Engineering Reviews</u> (2022): 1-26.

[95]   Zhong, J., et al. Prevention of angiotensin II–mediated renal oxidative stress, inflammation, and fibrosis by angiotensin-converting enzyme 2. <u>Hypertension</u> 57(2) (2011): 314-322.

[96]   Alenina, N., Xu, P., Rentzsch, B., Patkin, E.L., and Bader, M. Genetically altered animal models for Mas and angiotensin-(1–7). <u>Experimental physiology</u> 93(5) (2008): 528-537.

[97]   Basu, R., Poglitsch, M., Yogasundaram, H., Thomas, J., Rowe, B.H., and Oudit, G.Y. Roles of angiotensin peptides and recombinant human ACE2 in heart failure. <u>Journal of the American College of Cardiology</u> 69(7) (2017): 805-819.

[98]   Dell'Italia, L.J., Collawn, J.F., and Ferrario, C.M. Multifunctional role of chymase in acute and chronic tissue injury and remodeling. <u>Circulation research</u> 122(2) (2018): 319-336.

[99]   Patel, V.B., et al. Angiotensin II induced proteolytic cleavage of myocardial ACE2 is mediated by TACE/ADAM-17: a positive feedback mechanism in the RAS. <u>Journal of molecular and cellular cardiology</u> 66 (2014): 167-176.

[100] Ishiyama, Y., Gallagher, P.E., Averill, D.B., Tallant, E.A., Brosnihan, K.B., and Ferrario, C.M. Upregulation of angiotensin-converting enzyme 2 after myocardial

infarction by blockade of angiotensin II receptors. <u>Hypertension</u> 43(5) (2004): 970-976.

[101] Ferrario, C.M., et al. Effect of angiotensin-converting enzyme inhibition and angiotensin II receptor blockers on cardiac angiotensin-converting enzyme 2. <u>Circulation</u> 111(20) (2005): 2605-2610.

[102] Scholz, A.J., Steinback, C., Kruse, S.A., Mertens, M., and Silverman, H. Incorporation of spatial and economic analyses of human-use data in the design of marine protected areas. <u>Conservation Biology</u> 25(3) (2011): 485-492.

[103] Ferrario, C.M., Trask, A.J., and Jessup, J.A. Advances in biochemical and functional roles of angiotensin-converting enzyme 2 and angiotensin-(1–7) in regulation of cardiovascular function. <u>American Journal of Physiology-Heart and Circulatory Physiology</u> 289(6) (2005): H2281-H2290.

[104] Gembardt, F., et al. Organ-specific distribution of ACE2 mRNA and correlating peptidase activity in rodents. <u>Peptides</u> 26(7) (2005): 1270-1277.

[105] Lo, C.-S., et al. Dual RAS blockade normalizes angiotensin-converting enzyme-2 expression and prevents hypertension and tubular apoptosis in Akita angiotensinogen-transgenic mice. <u>American Journal of Physiology-Renal Physiology</u> 302(7) (2012): F840-F852.

[106] Koka, V., Huang, X.R., Chung, A.C., Wang, W., Truong, L.D., and Lan, H.Y. Angiotensin II up-regulates angiotensin I-converting enzyme (ACE), but down-

regulates ACE2 via the AT1-ERK/p38 MAP kinase pathway. The American journal of pathology 172(5) (2008): 1174-1183.

[107]   Scott, A.J., et al. Reactive oxygen species and p38 mitogen-activated protein kinase mediate tumor necrosis factor α-converting enzyme (TACE/ADAM-17) activation in primary human monocytes. Journal of Biological Chemistry 286(41) (2011): 35466-35476.

[108]   Xu, P. and Derynck, R. Direct activation of TACE-mediated ectodomain shedding by p38 MAP kinase regulates EGF receptor-dependent cell proliferation. Molecular cell 37(4) (2010): 551-566.

[109]   Gheblawi, M., et al. Angiotensin-converting enzyme 2: SARS-CoV-2 receptor and regulator of the renin-angiotensin system: celebrating the 20th anniversary of the discovery of ACE2. Circulation research 126(10) (2020): 1456-1474.

[110]   Liu, X., Raghuvanshi, R., Ceylan, F.D., and Bolling, B.W. Quercetin and its metabolites inhibit recombinant human angiotensin-converting enzyme 2 (ACE2) activity. Journal of agricultural and food chemistry 68(47) (2020): 13982-13989.

[111]   Hou, T., Wang, J., Zhang, W., and Xu, X. ADME evaluation in drug discovery. 6. Can oral bioavailability in humans be effectively predicted by simple molecular property-based rules? Journal of Chemical Information and Modeling 47(2) (2007): 460-463.

[112]   Veber, D.F., Johnson, S.R., Cheng, H.-Y., Smith, B.R., Ward, K.W., and Kopple, K.D. Molecular properties that influence the oral bioavailability of drug candidates. Journal of medicinal chemistry 45(12) (2002): 2615-2623.

[113]   Shen, J., Yang, Y., Broughton, H., Watson, I.A., and Desai, P.V. High-throughput hydrogen bond strength calculation and its applications in optimizing drug ADME properties. Future Medicinal Chemistry 11(6) (2019): 511-524.

[114]   Sawada, K., et al. Isolation and structural elucidation of unique γ-oryzanol species in rice bran oil. Food Chemistry 337 (2021): 127956.
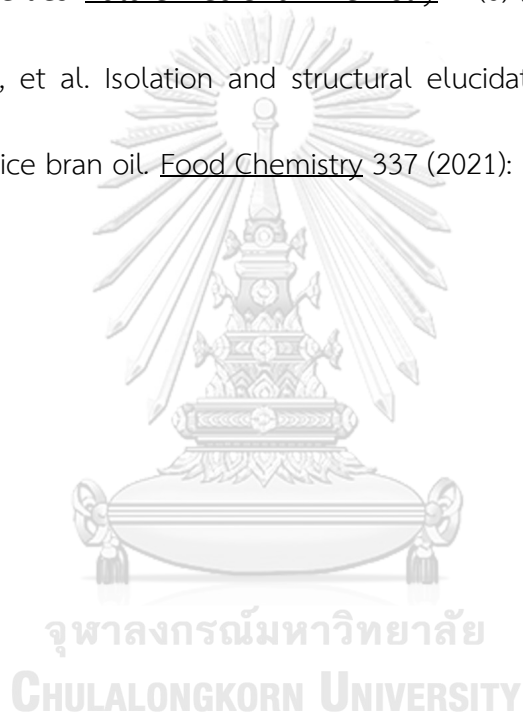
APPENDIX
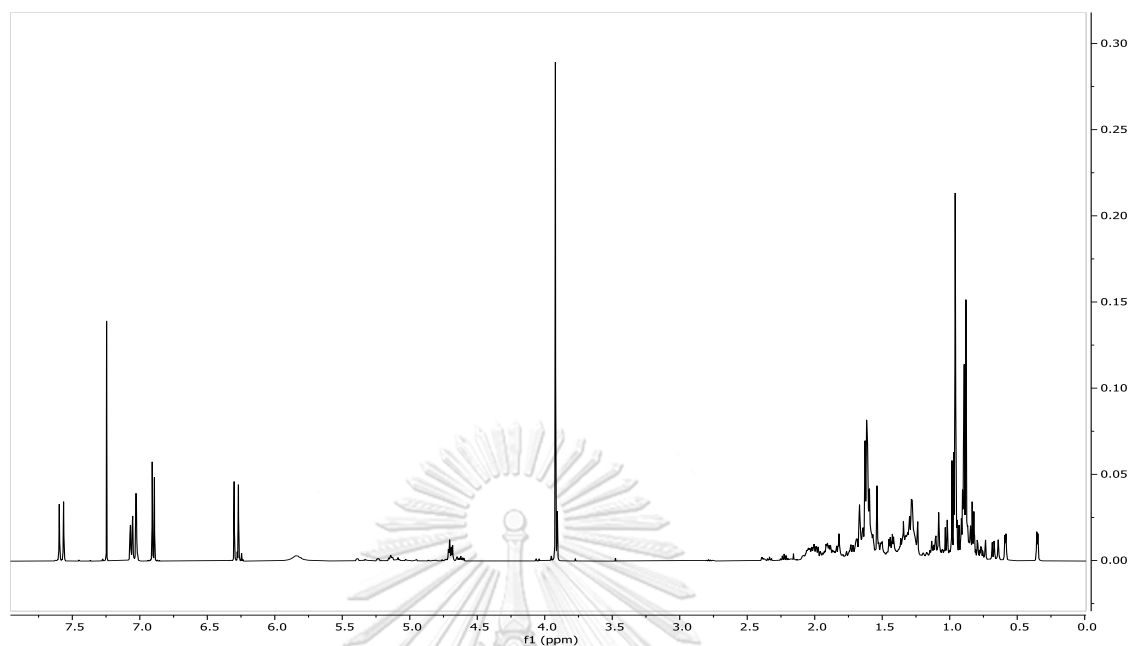
Figure A.1 ^{1}H NMR spectrum (500 MHz, CDCl$_3$) of compound 1
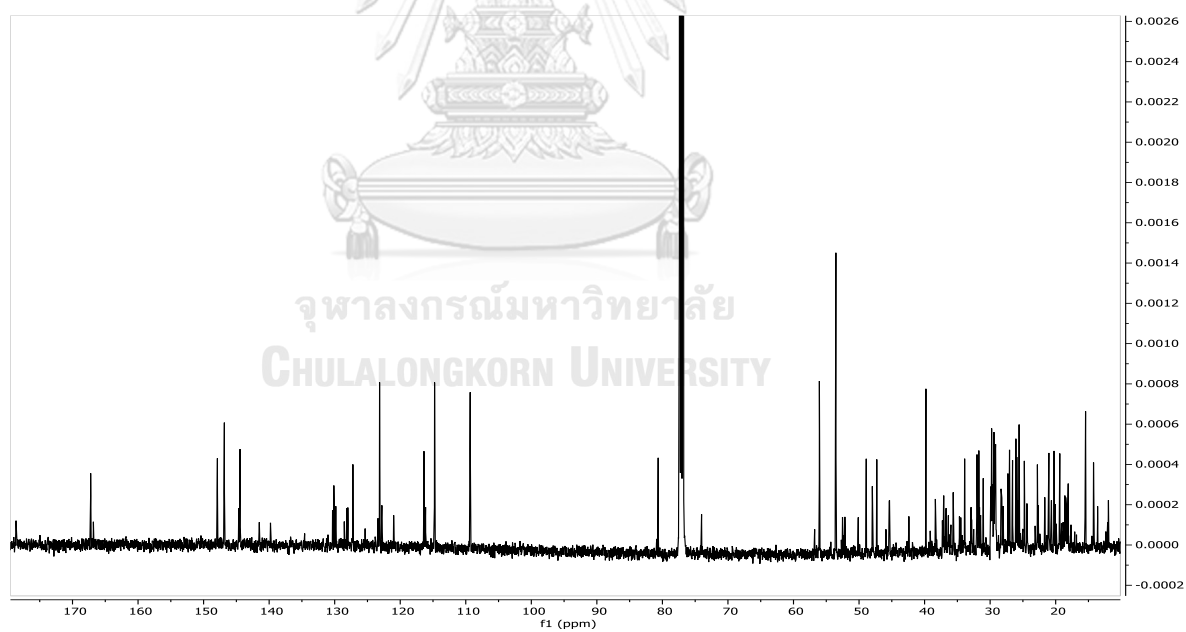
Figure A.2 ^{13}C spectrum NMR spectrum of compound 1
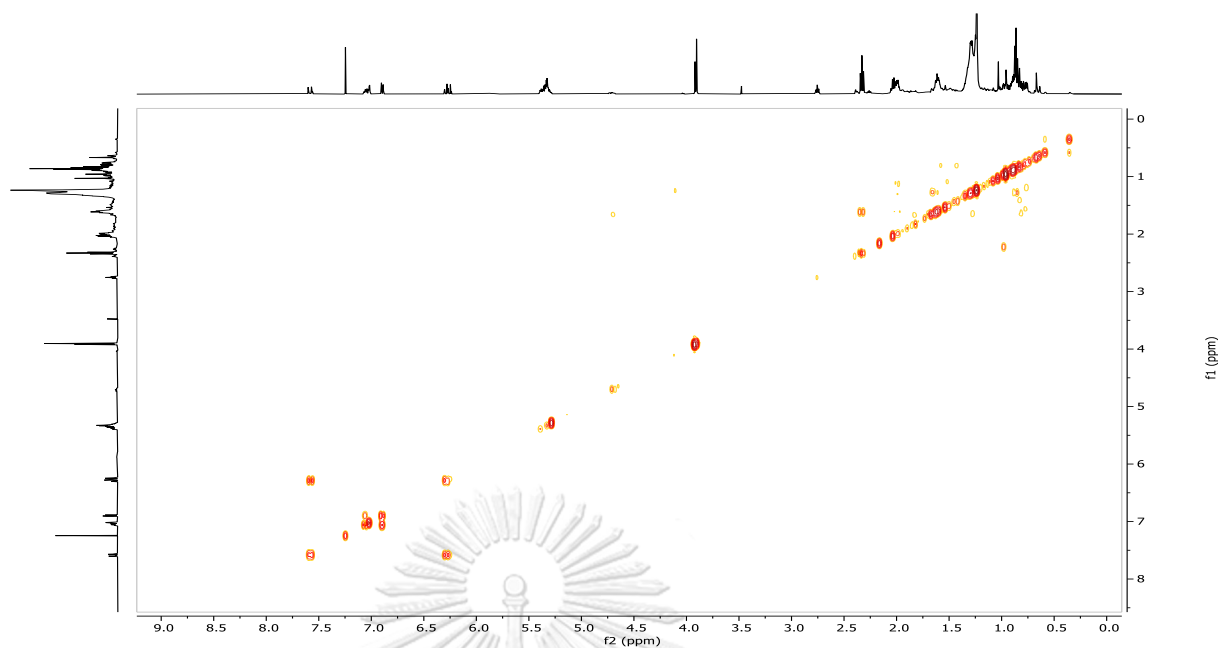
Figure A.3 ^{1}H-^{1}H COSY spectrum (500 MHz, CDCl$_3$) of compound 1
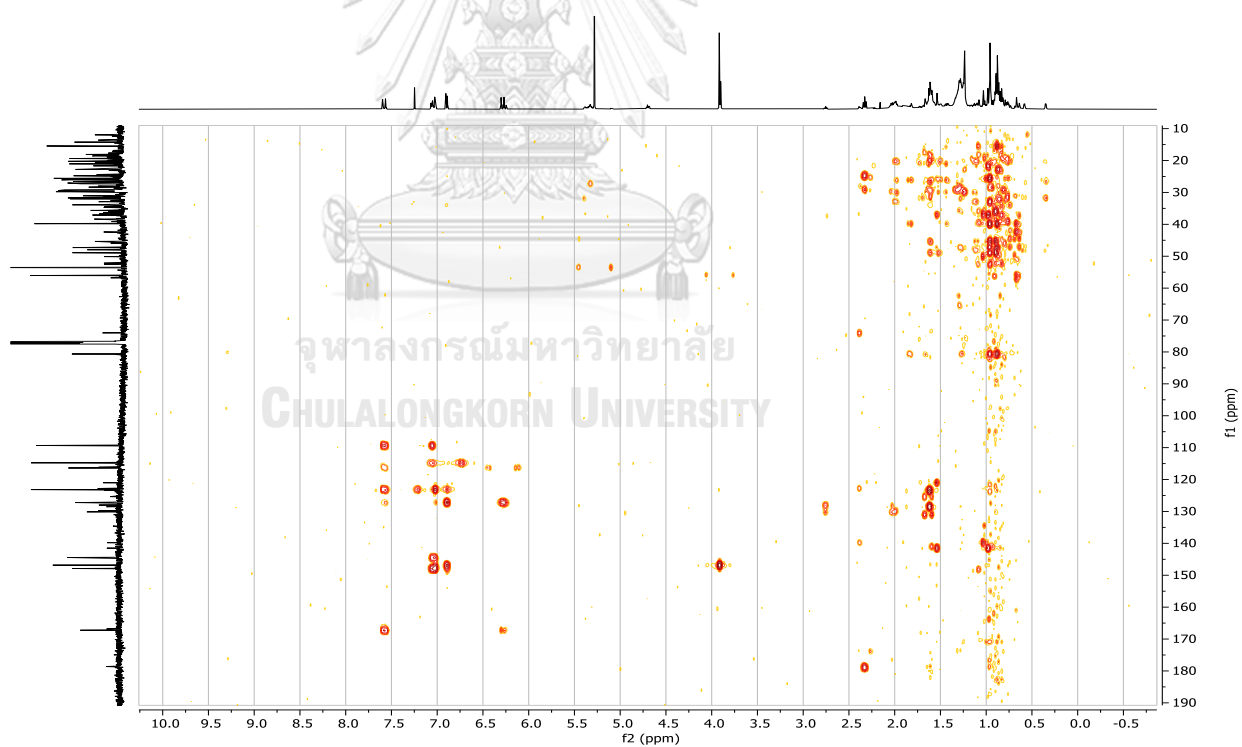
Figure A.4 HMBC spectrum (500 MHz, CDCl3) of compound 1
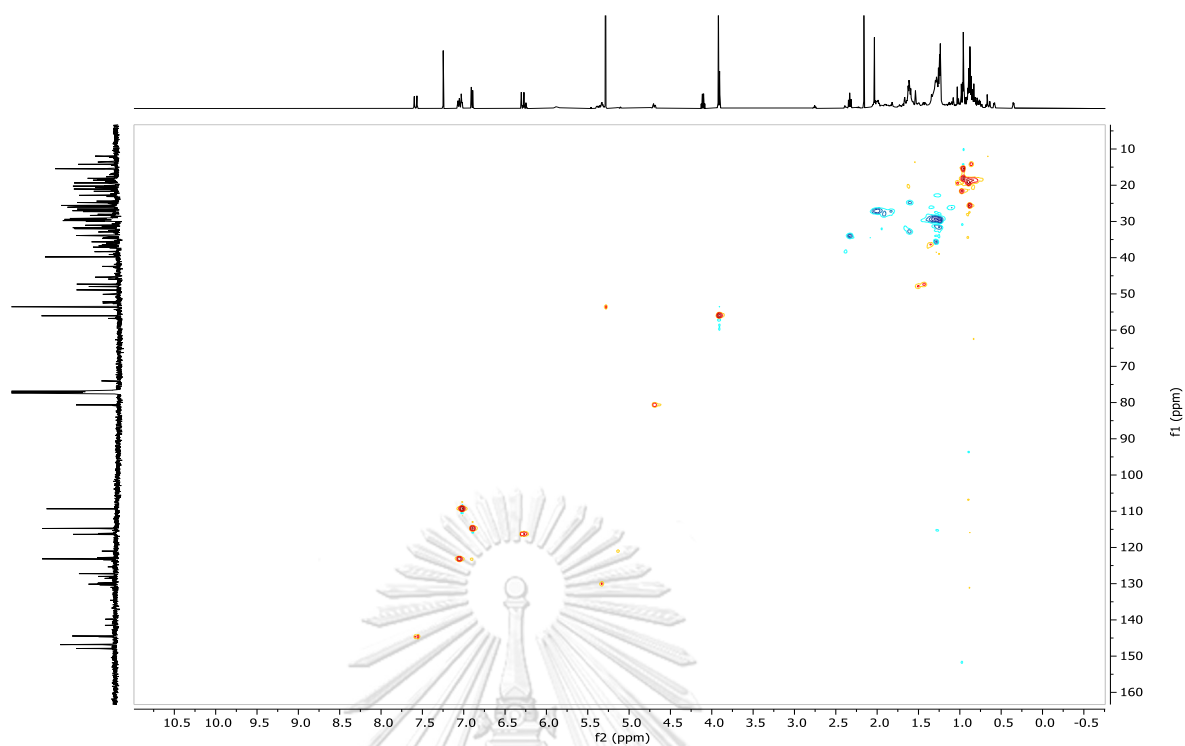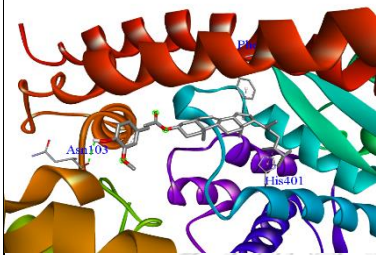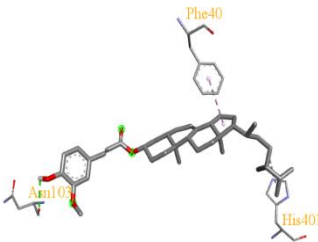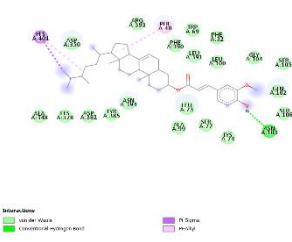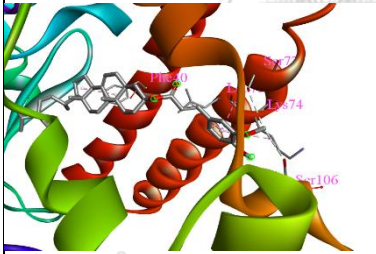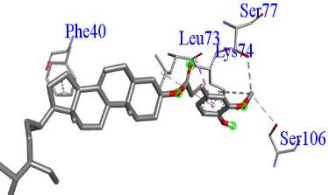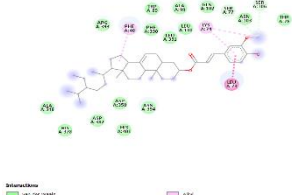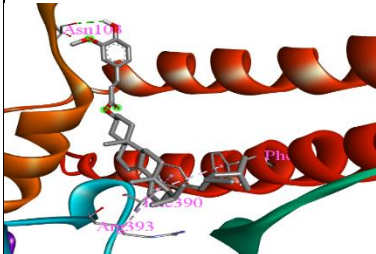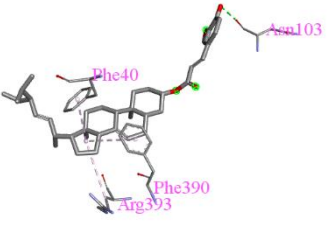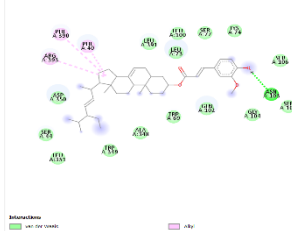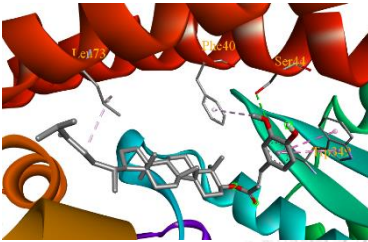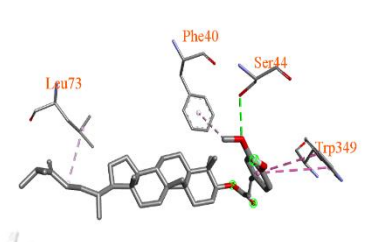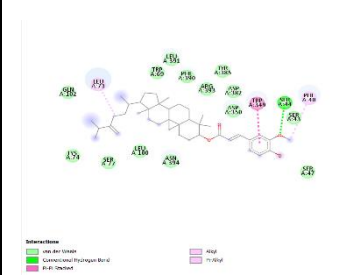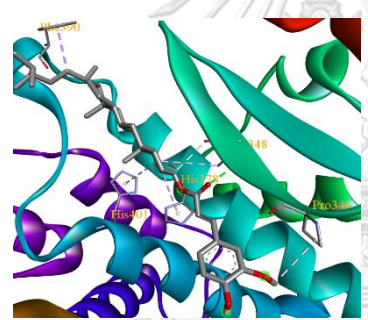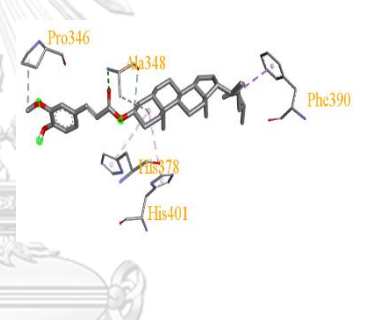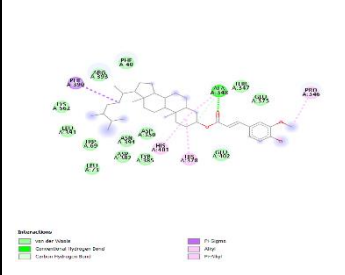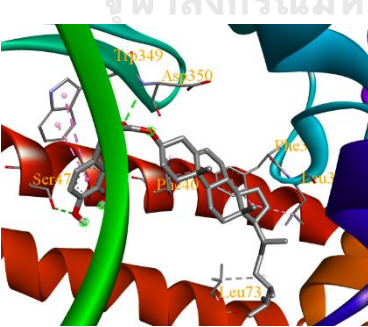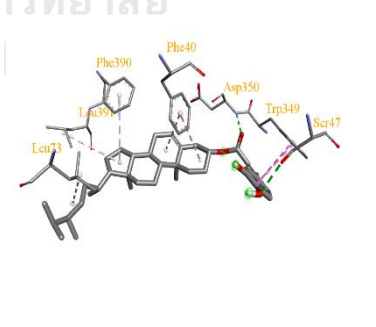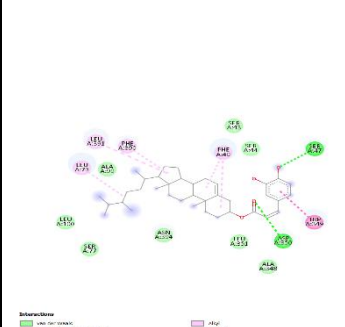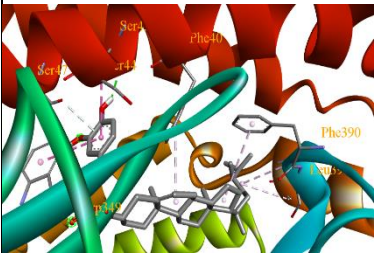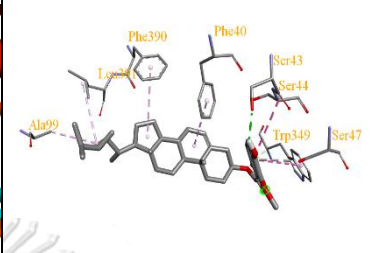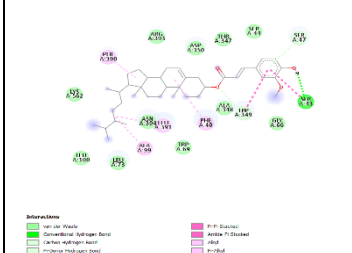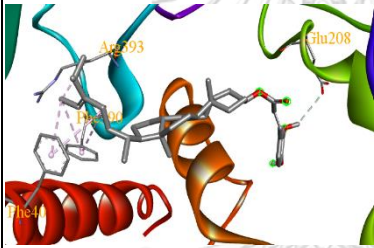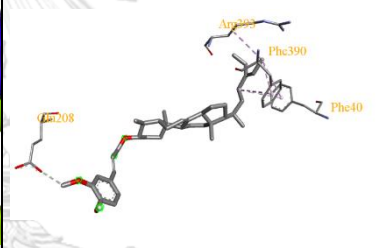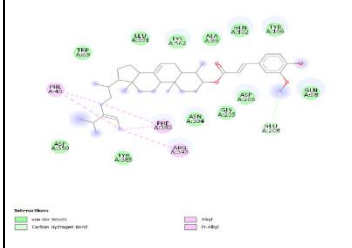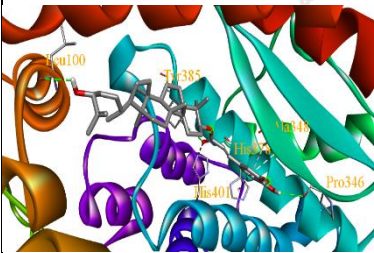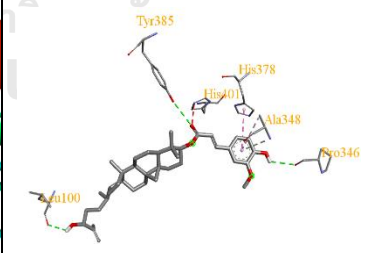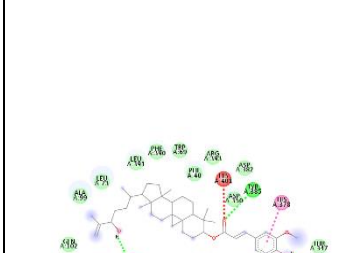
Figure A.5 HSQC spectrum (500 MHz, CDCl3) of compound 1
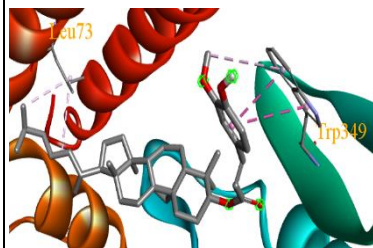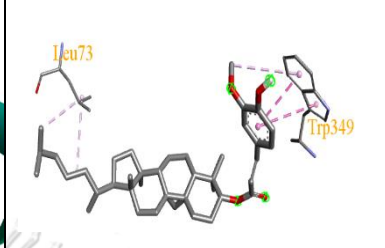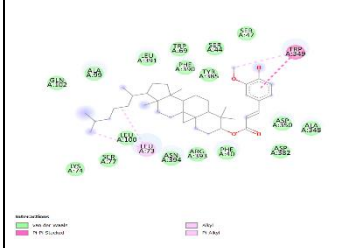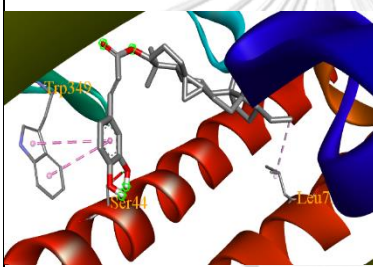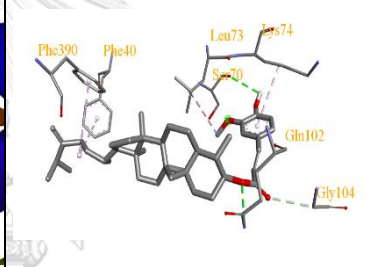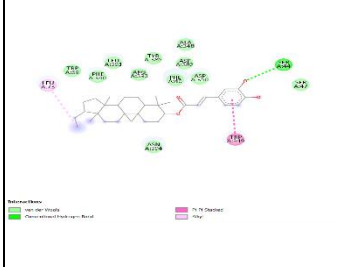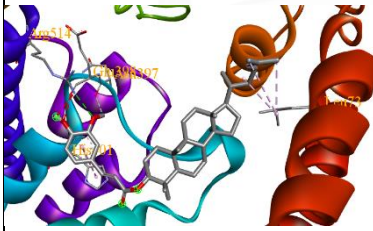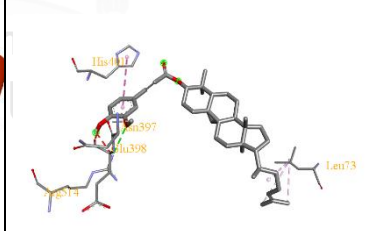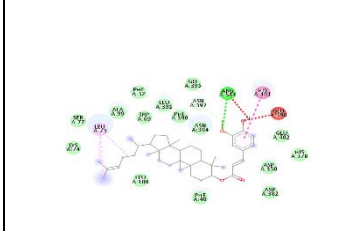
Table A.1 *In silico* approach of the phytochemicals in the active site of ACE2 (PDB ID: 1R42)
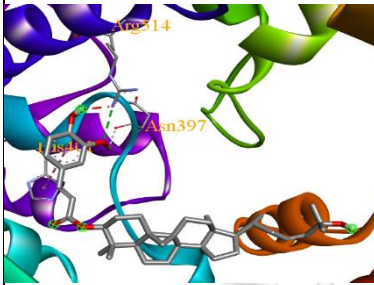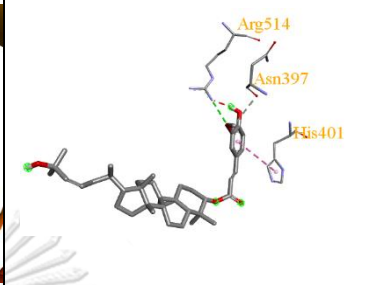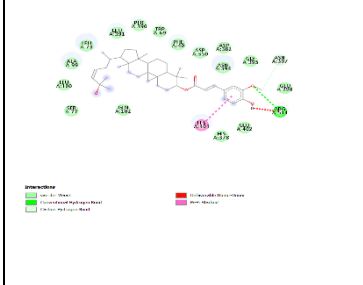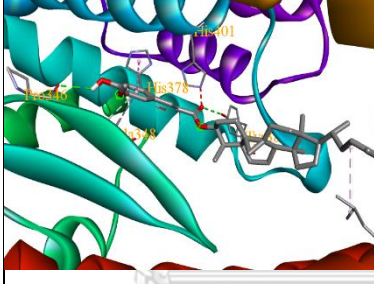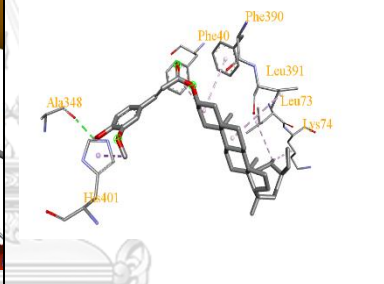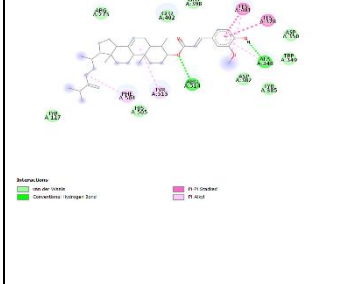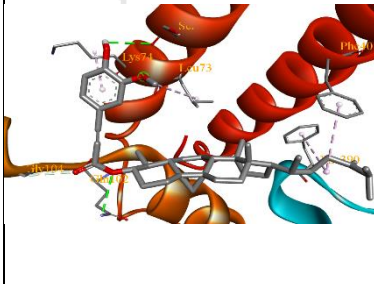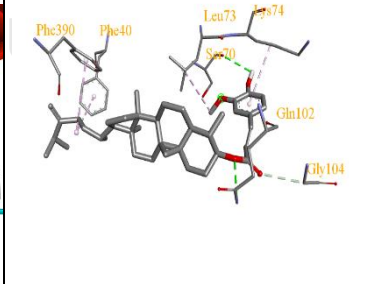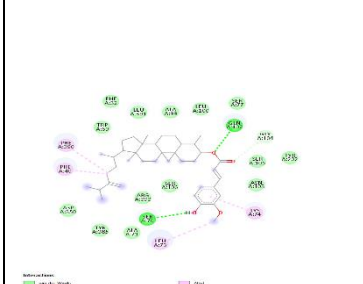
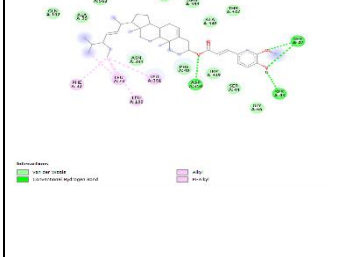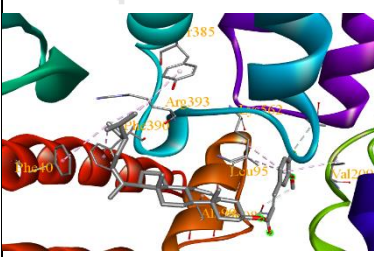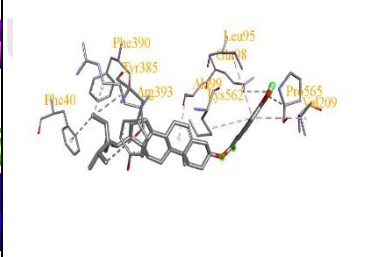| Phytochemical name	Binding energy (kcal/mol)	Phytochemicals in the active site of ACE2	3D molecular amino acid interaction	2D molecular amino acid interaction
Δ⁷-Campestenyl ferulate	-9.0			
Δ⁷-Sitostenyl ferulate	-8.5			
Δ⁷-Stigmastenyl ferulate	-10.2			
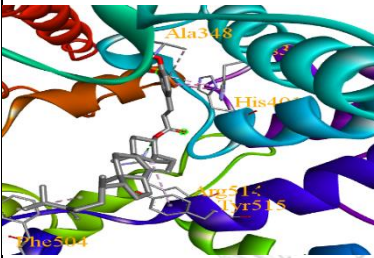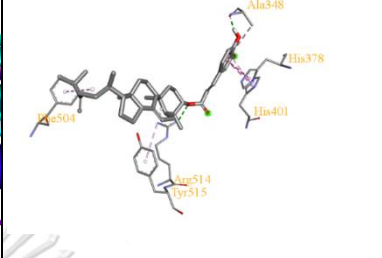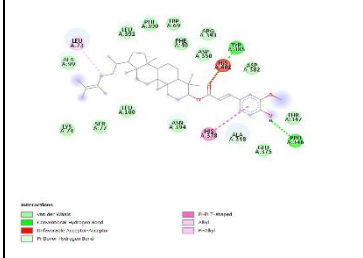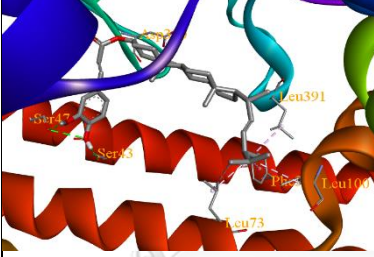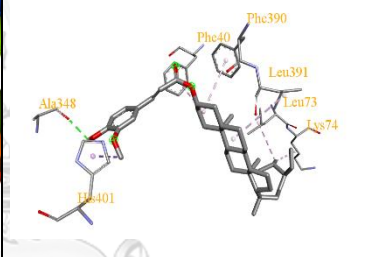
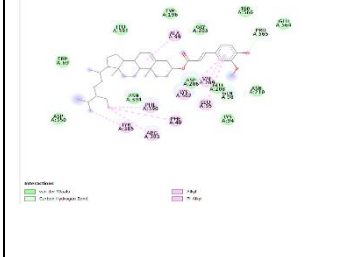| Phytochemical name	Binding energy (kcal/mol)	Phytochemicals in the active site of ACE2	3D molecular amino acid interaction	2D molecular amino acid interaction
24-Methylene-cycloartanyl ferulate	-9.3			
Campestanyl ferulate	-9.4			
Campesteryl caffeate	-9.4			

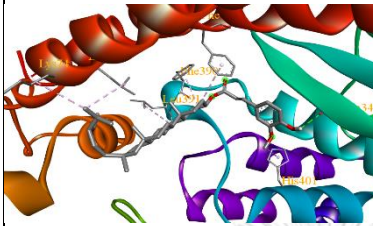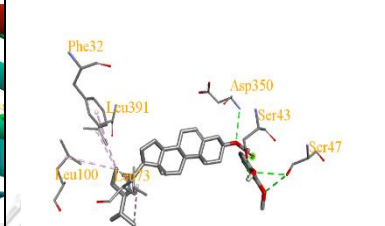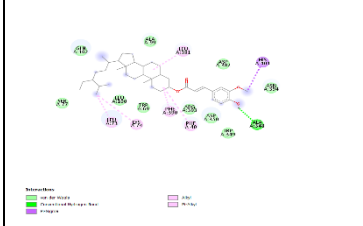| Phytochemical name	Binding energy (kcal/mol)	Phytochemicals in the active site of ACE2	3D molecular amino acid interaction	2D molecular amino acid interaction
Campesteryl ferulate	-9.3			
Citrostadienyl ferulate	-9.4			
Cycloart-23-Z-ene-3β, 25-diol-3β-trans ferulate	-9.9			

Phytochemical name	Binding energy (kcal/mol)	Phytochemicals in the active site of ACE2	3D molecular amino acid interaction	2D molecular amino acid interaction
Cycloartanyl ferulate	-9.5			
Cycloartenyl caffeate	-8.9			
Cycloartenyl ferulate	-9.7			

Phytochemical name	Binding energy (kcal/mol)	Phytochemicals in the active site of ACE2	3D molecular amino acid interaction	2D molecular amino acid interaction
(24)-cycloart-25-ene-3β, 24-diol-3β-trans ferulate	-9.4			
Cyclobranyl ferulate	-9.8			
Cycloeucalenyl ferulate	-9.3			

Phytochemical name	Binding energy (kcal/mol)	Phytochemicals in the active site of ACE2	3D molecular amino acid interaction	2D molecular amino acid interaction
Gramisteryl ferulate	-9.5			
Sitostanyl ferulate	-8.8			
Sitosteryl ferulate	-8.7			

Phytochemical name	Binding energy (kcal/mol)	Phytochemicals in the active site of ACE2	3D molecular amino acid interaction	2D molecular amino acid interaction
Stigmasteryl ferulate	-9.0			

VITA

NAME	Muhammad Waqar Nasir
DATE OF BIRTH	3 August 1997
PLACE OF BIRTH	Pakistan
INSTITUTIONS ATTENDED	- Bachelor of Science in Chemistry, University of Management and Technology Lahore, Pakistan.
	- Master of Science in Chemistry, Chulalongkorn University, Bangkok, Thailand.
HOME ADDRESS	House No 195, Street No 32, Sector I-8/2 (District), Islamabad (Province), Pakistan